UNIVERSITEIT VAN PRETORIA
UNIVERSITY OF PRETORIA
YUNIBESITHI YA PRETORIA

DITHIOCARBONATE AND TRITHIOCARBONATE INTERACTIONS WITH PYRITE AND COPPER

by

Jan Albert Venter

Submitted as partial fulfillment of the requirements for the degree

Magister Scientiae (Metallurgy)

In the Faculty of Engineering, Built Environment and Information Technology.

Supervisor: Dr. M.K.G. Vermaak

Finally an answer to the perennial question:

“Nou is ek klaar.”

Acknowledgements

I want to thank the Lord for giving me the ability and strength to be able to complete this study.

I also want to thank the following people:

- My family for their support and patience
- Thys Vermaak for the guidance he provided me and especially all the time he sacrificed listening to my ideas
- Prof. Chris Pistorius for all the discussions, scheduled and impromptu, even on weekends and holidays
- Robin Muir for the exchange of ideas and manufacturing of several pieces of glassware
- Friends for their support and encouragement
- The Department of Materials Science and Metallurgical Engineering for providing me with the opportunity and necessary funds for this study

DITHIOCARBONATE AND TRITHIOCARBONATE INTERACTIONS WITH PYRITE AND COPPER

By

Jan Albert Venter

Supervisor: Dr. M.K.G. Vermaak

Magister Scientiae (Metallurgy)

Abstract

Extensive research has been performed on the interaction of dithiocarbonates (xanthate) with a wide variety of substrates. This study the focuses on the interaction of trithiocarbonates (TTC) with pyrite and copper. The mechanism of adsorption of the xanthate is compared to that of the TTC. For the xanthate to adsorb it is necessary for an oxidant to be present, since xanthate adsorbs via charge transfer processes (electrochemical processes). It was found by the use of cyclic voltammetry and contact angle measurements that collector adsorption of the TTC can occur in both oxidising and reducing (thus the absence of an oxidant) conditions. Neither the TTC monomer nor the dimer could be detected on the surface by the use of Raman spectroscopy. The collector species on the surface was the TTC decomposition products namely the thiol or thiolate. Electrochemical impedance spectroscopy (EIS) confirmed that the TTC can interact under oxidising and reducing conditions. EIS showed that the rate of adsorption of the collector species for anodic currents increases relatively to the rate of adsorption for cathodic currents. Different adsorption mechanisms are realised for the different polarisation conditions. It is postulated that the TTC species serves as an intermediate for the adsorption of the thiol or thiolate on the surface, ultimately rendering the surface hydrophobic. Decomposition tests, performed by employing UV/Vis spectroscopy,

indicated that the TTC is very unstable between a pH of 4 and 11. The thiol or thiolate however does not readily adsorb onto the substrates (indicated by the EIS measurements). Microflotation tests confirmed the thiolate's inability to render pyrite hydrophobic. The microflotation tests also indicated that the TTC became less effective in recovering pyrite after it was left to decompose for a couple of hours.

Keywords: Xanthate, TTC, pyrite, copper, cyclic voltammetry, contact angle measurements, Raman spectroscopy, EIS, UV/Vis spectroscopy and microflotation

Contents Page

1. Introduction

Flotation is a very versatile and important concentration step for low-grade and complex ores that need to be ground very fine to achieve liberation. The collectors are surface-active chemicals that selectively adsorb onto the minerals of interest. The target mineral is rendered hydrophobic by the collector. When gas (either air or nitrogen) is passed through the pulp, the gas bubbles attach to the hydrophobic particles and the particle-bubble collectives then rise to the surface of the pulp, where the target mineral is collected.

Flotation is used extensively in the base metal, gold and platinum-group element (PGE) industries. In the latter two industries, although less frequently in the case of the gold industry, the noble elements can be associated with base-metal sulfides, e.g. pyrite in the case of gold. So by concentrating these base-metal sulfides, the noble metals are co-concentrated.

Dithiocarbonates (xanthate) collectors have been the workhorses of the sulfide flotation industry for more than 80 years. Extensive work has been done on the interaction of different thiol collectors with different substrates (Woods, 1996, and Finkelstein & Poling, 1977). More recently, trithiocarbonates (TTC) have also been employed in the recovery of base-metal sulfides, mainly in precious metal ores. Indications are that improved grades and recoveries are realised with the use of TTCs (Breytenbach *et al.*, 2003, Du Plessis *et al.*, 1999, 2002 & 2003, and Vos *et al.*, 2006). However, the best flotation results were obtained by replacing a small amount of xanthate (less than 25 molar percentage) with an equal-molar quantity of TTC (Breytenbach *et al.*, 2003). The initial work by Du Plessis *et al.* (1999 & 2002) indicated that it is possible to achieve sufficient hydrophobicity at potentials significantly more negative than the reversible potential of the TTC monomer/dimer couple. This would indicate that in reducing conditions, only the TTC monomer might be present or – as stated by Du Plessis (2003) – a decomposition product of the TTC. Du Plessis (2003) indicates that at potentials more positive than the reversible potential of the TTC monomer/dimer couple, both the monomer and dimer are present on the surface.

The purpose of this work is to investigate the mechanism of adsorption of the TTC onto the surfaces of pyrite and copper. The aim is to investigate, by employing contact angle measurements, electrochemistry, Raman spectroscopy and electrochemical impedance measurements, whether the xanthate and the TTC follow similar adsorption mechanisms.

2. Literature review

2.1 Dithiocarbonate (xanthate) and trithiocarbonate (TTC)

2.1.1 Xanthate

The introduction of short-alkyl-chain xanthates (Figure 1) as collectors in 1925 was a major advance in flotation technology, because these collectors were more selective than the previously utilised collectors (Woods, 1996).

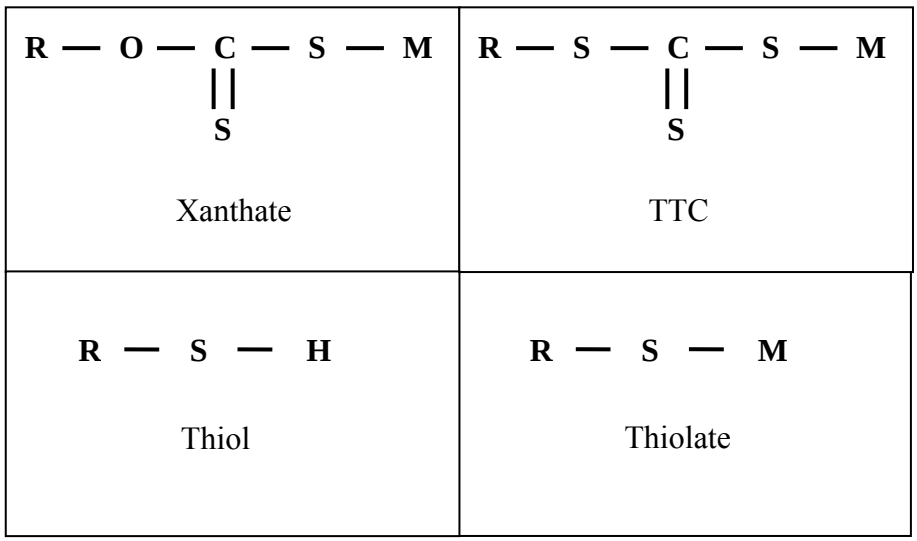

R : non-polar organic hydrocarbon chains
M: alkaline metal

Figure 1: Structures of collector species

The precise interactions between the mineral surface and xanthate have been debated for quite some time (Woods, 1996, and Finkelstein & Poling, 1977). The general consensus is that the xanthate chemisorbs via charge transfer onto the sulfide metal to form a layer. If the mixed potential of the mineral is more positive than the reversible potential of the xanthate/dixanthogen couple, then the xanthate will be oxidised to dixanthogen (X_2) (Steyn, 1996). This secondary step is electrochemical adsorption.

Chemisorption of xanthate on mineral via charge transfer (Woods, 1996):

$$M_{surf} + X^- \rightarrow M_{surf}X_{ads} + e^- \quad (1)$$

Electrochemical oxidation:

$$2X^- \rightarrow X_2 + 2e^- \quad (2)$$

According to Woods (1996), electrochemical oxidation occurs as follows:

$$M_{surf}X + X^- \rightarrow M_{surf}X_2 + e^- \quad (3)$$

Or

$$2M_{surf}X \rightarrow M_{surf}X_2 + e^- \quad (4)$$

$$M_{surf}X_2 \rightarrow X_2 + M_{surf} \quad (5)$$

The oxidation reactions above are balanced out by the reduction of oxygen in alkaline solutions.

$$^1/_2O_2\,(ads) + H_2O\,(l) + 2e^- = 2OH^-\,(aq) \quad (6)$$

This means that the mineral surface behaves as a catalyst for the oxidation of the xanthate. Therefore it can be seen that when the xanthate chemisorbs via charge transfer, it forms an ionic bond to the mineral surface; and when it is electrochemically oxidised it is bonded to the surface due to Van Der Waals forces.

2.1.2 TTC

Slabbert (1985) showed that the short chain TTCs (Figure 1) increase the recovery of PGMs significantly on plants that previously used other collectors. Due to the foul odour of the short chain TTCs and the withdrawal of the United States from South Africa, the use of TTCs has been very limited until recently. With the development of C_{12}-TTCs the use of this type of thiol collectors has increased.

Although limited research has been done on the interaction of TTCs with mineral surfaces, the adsorption mechanism is believed to be similar to that of xanthates at potentials more positive than the reversible potential of the monomer/dimer couple; initial chemisorption via transfer followed by the electrochemical oxidation (Du Plessis, 2003). Du Plessis (2003) however indicated that, at potentials more negative than the reversible potential of the monomer/dimer couple, the TTC's corresponding thiol was the only detectable species.

The following is a brief summary of the techniques employed in fundamental investigations of the interaction between a substrate and collector.

2.2 Potentiometry

Du Plessis (2003) has determined the reduction potentials for different xanthate/dixanthogen and TTC/$(TTC)_2$ couples. A glassy carbon indicator electrode was covered with a dimer and placed in a solution of the corresponding monomer. The open-circuit potential was subsequently measured, which corresponds to the redox potential of the couple. Their results are illustrated in Figure 2 and Table 1.

It is clear from these results that as the alkyl group increases in length, the redox potential decreases because with the increase in the size of the alkyl group, the inductive effect becomes more significant. This means that the monomer can be more easily oxidised. This would be expected for alkyl groups of up to about three carbons (Winter & Woods, 1973). The continued change in E^o may be due to the selection of the standard state of the oxidised species. The overall free energy that is measured includes the free energy of dissolution, since the species transforms from a thio-ion to a deposited oil or solid.

Du Plessis (2003) reports that the TTC decomposes during the measurements. This calls into question whether the oxidation of the TTC or only the side decomposition reaction was in fact measured. The decomposition also influences the calculation of the standard redox potentials, since the concentration of the TTC monomer in solution is unknown.

Table 1: Standard redox potentials for different thiocarbonate couples (Solutions saturated with dimer, mV vs. SHE) (Du Plessis, 2003)

Hydrocarbon group	**Monothiocarbonate MTC/$(MTC)_2$**	**Dithiocarbonate DTC/$(DTC)_2$**	**Trithiocarbonate TTC/$(TTC)_2$**
Methyl	20	-2 ± 9.5	-
Ethyl	2	-54.4 ± 12.1	-
n-Propyl	-22	-83.3 ± 13.3	-144.5 ± 10.3
Iso-Propyl	-	-91.7 ± 6.7	-
n-Butyl	-38	-118.8 ± 13.0	-187.6 ± 14.2
Iso-Butyl	-	-131.7 ± 11.7	-
n-Amyl	-88	-148.8 ± 12.2	-247.7 ± 12.7
Hexyl	-120	-156.0 ± 1.4	-275.8 ± 14.9

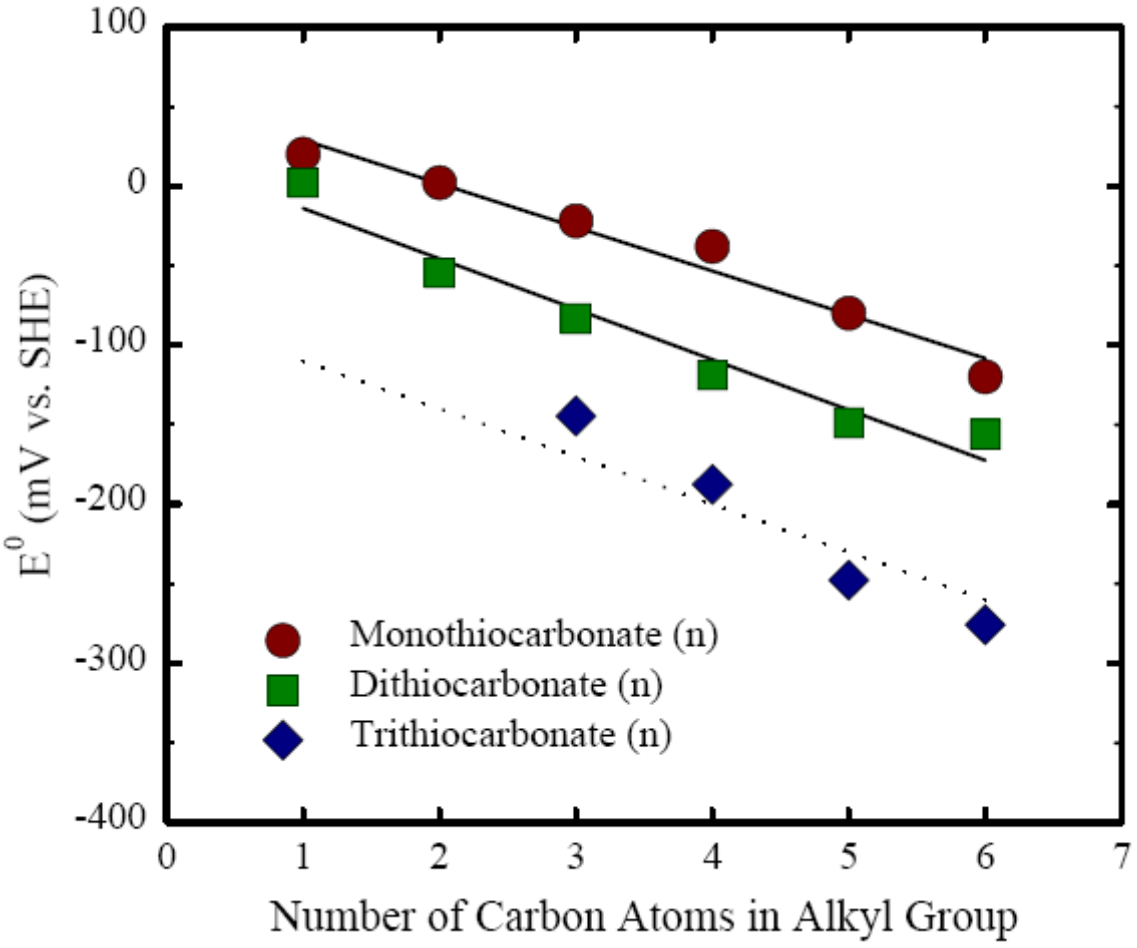

Figure 2: Standard redox potentials of thiocarbonate collectors (Du Plessis, 2003)

2.3 Voltammetry

The mechanism of adsorption for xanthates has been derived from voltammetric experiments. Figure 3 (Woods, 1976) illustrates the difference in the cyclic voltammograms of copper sulfide electrodes with and without xanthate. Peaks A_1 and A_2 are due to the chemisorption of the xanthate onto the copper sulfide surface. Peak A_3 is the formation of bulk copper xanthate, which is approximately 150 mV (SHE) more negative than the oxidation of xanthate to dixanthogen (Woods, 1976). Peaks A_1 and A_2 occur at potentials more negative than those of the reversible potential for the formation of the metal xanthate and dixanthogen. This type of pre-wave is indicative of the chemisorption of the xanthate onto the copper sulfide surface, as described by reaction (1) – therefore xanthate would be the only species present on copper sulfide.

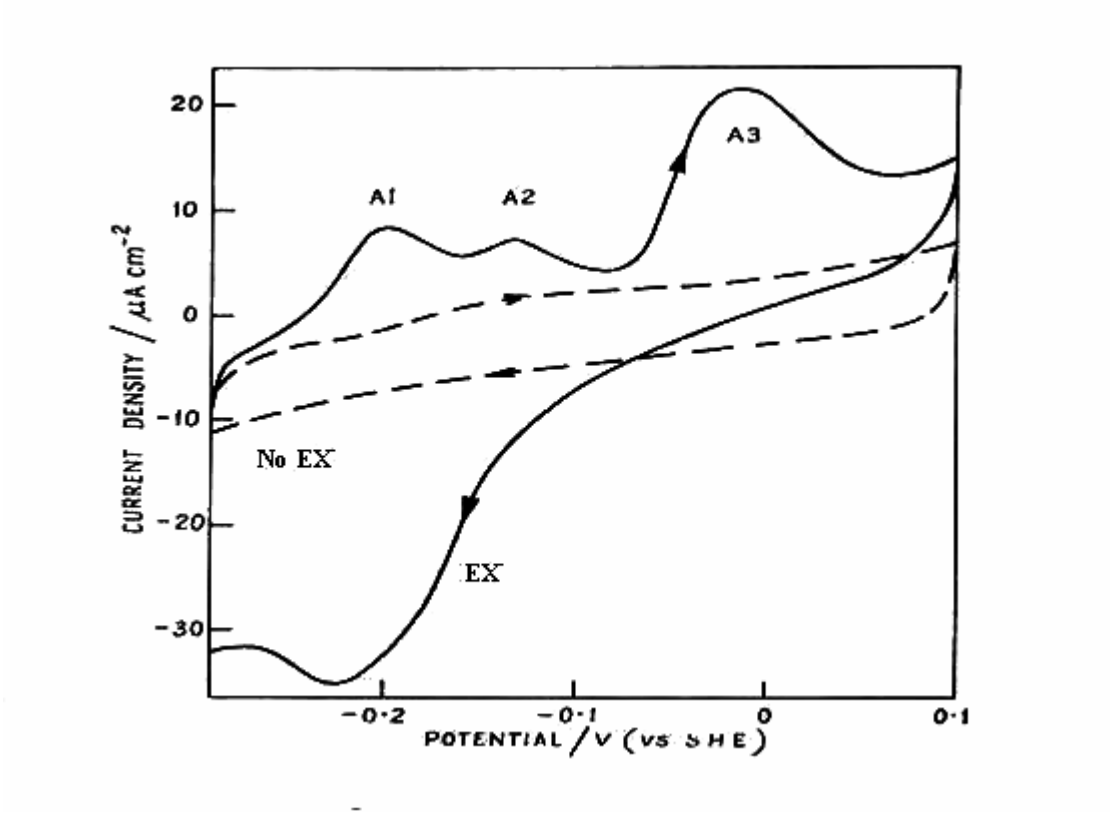

Figure 3: Cyclic voltammograms of copper sulfide electrodes with and without ethyl xanthate (3.97×10^{-4} M) in 0.1 M sodium fluoride solution (Woods, 1976).

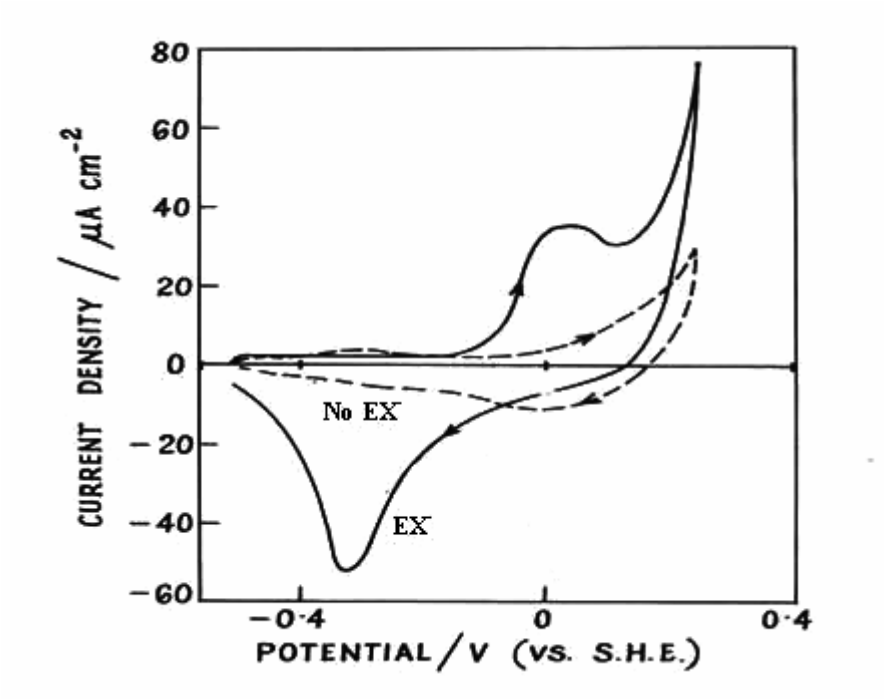

Figure 4: Voltammogram for a galena electrode in a 0.1 M borate solution, with and without ethyl xanthate (9.5×10^{-3} M) (Woods, 1976).

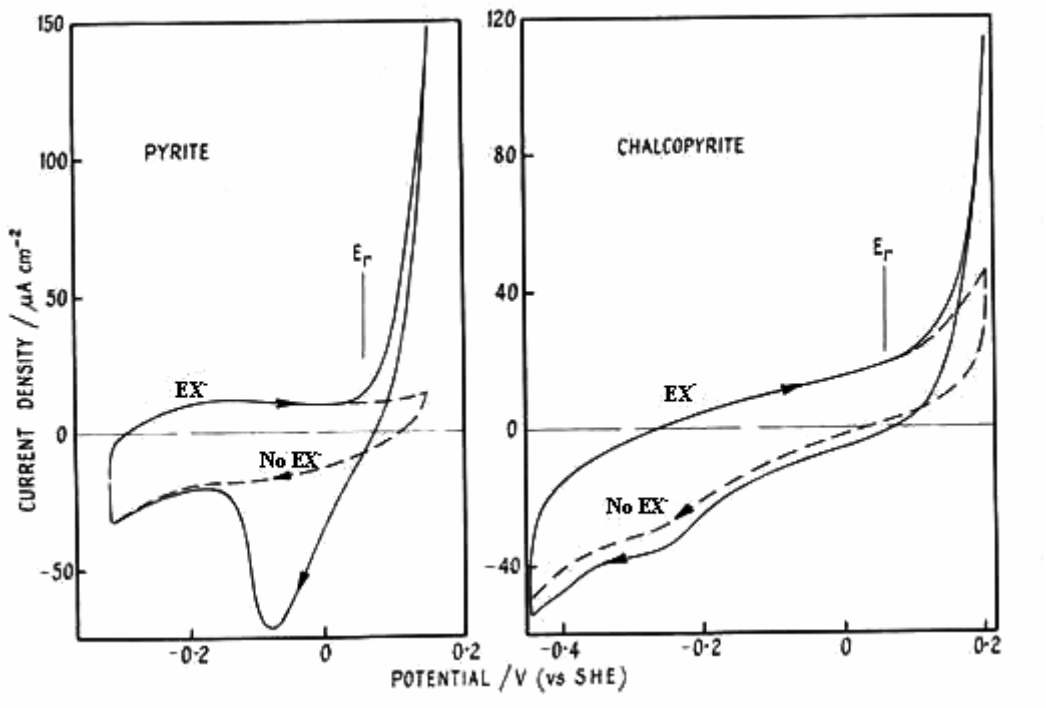

Figure 5: Voltammograms of pyrite and chalcopyrite electrodes in a 0.05 M borate solution, with and without ethyl xanthate (1×10^{-2} M); E_r is the reversible potential of xanthate-dixanthogen (Woods, 1976)

This type of pre-wave is also visible on galena electrodes (Woods, 1976). In Figure 4 a peak at ~0 mV (SHE) is visible when the galena is polarised in a xanthate solution. Furthermore, an increase in the current from potentials more positive than the reversible potential of xanthate-dixanthogen is observed in Figure 4. This indicates that dixanthogen can form on galena if the surface potential is high enough.

By contrast, only the oxidation peak of xanthate to dixanthogen is evident on platinum, gold, pyrite and chalcopyrite electrodes (Figure 5). The Tafel slopes for the anodic oxidation of xanthate on these electrodes indicate that the oxidation reaction is also preceded by the chemisorption of the xanthate [see reaction (1)].

Several different techniques have been employed to verify the species that are present at specific potentials. These techniques include infrared spectroscopy, Raman spectroscopy, nuclear magnetic resonance, X-ray photoelectron spectroscopy and ultraviolet spectroscopy (see later in this study).

2.4 Collector efficiency

The most important property of a collector is its efficiency. The best way to determine the efficiency of a collector is to determine the flotation recovery obtained with the collector. As knowledge of the precise interaction with the surface is not as important as the collector's ability to recover the concentrate, it is important to measure the hydrophobicity of a conditioned surface. A useful technique for this purpose is to measure the three-phase gas-liquid-solid contact angle (Figure 6).

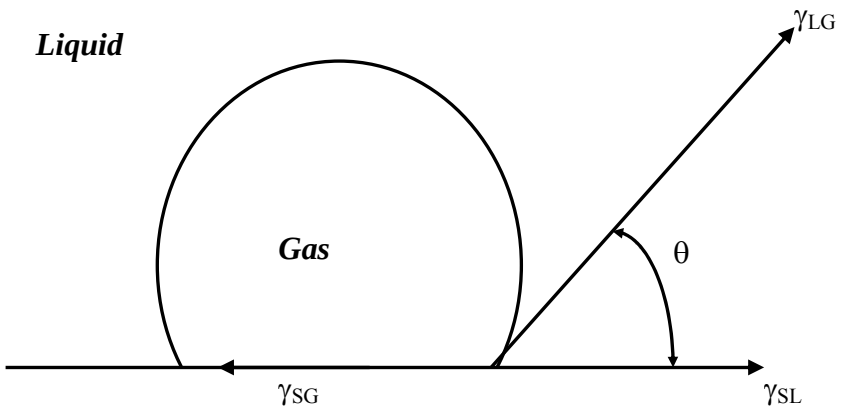

Figure 6: Diagram of the three-phase equilibrium on the gas-liquid-solid interface, with the contact angle θ between the gas and solid phases (Fuerstenau *et al.*, 1976)

This equilibrium condition can be described by Young's formula (Fuerstenau *et al.*, 1976):

$$\gamma_{SG} = \gamma_{SL} + \gamma_{LG} \cos \theta \quad (7)$$

where γ_{SG}, γ_{SL} and γ_{LG} are the tensions of the solid/gas, solid/liquid and liquid/gas interfaces and θ is the contact angle. The change in the free energy due to the change of interfaces is given by Dupre's equation (Fuerstenau *et al.*, 1976):

$$\Delta G = \gamma_{SG} - (\gamma_{SL} + \gamma_{LG}) \quad (8)$$

Therefore, by combining these two equations it is possible to derive:

$$\Delta G = \gamma_{LG} (\cos \theta - 1) \quad (9)$$

This means that upon any attachment between a surface and a gas bubble, at any finite contact angle, there will be a decrease in free energy. When there is an increase in the contact angle there is a corresponding decrease in the free energy, indicating an increase in the hydrophobicity of the particle.

Measurements of contact angles have shown that the maximum contact angle for a particle collector system is not dependent on the functional group of the collector, but does depend on the hydrocarbon chain length and the amount of branching of the hydrocarbon chain (Woods, 1996). Figure 7 (Rao, 1971) indicates that as the hydrocarbon chain length of an alkyl xanthate increases, so does the maximum contact angle increases. In addition, branched hydrocarbon chains (*iso*-alkyl) compared to similar length straight hydrocarbon chains have larger maximum contact angles.

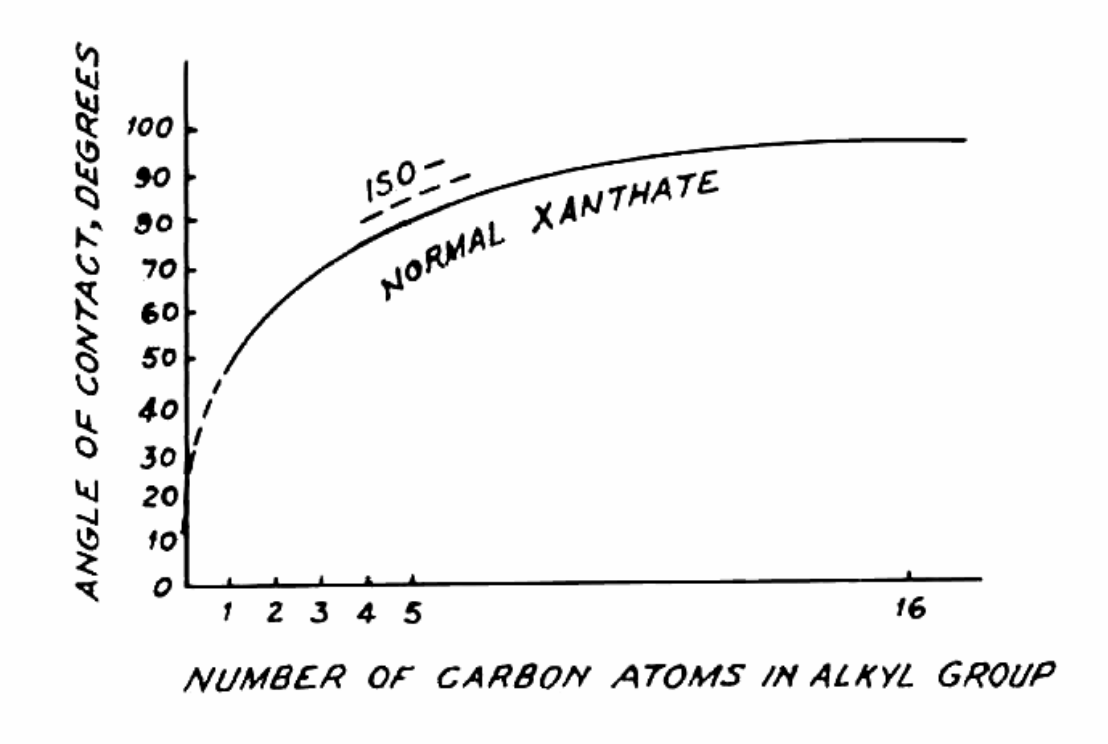

Figure 7: Dependence of contact angle on alkyl xanthate chain length (Rao, 1971).

Another useful application of contact angle measurements is to verify electrochemical measurements by measuring contact angles on electrode surfaces under potential control. The adsorption of xanthate is highly dependent on the type of substrate surface present (Woods *et al*., 1994). Figure 8 shows that silver (curve 1) forms finite (non-zero) contact angles at lower potentials than gold (curve 4). In fact, gold only forms non-zero contact angles at potentials more positive than the reversible potential of xanthate/dixanthogen. Silver adsorbs xanthate at lower potentials than the xanthate/dixanthogen couple, indicating that the xanthate present on the silver must

have been chemisorbed. The other two curves (2 and 3) are for silver-gold alloys, showing that silver enhances the hydrophobic surface state of the gold.

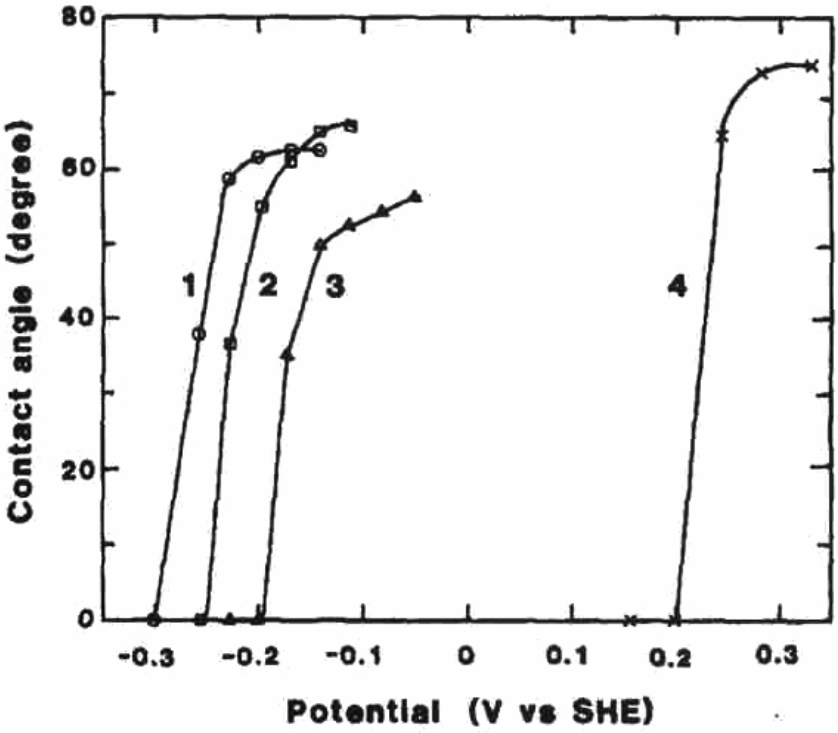

Figure 8: Dependence of contact angle on potential in a 1×10^{-3} M ethyl xanthate solution (pH 9.2) for: (1) silver; (2) 50:50 wt.% Ag-Au alloy; (3) 20:80 wt.% Ag-Au alloy; (4) gold (Woods *et al*., 1994)

Care should be taken when determining contact angles, since the size of the surface and bubbles can have a dramatic effect on the results. It is possible that the collector may not cover the entire surface; some parts are hydrophilic and some parts are hydrophobic (Woods *et al*., 1994). This means that the contact angle determined in a region of low adsorption density would not be a fair reflection of the hydrophobic state of the surface.

Figure 9 shows the relationship between fractional surface coverage and flotation recovery. At a fractional surface coverage of 0.2 the flotation recovery is already around 50% and when the fractional surface coverage reaches 0.5 the flotation recovery is 90%.

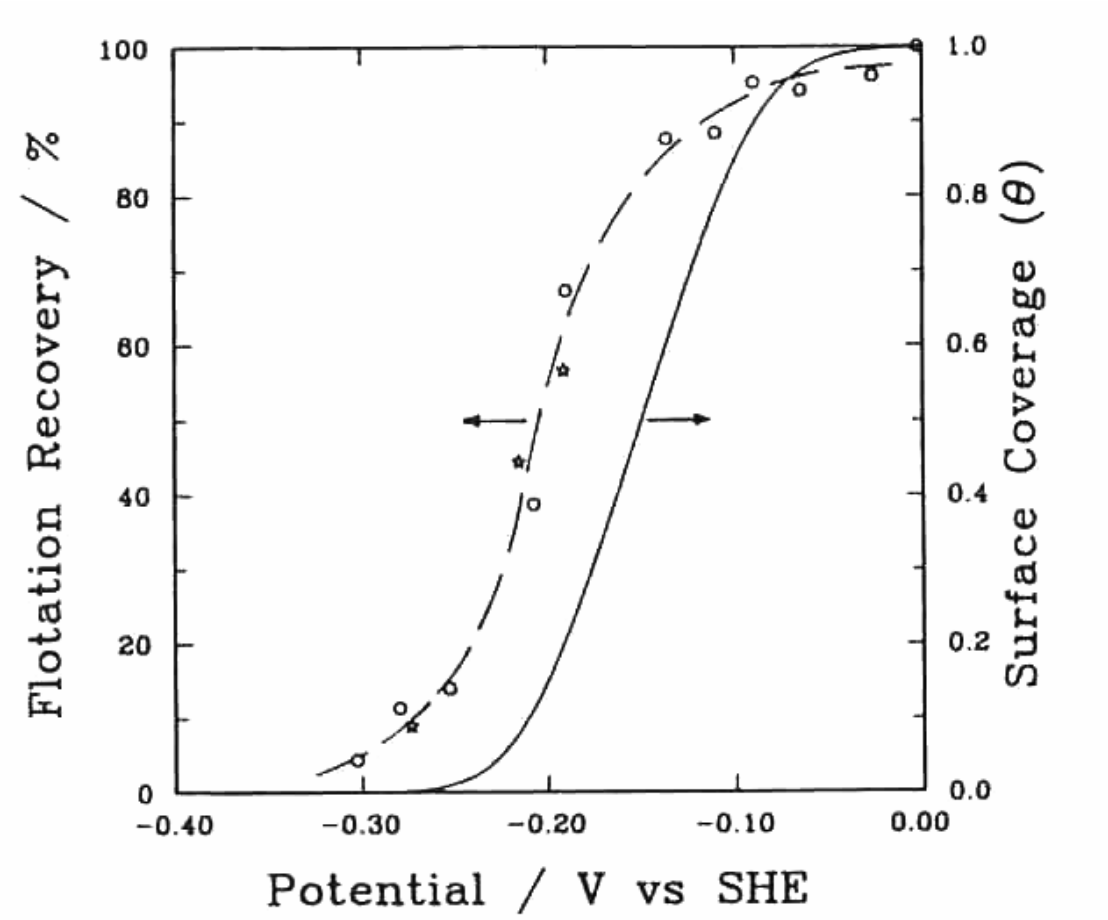

Figure 9: Comparison of the flotation recovery after one minute of chalcocite in 1×10^{-5} M ethyl xanthate solution (pH 9.2) with the adsorption isotherm for chemisorbed xanthate at this concentration (Woods, 1996).

Figure 9 illustrates that: (i) a complete monolayer is not required to be able to float very efficiently, (ii) a small increase in surface coverage results in a large increase in the recovery obtained.

2.5 Infrared (IR) spectroscopy

IR spectroscopy has been widely used in the determination of xanthate species; more recently it has also been used in the determination of TTC species. There are significant differences between the IR spectra of xanthate and dixanthogen, which is well illustrated in the IR spectra of sodium ethyl xanthate (NaEX) and ethyl dixanthogen (EX_2) as shown in Figure 10 (Rao, 1971) and Table 6 (Poling, 1976).

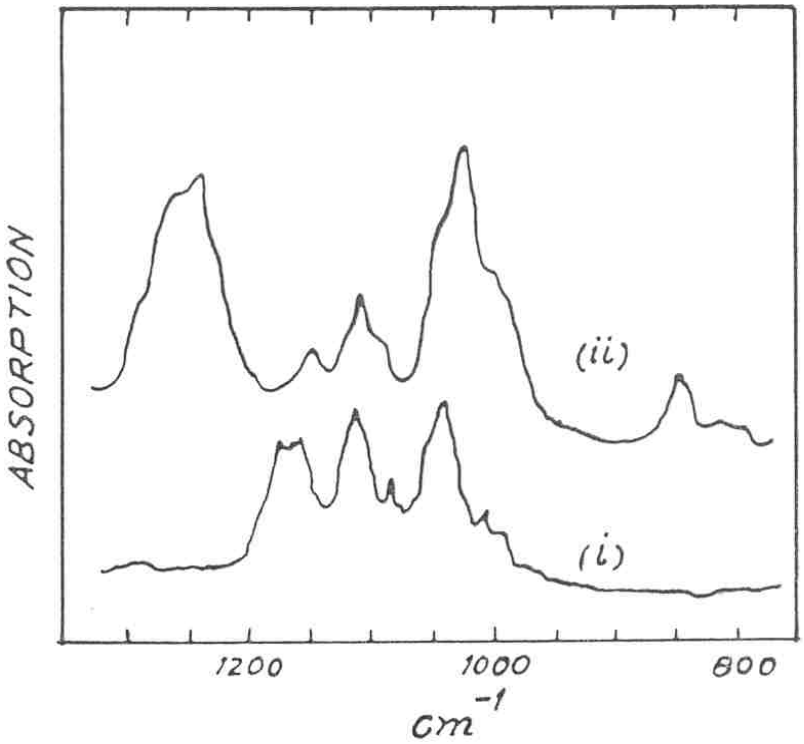

Figure 10: IR spectrum (*i*) NaEX and (*ii*) EX_2 (Rao, 1971)

Table 2: IR adsorption bands for xanthate and dixanthogen (Poling, 1976)

Functional group	**Xanthate**	**Dixanthogen**
	Wave number (cm^{-1})	
C-O-C	1100-1200 (2 bands)	1100-1265 (2 bands)
C=S	1010-1060	~1020
C-S	-	965-860

For the ionic xanthate, the charge on the sulfur is delocalised through the π-electrons, so the σ-bond of the C-S group would acquire a π-bond character. This means that the C-S bond would only be clearly visible on the infrared spectrum of the dixanthogen.

The two bands observed in the region 1100-1265 cm^{-1} are the symmetrical and asymmetrical stretching of the C-O-C group. The symmetrical stretching gives a weaker band than the asymmetrical stretching. This is clearly visible with the dixanthogen, where the asymmetrical stretching appears as a strong absorption peak at ~1265 cm^{-1} whereas the symmetrical stretching appears as a weak absorption peak at ~1150 cm^{-1}.

In the case of the xanthate, the asymmetrical and symmetrical C-O-C stretching absorption peaks are both of similar intensities. The reason is that the σ-bond of the one C-O group acquires some π-bond character from the delocalising of the charge. This means that the intensity of the symmetrical stretching of the C-O-C group will become greater. This is also evident from the spectrum in Figure 10. The asymmetrical absorption peak also shifts more, owing to the change from a non-polar to a polar molecule. The symmetrical C-O-C stretching for the xanthate is at ~1150 cm^{-1} (~1150 cm^{-1} for dixanthogen) and the asymmetrical stretching absorption is at ~1100 cm^{-1} (~1265 cm^{-1} for dixanthogen).

Du Plessis *et al.* (1999) recorded IR spectra for *n*-amyl xanthate, *n*-amyl TTC and their respective dimers. These spectra are shown in Figures 11 and 12. The authors state that the two bands observed for the xanthate in the region 1200-1125 cm^{-1} (Figure 11) are due to the C-O-C stretching vibration. These stretching vibrations are not present for the TTC. The peaks in the region 1010-1080 cm^{-1} for the xanthate and TTC are due to the C=S stretching vibration. The band at 840 cm^{-1} observed in the spectra for the TTC is probably due to the C-S stretching vibration. For the dimers, the C-O-C stretching vibration is again apparent for the dixanthogen in the region 1200-1300 cm^{-1} (Figure 12). For both dimers, the C=S stretching absorption peaks are visible in the region 1000-1050 cm^{-1}. It is clear from these spectra that it is possible to distinguish between the two collectors and also that it is possible to distinguish between the monomers and the dimers.

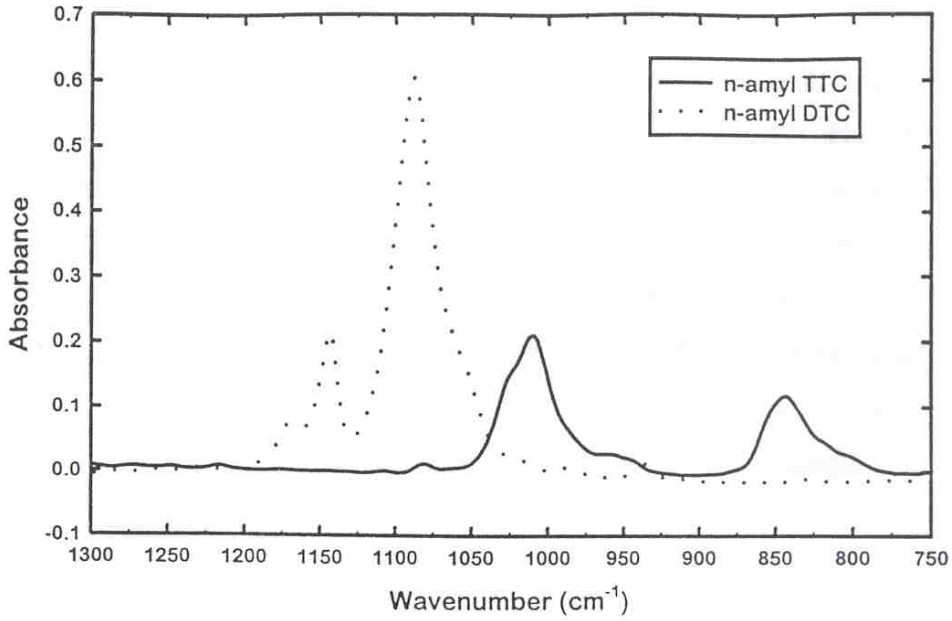

Figure 11: IR spectra of *n*-amyl xanthate and *n*-amyl TTC (Du Plessis *et al*., 1999).

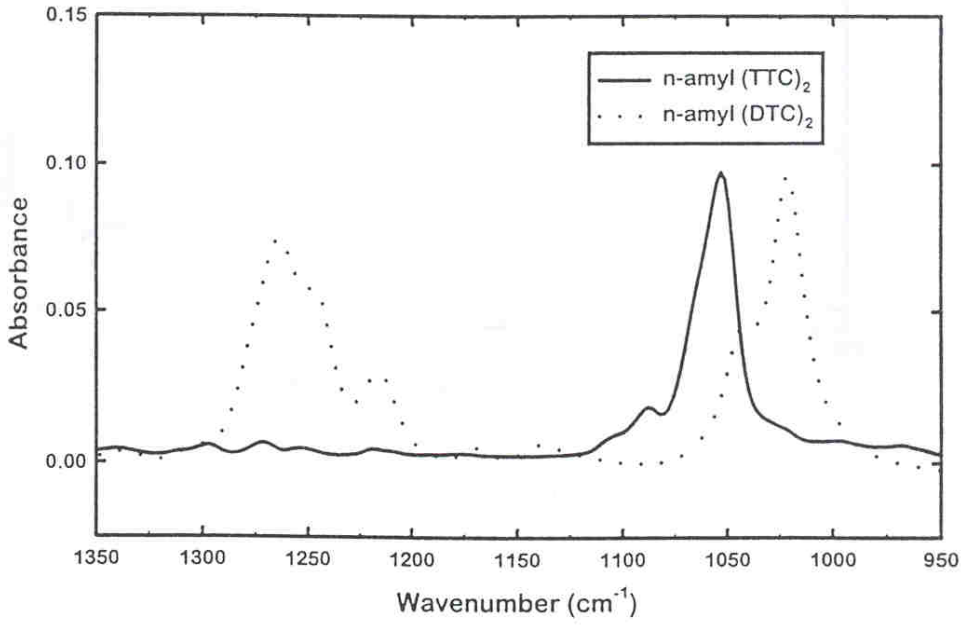

Figure 12: IR spectra of *n*-amyl dixathogen and *n*-amyl $(TTC)_2$ (Du Plessis *et al*., 1999).

IR has been utilised to determine the species present on the surface of the minerals in the flotation process. The technique most commonly used is to have a polished mineral or metal electrode under potentiometric control. The electrode is placed in a collector solution and held at a fixed potential. The electrode is then analysed to determine the species present on its surface.

At first the electrodes were always analysed *ex situ* owing to the strong influence of the water in the IR absorption region. The species were then either extracted from the electrode surface and then analysed in an IR spectrometer or determined by infrared external reflectance. The infrared reflectance method is preferred because it is difficult to ensure the integrity of the surface species when it is extracted. More recently, some *in situ* IR determinations have been done with the infrared reflectance technique. The IR spectra acquired during these procedures are then compared to the IR spectra of synthesised pure collector compounds in their different forms.

The orientation as well as the thickness of the adsorbed layers can be estimated with external reflectance IR. In addition, possible changes in the surface species exposed to the atmosphere are inhibited with the use of the *in situ* method. By using the technique of external reflectance infrared, Mielczarski *et al.* (1989) concluded that xanthate that is adsorbed onto chalcocite is orientated (Figure 13). The authors also concluded that a monolayer could be formed in a couple of minutes, though it took about 2½ hours for a near three-monolayer film to form.

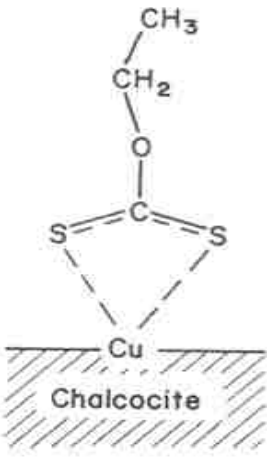

Figure 13: Orientation and co-ordination of ethyl xanthate on chalcocite (Mielczarski *et al.*, 1989)

Bozkurt *et al.* (1999) found that, by using s- and p-polarised external IR reflection, the monolayer of xanthate adsorbed onto the surface of a copper electrode was orientated similarly to that of xanthate on chalcocite (Figure 13). Bozkurt *et al.* (1999) did not observe more than one layer of xanthate adsorbing onto the surface, but only an increase in the coverage of the monolayer. Bozkurt *et al*. (1999) also investigated the orientation of dixanthogen; they found the dixanthogen produced was randomly orientated. This possibly indicates that the dixanthogen is randomly orientated on the orientated metal xanthate layer through hydrophobic interaction.

Mielczarski *et al.* (1998) give further evidence of the possibility that both species are present when the dixanthogen is formed and adsorbed. The authors found that cuprous xanthate was present even after the formation of the dixanthogen. In addition, the authors found that amyl xanthate, adsorbed only as a monolayer on the surface of the mineral and dixanthogen, was present as multilayers on this monolayer. With ethyl xanthate Mielczarski *et al.* (1998) found that more than a monolayer cuprous ethyl xanthate formed – again the dixanthogen formed on these layers. This may indicate that chemisorbed xanthate is needed for dixanthogen to be present on the surface. This is a possible explanation for the poor recoveries obtained when dixanthogen is produced *ex situ* and used as a collector (Ackerman *et al.*, 1987).

Du Plessis (2003) states that, by employing infrared reflectance spectroscopy, dixanthogen formed after 15 minutes of polarisation at 0.1 V (Ag/AgCl) in a xanathate solution (1×10^{-3} M). In addition the author found that the TTC dimer formed after 15 minutes of polarisation at 0.1 V (Ag/AgCl) in a TTC-containing solution (1×10^{-3} M). This correlates well with the potentiometric measurements done by Du Plessis (2003) which indicate that the TTC oxidises at more negative potentials than 0.1 V (Ag/AgCl). Furthermore, the author found that the TTC formed finite contact angles at lower potentials than the xanthate (Figure 14). The author identified the presence of the TTC by comparing IR external reflectance measurements with those of the TTC monomer and dimer. Furthermore, Du Plessis found that, at a potential of -0.5 V (Ag/AgCl) – which is more negative than the reversible potential of the TTC monomer/dimer couple – only the TTC's corresponding thiol could be detected on the surface. The author found that the

xanthate only formed measurable contact angles at potentials where the dixanthogen formed and concluded that pyrite could only be floated in the presence of the dixanthogen. Care should be taken when considering this interpretation, since the metal xanthate that forms on a mineral during adsorption is hydrophobic and will induce flotation. This stems from the fact that the author could only measure contact angles at potentials where dixanthogen formed. Woods (1996) states that only the oxidation of the dixanthogen is visible from the voltammograms of pyrite. However, similarly to gold, the Tafel slopes indicate that the adsorption and oxidation of the xanthate on the surface of the pyrite occur in the same potential region. This shows that a hydrophobic surface state can only be established in a region where dixanthogen is present, but it does not denote the sole presence of dixanthogen, as proven by Bozkurt *et al*. (1999) and Mielczarski *et al*. (1998). Figure 14 indicates that Du Plessis *et al*. (1999) measured zero contact angles at a potential of -1400 mV (Ag/AgCl), but this is already in the hydrogen evolution potentialrange (Wang *et al.*, 1989). The hydrogen will form nano bubbles that result in a hydrophobic surface, therefore one would expect a finite contact angle in this potential region.

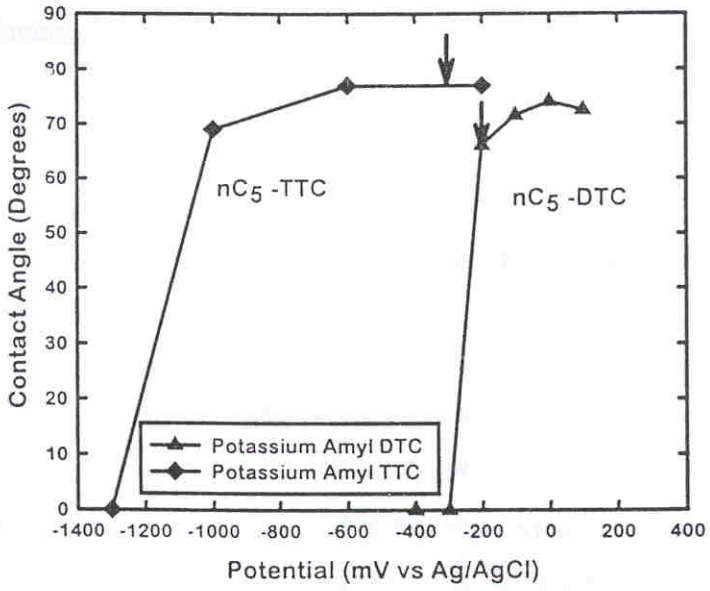

Figure 14: Contact angle measurements for potassium *n*-amyl xanthate and TTC (1×10^{-3} M) as a function of applied potential (pH 4.7) (Du Plessis *et al.*, 1999)

2.6 Raman spectroscopy

More recently, Raman spectroscopy has been used to identify the surface species in flotation. The reason for the interest in this technique is the development of Fourier transform Raman spectroscopy (FT-Raman) that has made it possible to generate infrared vibration spectra. As a result, species such as dixanthogen and xanthate can be identified. By roughing the substrate with an oxidation and reduction cycle it is possible to obtain an enhanced Raman spectrum of up to 10^3 times. With the use of surface-enhanced Raman spectroscopy (SERS) it is possible to analyse sub-monolayers on surfaces.

Woods *et al*. (1998a) used FT-Raman to generate spectra of different xanthate compounds including copper, gold and silver xanthate. With Raman spectroscopy it is relatively easy to distinguish a metal xanthate from dixanthogen, since a strong band occurs in the latter at 498 cm^{-1} due to the S-S stretching. In IR spectroscopy this band is weak or non-existent; a non-polar group is not as active in infrared spectroscopy. In Figure 15 (Woods *et al.*, 1998a) the spectral differences between gold ethyl xanthate and diethyl dixanthogen are unambiguously distinguishable; this eases the identification of either xanthate or dixanthogen or even both species on the surface of a mineral. Another advantage of Raman spectroscopy is that water does not influence the spectra as much as it does in IR spectroscopy due to the absorption of infrared by water. Consequently, this technique lends itself much more towards *in situ* measurements of the interactions between the collectors and the mineral surface. Another advantage is the possibility of focusing the laser beam on the surface of the mineral so as to obtain mainly the spectra of the species present at the interface, not in the bulk solution.

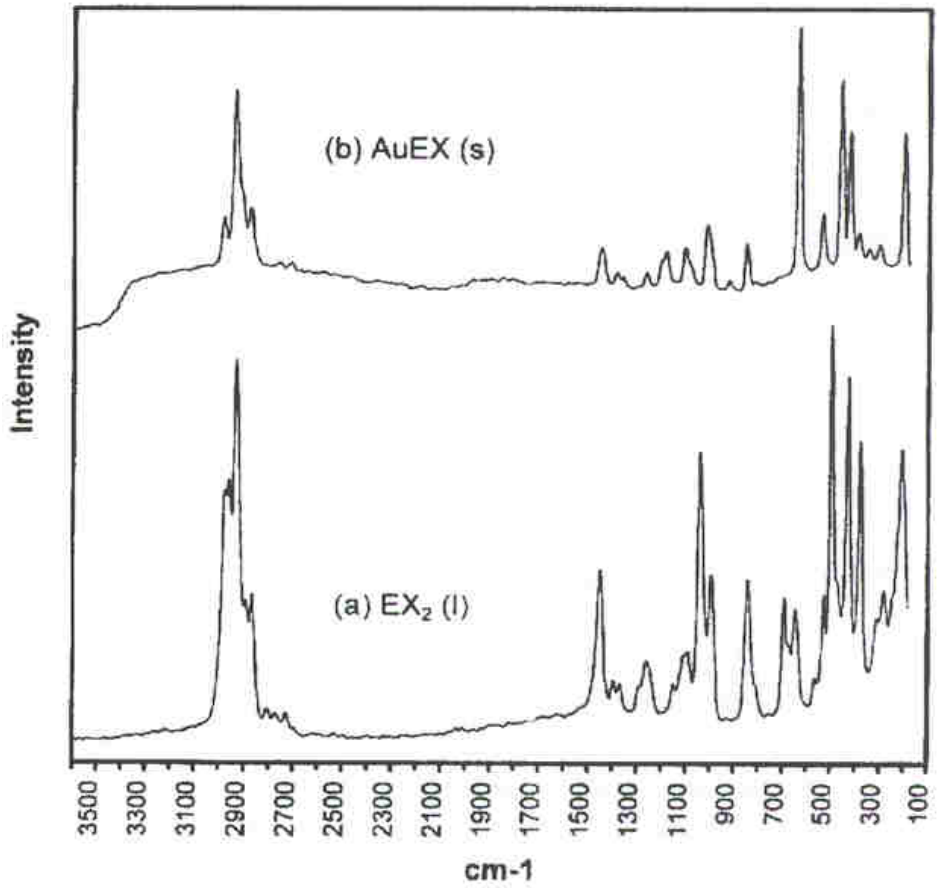

Figure 15: Ft-Raman spectra for (a) liquid diethyl dixanthogen and (b) solid gold ethyl xanthate (Woods *et al*., 1998a)

Woods *et al.* (1998c) analysed the interaction between xanthate and gold by using SERS. The authors found that gold ethyl xanthate was present on the gold surface at a potential of 100 mV (SHE); this potential is more negative than the reversible potentials of gold ethyl xanthate (160 mV (SHE)) and xanthate-dixanthogen (138 mV (SHE)). This result indicates that the underpotential deposition of xanthate on gold occurs. When applying a potential of 500 mV (SHE), xanthate and dixanthogen were both identified on the gold surface. This was confirmed by drying the electrode in dry nitrogen for two hours; the dixanthogen is volatile and evaporates from the surface. After two hours of drying, only gold ethyl xanthate was present (Figure 16) confirming that both species had initially been present.

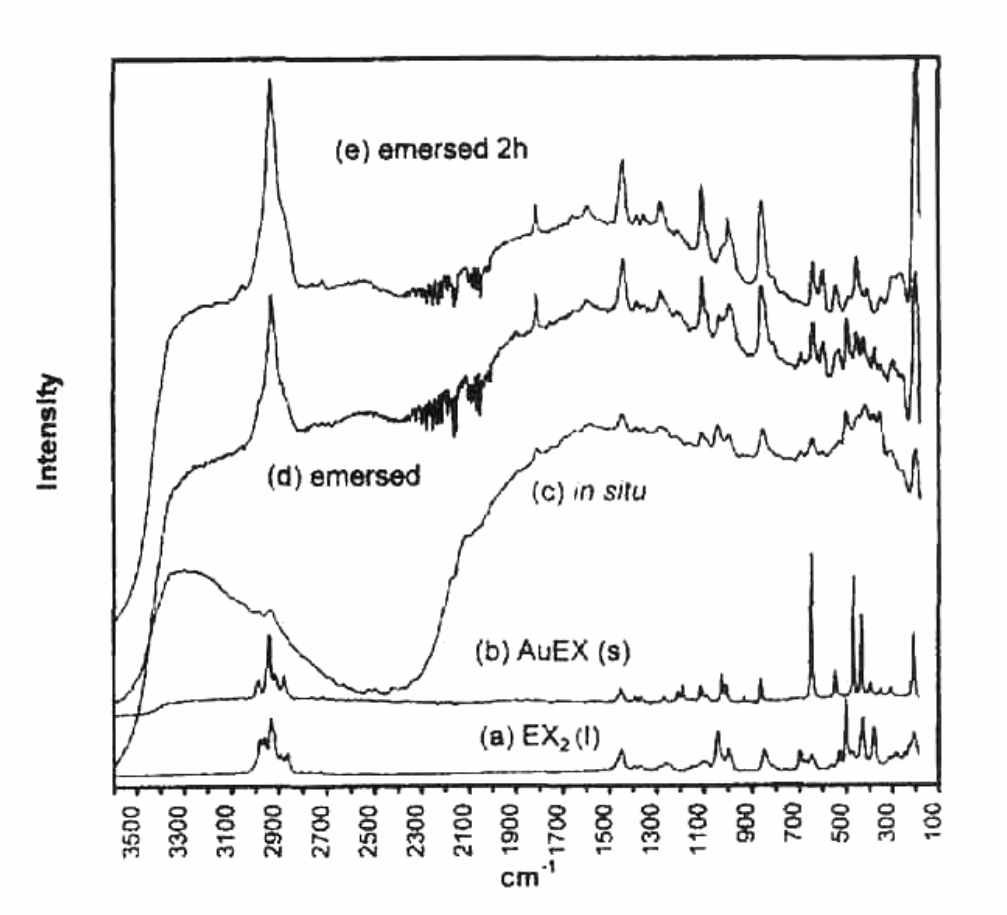

Figure 16: (a) FT-Raman spectrum of liquid diethyl dixanthogen. (b) FT-Raman spectrum of solid gold xanthate. SERS spectra of gold electrode at 0.50 V in 0.5 M sodium tetraborate solution containing 5×10^{-4} M potassium ethyl xanthate: (c) *in situ*; (d) immediately after emersion; (e) two hours after emersion with dry nitrogen flowing over electrode surface (Woods *et al.*, 1998c).

Under these conditions (high overpotential) more dixanthogen than AuEX should have formed, resulting in a more intense dixanthogen peak. It is clear from the spectra, however, that the two species have similar intensities resulting from a more pronounced enhancement of AuEX compared to the diethyl dixanthogen. Woods *et al*. (1998c) state that this might be due to a layer AuEX that forms on the surface and interacts with the surface and is subsequently enhanced. By contrast, the dixanthogen is believed to be bonded to this layer of AuEX through hydrophobic interactions and should be situated a distance away from the surface; as a result the dixanthogen cannot interact with the surface and be enhanced. This supports the findings of

Mielczarski *et al.* (1998) and Bozkurt *et al.* (1999); there is a layer of xanthate present on the surface and dixanthogen is bonded to this layer.

2.7 X-ray photoelectron spectroscopy (XPS)

Further validation of the species on the surface has been obtained through the use of XPS [Kartio *et al*.(1992) and Laajalehto *et al.* (1999)]. There are, however, some limitations involved in employing XPS since dixanthogen, which has a high vapour pressure, evaporates in the ultra-high vacuum. Kartio *et al*. (1992) overcame this limitation by developing a technique to dry and cool the substrate, while keeping the surface species intact. A further advantage of this technique is that it prevents the oxidation of the surface species after removing the mineral from the collector solution.

There have been quite a number of inconsistent interpretations of the results obtained with XPS. Kartio *et al*. (1992) state that they found diaxanthogen was present on the pyrite surface at 130 K after following the evacuation technique described in the text. Upon heating the sample to 300 K, no dixanthogen could be detected on the surface but the authors were able to detect a small amount of ethyl xanthate – this finding was corroborated by Laajalehto *et al.* (1999). These findings are in accordance with the previously discussed findings of Mielzcarski *et al.* (1998), Bozkurt *et al.* (1999) and Woods *et al.* (1998c) – both species (xanthate and dixanthogen) are present on the substrate's surface when dixanthogen is formed. In addition, Kartio *et al.* (1992) and Laajalehto *et al.* (1999) detected only a small amount of xanthate on the pyrite surface, which can be correlated to a monolayer or sub-monolayer coverage.

2.8 Ultraviolet (UV) absorption

UV absorption is another useful technique to determine the presence of xanthate and dixanthogen. It is possible to determine the amount of the different types of collector species quantitatively with this technique – it is a very useful technique in studying the kinetics of the adsorption and decomposition of the collectors.

Xanthate and its related compounds have different wavelength UV absorptions, as indicated in Table 3 (Leja, 1982). Du Plessis *et al*. (1999) determined the UV absorption of *n*-amyl TTC and compared it with the UV absorption of *n*-amyl xanthate (Figure 17). Du Plessis (2003) identifies the peaks at approximately 305 nm and 333 nm due to presence of the TTC and the peak at 232 nm due to the presence of the TTC's corresponding thiol.

Table 3: UV absorption of xanthate and related compounds (Leja, 1982)

Compound	**Wavelength (nm)**
CS_2	206.5
Monothiocarbonate	223
Xanthate ion	226 301
Dixanthogen	238 283
Xanthic acid	270

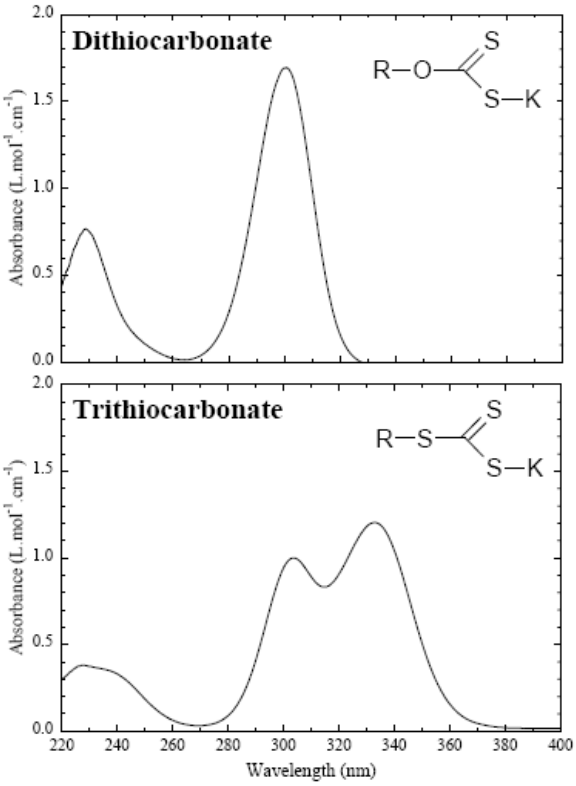

Figure 17: UV spectra of *n*-amyl xanthate and *n*-amyl TTC (Du Plessis, 2003)

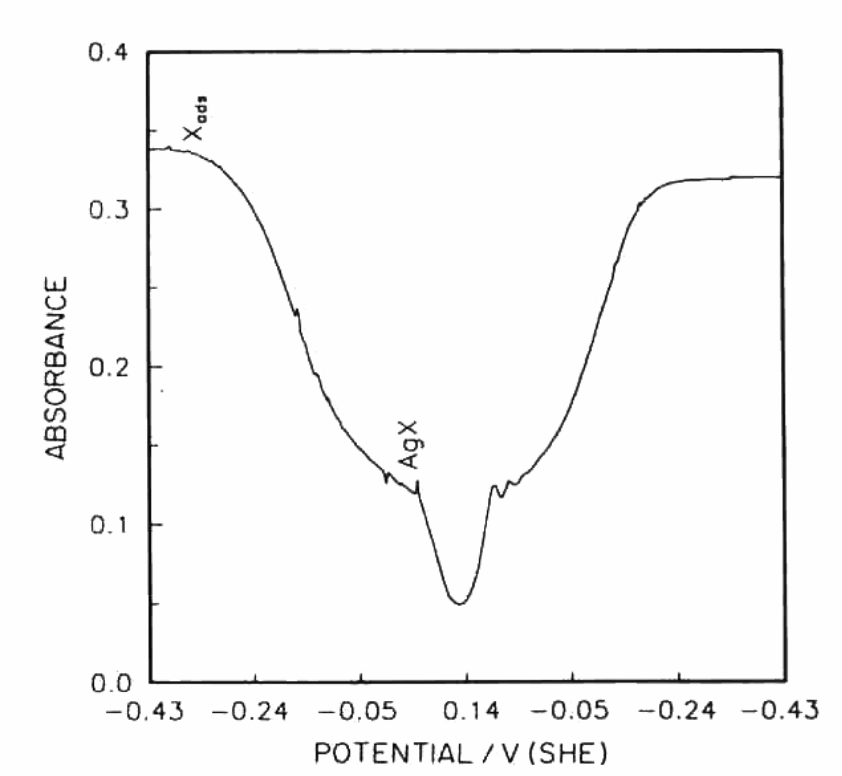

Figure 18 : Absorbance at 301 nm of ethyl xanthate (2×10^{-3} M) solution (pH 9.2) circulating through a silver wool electrode that was held at – 0.43 V (SHE) for two minutes and then a triangular potential cycle of 1 mV/sec between – 0.43 V (SHE) and 0.14 V (SHE) was applied (Woods, 1996).

Woods (1996) was able to show that xanthate adsorbs at potentials lower than those for the formation of metal xanthate through the use of *in situ* UV measurements and potential control of a silver wool electrode. In Figure 18 it is evident that xanthate adsorbs onto the silver; upon reaching the potential where AgX forms, the tempo of adsorption increases. It is clear from Figure 18 that the adsorbed xanthate desorbs again when the potential is lowered. These results confirm the theory that xanthate adsorbs via an underpotential deposition mechanism.

Extensive studies have been performed to determine the products and rate of decomposition of xanthate and dixanthogen. UV has played a central role in determining the kinetics of the decomposition. Figure 19 gives an indication of the pH dependency of the xanthate and dixanthogen compounds. Xanthate and dixanthogen are reasonably stable in a pH region of 6-9. When the solution pH moves

higher or lower than these boundary values, the tempo of decomposition of either xanthate or dixanthogen increases.

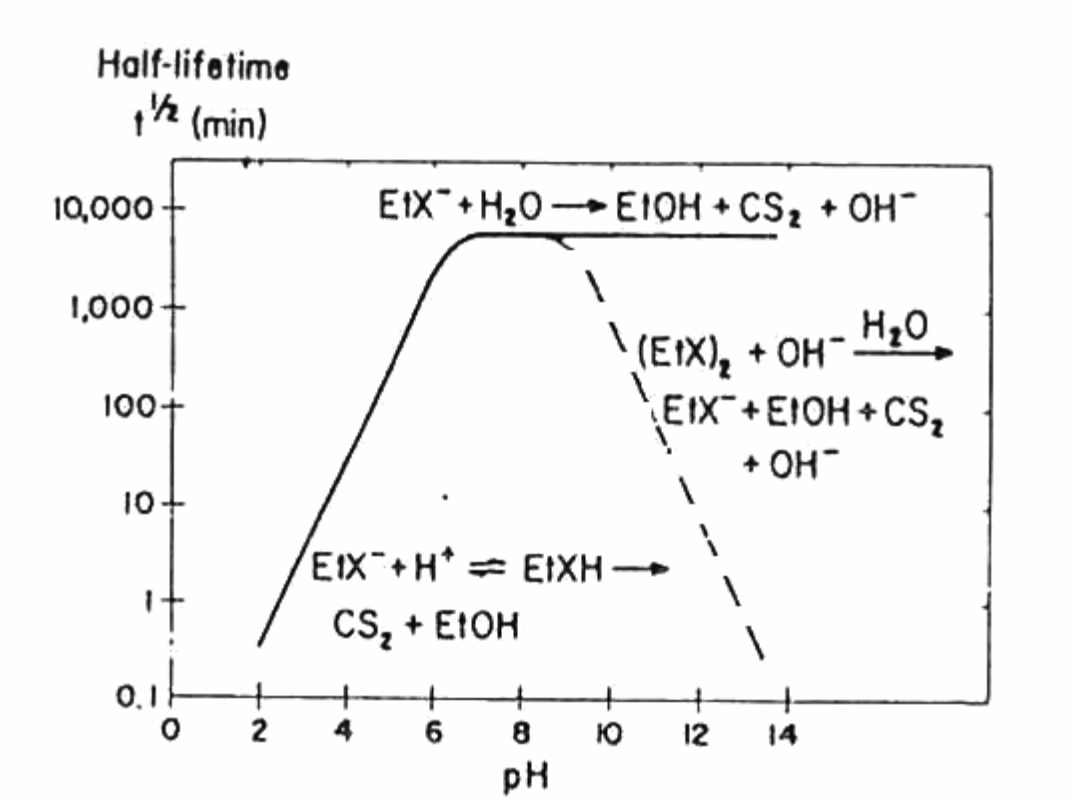

Figure 19: Half-life times of ethyl xanthate and diethyl dixanthogen (Leja, 1982).

2.9 Conclusions

From the studies performed in the past, it would appear that the xanthate initially chemisorbs (reaction (1)) in all cases. This may be followed by the oxidation of the xanthate to the dixanthogen if the mixed potential on the surface is sufficiently positive. The adsorbed xanthate is bonded via an ionic bond to the surface whereas in the case of the dixanthogen, it is apparently bonded due to Van der Waals forces via the adsorbed xanthate. The surface serves as a catalyst for the oxidation reaction.

In the case of TTC, only a limited amount of research has been performed. The current perception is that the TTC follows a similar mechanism for adsorption, but it occurs at more negative potentials than in the case of the xanthate. The initial investigations seem to confirm the presence of the TTC at more negative potentials and possibly even the presence of the TTC dimer. The TTC appears to be much more

reactive and this was also observed by the decomposition when determining the reversible potential for the monomer/dimer couple. The measured onset of hydrophobicity is from significantly more negative potentials than the reversible potential of the TTC monomer/dimer couple (Figure 14). Therefore if the same collector mechanism is involved for the TTC (compared to that of the xanthate), then chemisorption should occur at significantly more negative potentials. This work is aimed at investigating the electrochemical behaviour of the TTC with the substrate and at verifying whether the TTC does indeed chemisorb at significantly more negative potentials. Secondly, this study is aimed at verifying whether the dimer of the TTC is the collector species on the substrate surface after the onset of hydrophobicity – no conclusive identification has as yet been performed.

3. Experimental procedure

3.1 Collectors

Synthesis grade potassium ethyl xanthate (KEX), 95% pure, from Merck-Schuchardt was purified by recrystallisation from acetone by the addition of diethyl ether (RAO, 1971). Analytical grade acetone and diethyl ether were used. The purified xanthate was stored under vacuum in a desiccator.

Potassium dodecanetrithiocarbonate (KC_{12}-TTC) was synthesised by adding disulfide to the solution of potassium hydroxide in dodecanethiol (Drake & Yang, 1994). All the reagents were analytical grade. The KC_{12}-TTC was stored under vacuum in a desiccator.

Potassium dodecanethiolate (C_{12}-SK) (see Figure 1) was synthesised by adding excess dodecanthiol to potassium hydroxide. The dodecanthiolate was washed with cold diethyl ether to remove the remaining dodecanethiol. All the reagents were analytical grade. The potassium dodecanethiolate was stored under vacuum in a desiccator.

3.2 Electrodes

Pyrite and copper were the substrates of choice for this study. Pyrite was chosen since it is a mineral which is commonly recovered by flotation in industry. Copper was chosen for its electrochemical interaction with xanthate; pre-wave at potentials significantly lower than the reduction potential of the xanthate /dixanthogen couple.

A natural crystal of pyrite from Ward's Natural Science Establishment, which originated from Zacatecas, Mexico, was used as an electrode. The pyrite was embedded in a resin and a geometric surface of approximately 0.46 cm^2 was exposed.

The copper electrode was similarly prepared by embedding a copper disk in a resin with a geometric exposed surface of approximately 0.55 cm^2.

3.3 Electrochemical measurements

A conventional three-electrode system was used. Potentials were measured against an Ag/AgCl reference electrode filled with saturated KCl, which has a potential of + 0.20 V against a standard hydrogen electrode (SHE). Experiments were conducted at 25° C (± 1° C) and in a 0.05 M sodium borate ($Na_2B_4O_7$) buffer solution (pH of 9.3). Two platinum electrodes fitted in glass tubes, with fritted glass ends, were utilised as counter-electrodes. These counter-electrodes were placed at equal distances from the working electrode. A Schlumberger 1287 potentiostat was used to construct the cyclic voltammograms.

The following steps were taken for each experimental run:

i) The pyrite surface was wet-ground using 2400 grit silicon carbide paper.
ii) The surface was then polished with a suspension of 0.05 μm Micropolish Alumina-B.
iii) Scans were performed in fresh de-aerated solutions [de-aerated for 2 hours with argon gas (99.999%) that had passed over zirconia turnings at 600° C].
iv) Cyclic voltammograms were recorded after the open-circuit potential had stabilised
v) Cyclic voltammograms were recorded by changing the potential linearly with time from the most negative potential to the upper potential and back at a rate of 1 mV/s.

3.4 Contact angle measurements

The captive bubble technique was utilised for the purpose of determining the contact angles. A modified three-electrode cell, with two parallel plate windows, was used. The electrochemical cell was washed with chromic acid between every experimental run to avoid contamination by the different collectors. De-ionised water with a resistivity of 18 MΩ.cm, that had been treated with UV to remove organics, was used for all solutions. For two hours, 0.05-M borate buffered solutions (pH 9.2) were de-aerated. Either KEX or KC_{12}-TTC (10^{-3} M collector concentration) was added immediately before the commencement of the polarisation. The electrochemical cell

was placed on the optical bench of the Ramé-Hart contact angle goniometer (Model: 100-00-230). As was the case with the electrochemical experiments, the surface of the electrodes was freshly prepared between the experimental runs. Repeatable contact angles were obtained by ensuring a completely flat electrode surface. The electrode was polarised potentiostatically, with a Schlumberger 1287 potentiostat, for 300 s before employing a nitrogen bubble during the contact angle measurements. At least three bubbles were employed and measured for each potential. No attachment was equated to a zero contact angle.

3.5 Raman spectroscopy

The Raman spectroscopy was done at the chemistry department of the University of Pretoria on a Z-24 DILOR spectrometer. A 514.5 nm Coherent Innova 90 Ar^{+}-laser was used for excitation. The power of the laser was varied from 10 mW to 100 mW. The approximate power at the electrode surface was a tenth of the original input power. The spectra were recorded in a back-scattering configuration with a long working distance 50× objective of an Olympus microscope attached to the instrument. A digital camera was also connected to the microscope. The instrument is equipped with a nitrogen-cooled CCD detector and the spectral resolution was at least 2 cm^{-1} for all the measurements.

The aim of the Raman spectroscopy was to identify which species of the collectors were present on the mineral surface at certain applied potentials (these potentials were predetermined from the electrochemical experiments). A specially designed *in situ* electrochemical cell was employed during the Raman spectroscopy. The cell was constructed from Perspex, except for a window of quartz glass. As Quartz glass does not adsorb light between 200 cm^{-1} and 3100 cm^{-1} it did not interfere with the measurements. The Raman cell consisted of two platinum electrodes, a glass luggin tube and the working electrode. An Ag/AgCl reference electrode filled with saturated KCl, which has a potential of + 0.20 V against a standard hydrogen electrode (SHE) was employed. The same pyrite and copper electrodes previously employed in the electrochemical measurements were used for the Raman investigations. A fresh electrode surface was prepared between the experimental runs by silicon carbide grinding followed by wet polishing, using 0.05 µm Alumina-B slurries. Before an

experimental run commenced, the system was flushed with Argon to prevent oxygen pick-up. The 0.05 M borate solutions (pH 9.2) were de-aerated for two hours before use. The cell was connected to a 500 ml conical flask immersed in a water bath to ensure a constant solution temperature of 25° C (± 1° C). The collectors were added immediately before the commencement of measurements (10^{-3} M collector concentration). A peristaltic pump was employed to circulate the solution between the flask and the electrochemical cell. The electrode potential was controlled with a Schlumberger 1287 potentiostat.

The spectra of the collector species were recorded in the macro cell of the Z-24 DILOR spectrometer. The spectra of the monomers of the collectors (in solution and in crystal form) as well as those of their dimers, were recorded. The dimers were synthesised by oxidising the monomers with ammonium persulfate (analytical grade). The spectra of possible decomposition products – dodecanethiol, potassium dodecanethiolate and CS_2 – were also recorded. These spectra were used as reference in comparison with the spectra recorded *in situ* to establish which species were present on the polarised surface.

3.6 Electrochemical impedance spectroscopy (EIS)

The same conventional three-electrode system previously used for the electrochemical measurements was also employed for the EIS measurements. Potentials were measured against an Ag/AgCl reference electrode filled with saturated KCl, which has a potential of + 0.20 V against a standard hydrogen electrode (SHE). Experiments were conducted at 25° C (± 1° C) and in a 0.05 M sodium borate ($Na_2B_4O_7$) buffer solution (pH of 9.2). Two platinum electrodes were utilised as counter electrodes. A Schlumberger 1287 potentiostat was used in conjunction with a Schlumberger 1260 frequency response analyser. The experimental solutions were de-aerated in the same way as stated in the previous section covering the electrochemical experimental procedure.. The same pyrite and copper electrodes used in the electrochemical measurements were employed for the EIS investigations. A fresh electrode surface was prepared between the experimental runs by silicon carbide grinding followed by wet polishing, employing 0.05 µm Alumina-B slurries.

3.7 Decomposition of TTC in solution

The decomposition tests were performed by measuring the concentration of the species in solution, employing a Perkin-Elmer Lamda 25 UV/Vis spectrometer. The absorbance of the TTC was measured at 333 nm (peak determined from UV/Vis scan between 200 nm and 400 m). The tests were conducted as a single batch of which the pH ranged between 4 and 11 and the temperature was kept constant at 18˚ C. The solution pH was adjusted by using 0.1 M KCl and 0.1 M NaOH solutions. After obtaining the required solution pH, the solution was de-aerated for two hours. The TTC was subsequently added, whereafter the collector concentrations were measured at 30 minute intervals. The solution pH was again measured at the end of the specific tests. The solutions were then allowed to decompose further for two days and the solution pH was monitored during this time. The same procedure was used for measuring the decomposition of the TTC in 0.05 M borate buffered solution (pH 9.2).

3.8 Microflotation of pyrite

Microflotation (Bradshaw & O'Connor, 1996) tests were performed on pyrite only (copper is too reactive and would therefore also introduce the effects of copper oxidation) to verify the findings of the spectroscopic and decomposition tests. Massive natural crystals of pyrite from Ward's Natural Science Establishment, which originated from Zacatecas, Mexico, were used for the test work – it was the same batch of pyrite used in the preceding experimental procedures. The massive pyrite was ground fine with a mortar and pestle and screened; only the 53 – 106 µm fraction was used for the microflotation investigations. All flotation tests were performed with dry air. Tests were performed in 0.05 M borate solution so that they would be comparable with the preceding investigations. Fresh 5×10^{-5} M KC_{12}-TTC, 5×10^{-5} M C_{12}-SK and 5×10^{-5} M KEX solutions were used during the microflotation tests. It was important to ensure that the flotation in the TTC solutions occurred as quickly as possible after preparation, due to the instability of the TTC. For this purpose, 100 ml 2.75×10^{-4} M KC_{12}-TTC solutions were prepared individually for each test. In each test 50 ml was used and the other half was allowed to decompose for four hours before it was used again.

A 275 ml microflotation cell was employed, consisting of a cylindrical glass tube with a conical section at the top to divert the bubbles into a catchment bowl. No frothers were used during the test work. The air was introduced by a needle at the bottom. The flow rate was kept constant at 6.5 $cm^3.min^{-1}$ during all tests. The pulp was kept in suspension by means of a peristaltic pump. The pulp was initially conditioned in the collector solution for three minutes before four sequential floats were performed at 3, 3, 4 and 10 minutes respectively.

4. Results and discussion

4.1 Electrochemical and contact measurements

4.1.1 Pyrite

Figure 20(a) shows the cyclic voltammograms that were recorded by changing the potential linearly with time between -400 mV (SHE) and 250 mV (SHE) at a scan rate of 1 mV/s. At the lower potentials, a cathodic current is visible in all three cases. This cathodic current is probably due to the presence of iron oxide and is therefore caused by the change in valence state of the iron (Gardner & Woods, 1977). The presence of the hydrophilic iron oxides is probably responsible for the small difference between the potential where dixanthogen can form and the potential where a finite contact angle is measured (see Figure 20(b)).

The cyclic voltammogram of the pyrite in the 0.05 M borate solution (without collectors) has a small cathodic current of up to approximately 150 mV (SHE), probably due to the presence of iron oxides. No significant oxidation was detected in the region of -400 mV (SHE) to 250 mV (SHE), resulting in the absence of a cathodic peak on the return cathodic scan. This correlates well with previous work (Woods, 1976).

In the presence of 10^{-3} M KEX a strong anodic peak was visible from potentials higher than the reversible potential of the xanthate/dixanthogen couple (121 mV (SHE)) (Vermaak *et al.*, 2005). On the return cathodic sweep, a cathodic peak was visible from approximately 120mV; this cathodic peak is due to the reduction of the dixanthogen that was formed during the anodic scan (Gardner & Woods, 1977). Bubble contact was only possible when the pyrite electrode was polarised at potentials more positive than the reversible potential of the xanthate/dixanthogen couple. These results are in good agreement with previous work (Gardner & Woods, 1977).

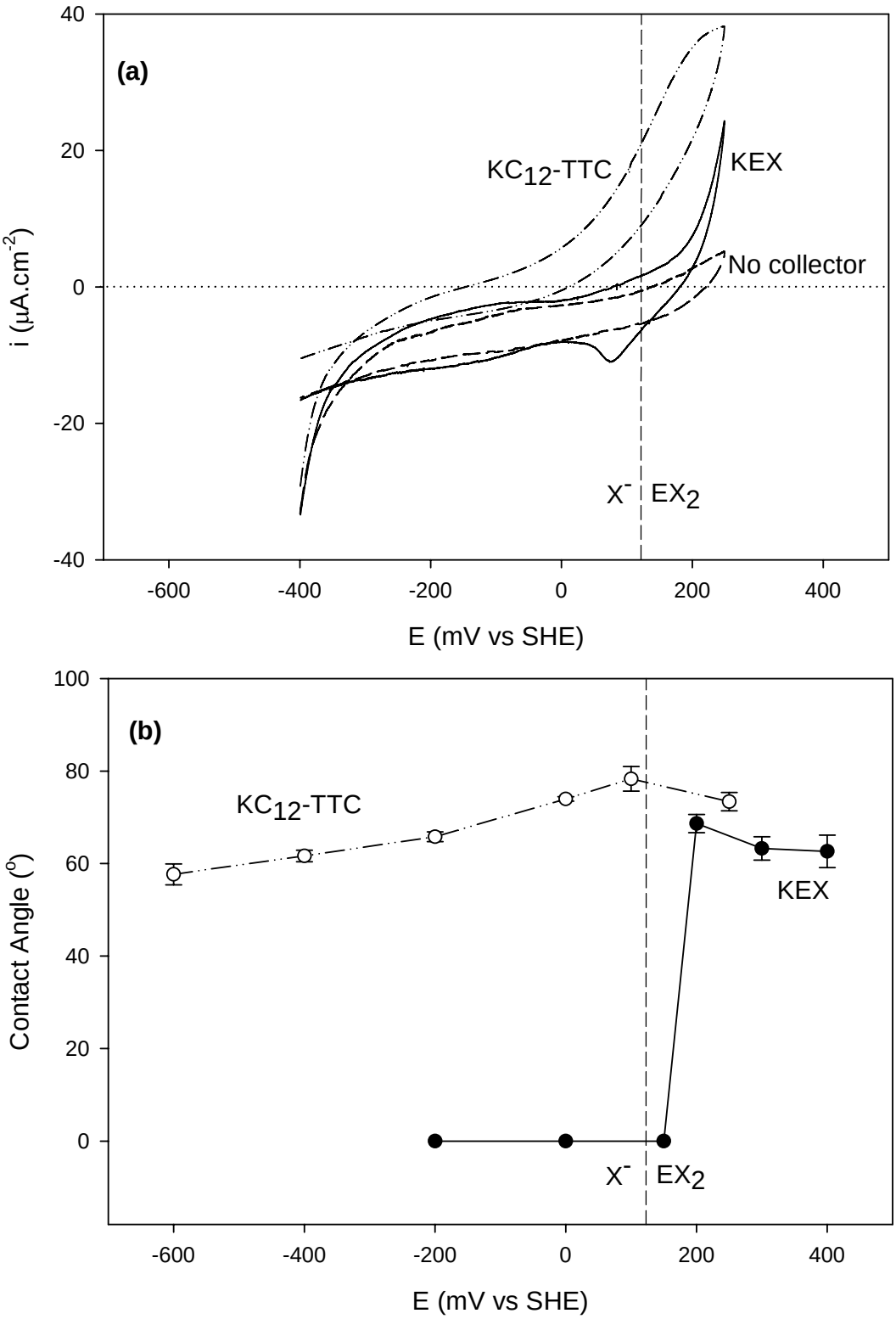

Figure 20: (a) Cyclic voltammograms scanned at 1 mV/s of pyrite in 0.05 M borate solutions with no collector, 10^{-3} M KEX and 10^{-3} M KC_{12}-TTC ; (b) contact angles for pyrite electrode polarised for 300 s in 0.05 M borate solutions with 10^{-3} M KEX and 10^{-3} M KC_{12}-TTC.

The results of the KC_{12}-TTC are significantly different from those of the xanthate. It was possible to measure finite contact angles even when only cathodic currents were detected. However, there was an increase of approximately 10° in the contact angle at a potential greater than -200 mV (SHE). The cyclic voltammogram (see Figure 20(a)) indicates that a significant anodic current is present from above -150 mV (SHE), but there is no cathodic peak present on the return cathodic scan. This indicates that the reaction responsible for the anodic current is not reversible. Cyclic voltammograms of TTC on a gold substrate reported by Groot *et al.* (2005) also indicated the absence of a reduction peak.

Some kind of product layer (electrode surface became dull) was visually detected at very low potentials (< -200mV). This correlates with the findings reported by Groot *et al.* (2005), which are briefly summarised as follows. Surface plasmon resonance (SPR) allows for the determination of the presence of material on the surface of the gold substrate. In the case of the xanthate collector there is only a change in the SPR angle (amount of collector on the surface) at potentials higher than the reversible potential of the xanthate/dixanthogen couple. No collector is detected below this potential; this corresponds to insignificant changes in the SPR angle. In the case of the TTC there is a significant change in the SPR angle from potentials at the onset of the anodic currents, but importantly at more negative potentials a small SPR angle was also measured; some material was present on the surface at low potentials before the onset of electrochemical reactions. In addition, Groot *et al.* (2005) also mention an increase in the amount of material present (larger SPR angles) on the gold surface at potentials where anodic currents are detected. This correlates well with the findings in this study (see Figure 20), showing an increase in the contact angle at potentials where anodic currents are measured.

The maximum contact angles measured (approximately 70°) in the xanthate solution were as expected (Gardner & Woods, 1977); but in the case of the KC_{12}-TTC, greater angles would be expected than those measured (approximately 75°) due to its longer chain length. The contact angles were smaller than expected because of the stabilisation of the bubble by the KC_{12}-TTC, as illustrated (see Figure 21) by bubble behaviour in contact with the pyrite surface. In Figure 21(a) the contact angle

obtained only by collision of the bubble with the surface is approximately 70°. Figure 21(b) shows the same bubble after the electrode was carefully vibrated; the contact angle changed to approximately 90°. This is closer to the expected values for long chain collectors (Gardner & Woods, 1977). In the case of the xanthate collector, there was no significant change in the contact angle when the pyrite electrode was carefully vibrated. Visual observations during the experimental runs indicated longer induction times for the bubbles in the KC_{12}-TTC solutions than for the bubbles in the xanthate solutions. Breytenbach *et al.* (2003) also allude to the stabilising effect of TTC, reporting the formation of more stable froths during batch flotation experiments, resulting in higher mass pulls. A further indication of the influence of KC_{12}-TTC on bubble stability was evident when the concentration of the collector was decreased during contact angle measurements. It was possible to achieve contact angles of approximately 100° (collision only) in 10^{-5}M KC_{12}-TTC solutions compared to the approximately 70° achieved in the 10^{-3}M KC_{12}-TTC solution; with the lower bulk concentration of the TTC one would expect that the interfacial concentration of the TTC on the bubble should be lower and so reduce the stabilisation effect of the TTC.

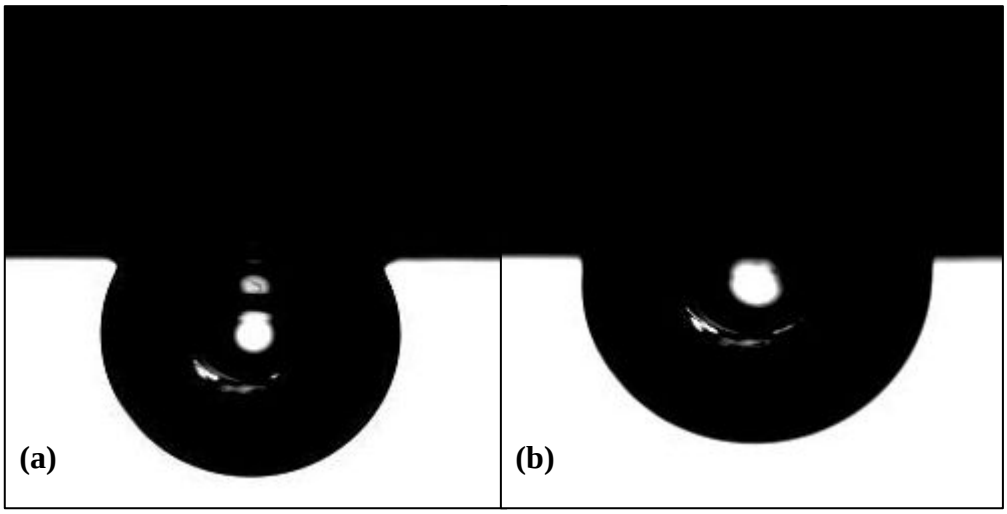

Figure 21: (a) Bubble due to collision with the surface of a pyrite electrode in a 0.05 M borate and 10^{-3}M C_{12}-TTC solution polarised for 300 s; (b) same bubble after electrode was carefully vibrated.

The electrochemical and contact angle measurements show that KC_{12}-TTC renders the pyrite surface hydrophobic at significantly more negative potentials than the xanthate collector. The contact angle measurements also indicated that the KC_{12}-TTC

significantly stabilises the bubbles. The latter effect is counterproductive, however, since one of the ideal characteristics of a collector is that it should have weak frothing characteristics (Wills, 1997).

It was apparent from successive scans in the same xanthate solution, each time with a freshly prepared pyrite surface, that there was no significant change in the electrochemical behaviour of the pyrite (Figure 22(I)). In the case of the KC_{12}-TTC, Figure 22(II), there was clearly a decrease in the detected anodic current in the successive scans. This was due to the decomposition of the KC_{12}-TTC, resulting in a significant decrease in the concentration of the KC_{12}-TTC. It was also clear that the decomposition product or products were not as electrochemically active, since no clear oxidation or reduction reactions could be observed, except for the decreasing anodic interaction of the TTC.

TTC probably decomposes to its corresponding thiolate or thiol and carbon disulfide (CS_2) according to the following equations:

$$RSCS_2^-(aq) = RS^-(aq) + CS_2\ (aq) \quad (10)$$

$$RS^-(aq) + H^+\ (aq) = RSH\ (aq) \quad (11)$$

where R is a hydrocarbon chain.

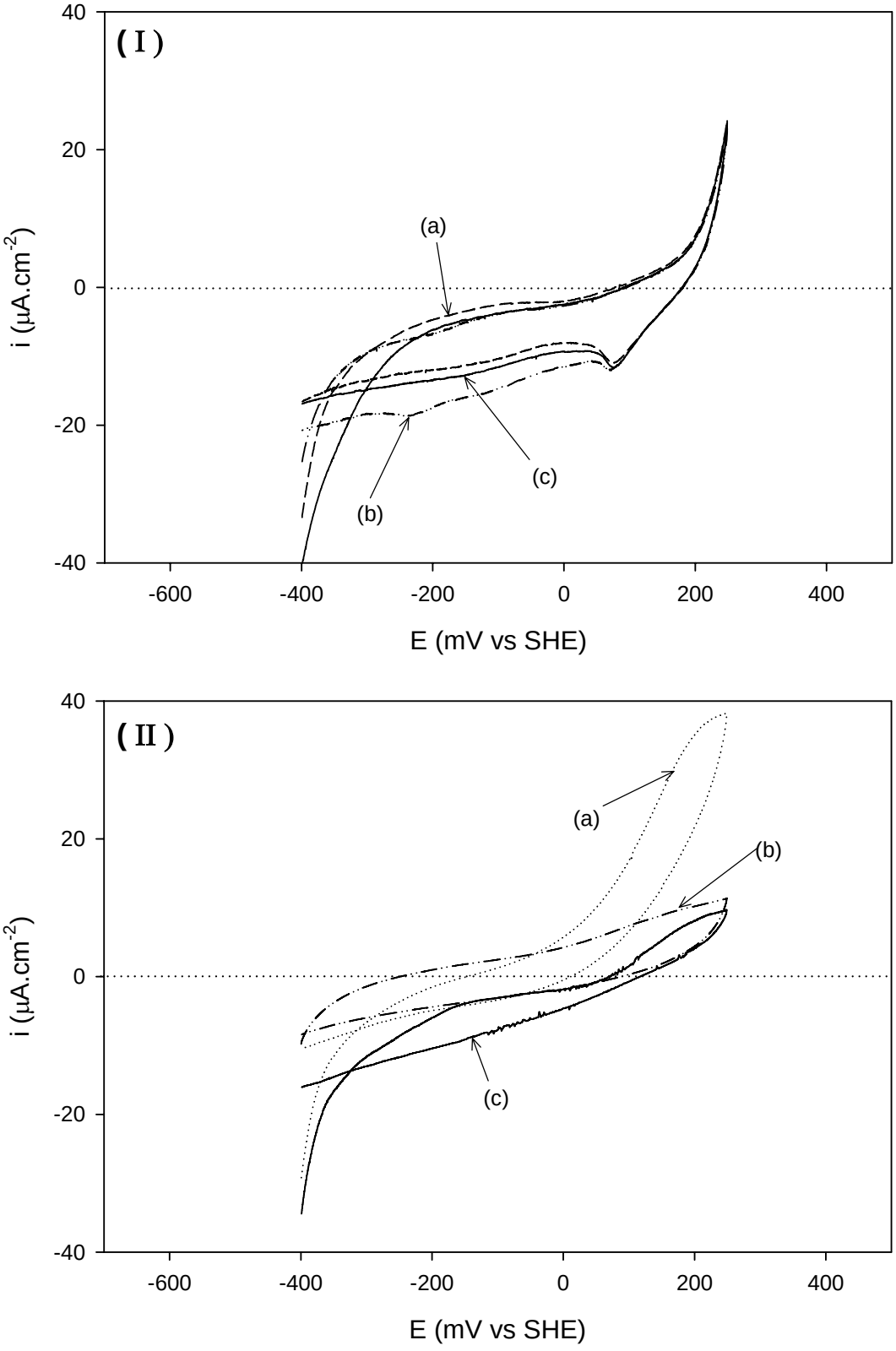

Figure 22: Cyclic voltammograms of pyrite scanned at 1 mV/s in 0.05 M borate solutions with (I) 10^{-3} M KEX and (II) 10^{-3} M KC_{12}-TTC; (a), (b) and (c) are successive scans in the same solution, each with a freshly prepared pyrite surface.

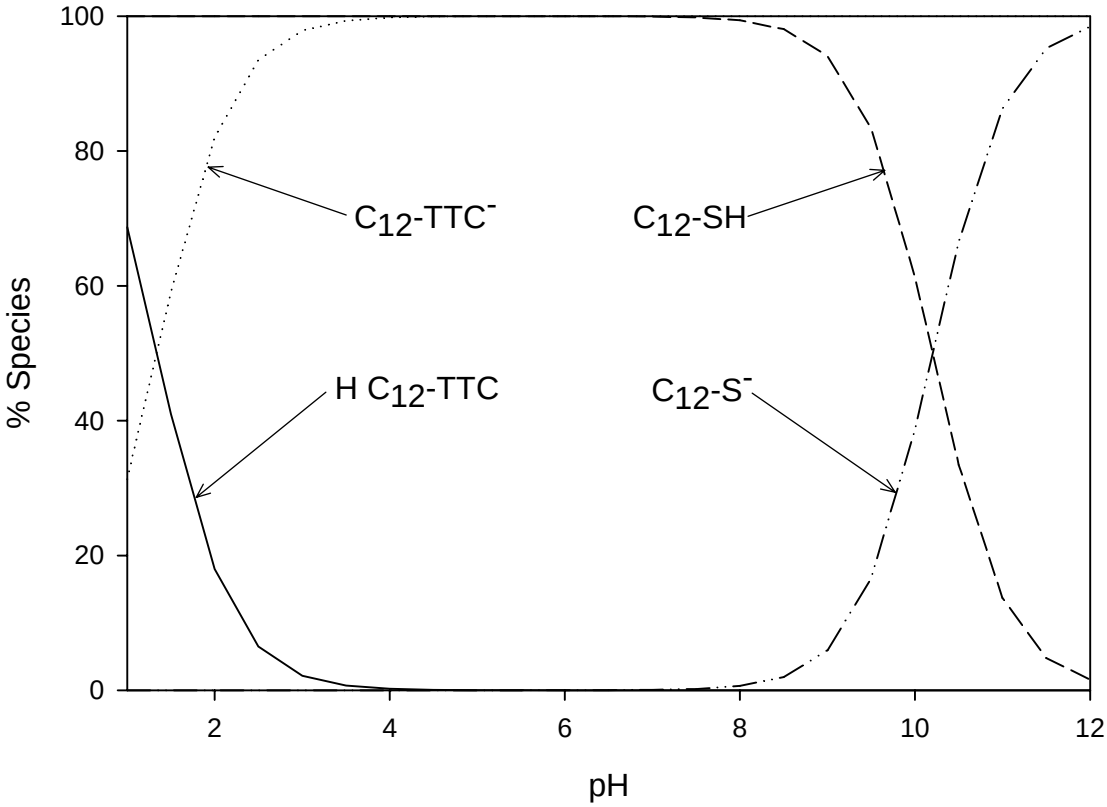

Figure 23: Microspecies distribution of KC_{12}-TTC and C_{12}-SK by pH at 25º C.

Thiol and thiolate are far less soluble than the corresponding TTC. The C_{12}-SH (solubility of 1.1×10^{-6} M) is present in a large excess at a pH of 9.2 as can be seen in Figure 23 (values calculated by utilising the ChemAxon Marvin software at the United States National Library of Medicine website at <http://chem.sis.nlm.nih.gov/chemidplus/>). This means that at equilibrium the concentration of the C_{12}-S^- will be approximately 1×10^{-7} M (calculated by using C_{12}-SH solubility and the microspecies data in Figure 23). It was necessary to heat the borate solution to dissolve the C_{12}-SK. Figure 24 shows a comparison of the electrochemical behaviour of the C_{12}-SK and KC_{12}-TTC (pyrite is used as a working electrode). It is evident from these cyclic voltammograms that there is no strong electrochemical interaction between the thiolate and pyrite. The behaviour is similar to the behaviour of the pyrite in the decomposed KC_{12}-TTC solution (Figure 22 c). The electrochemical behaviour of the thiolate is vastly different from the strong anodic current evident for the TTC.

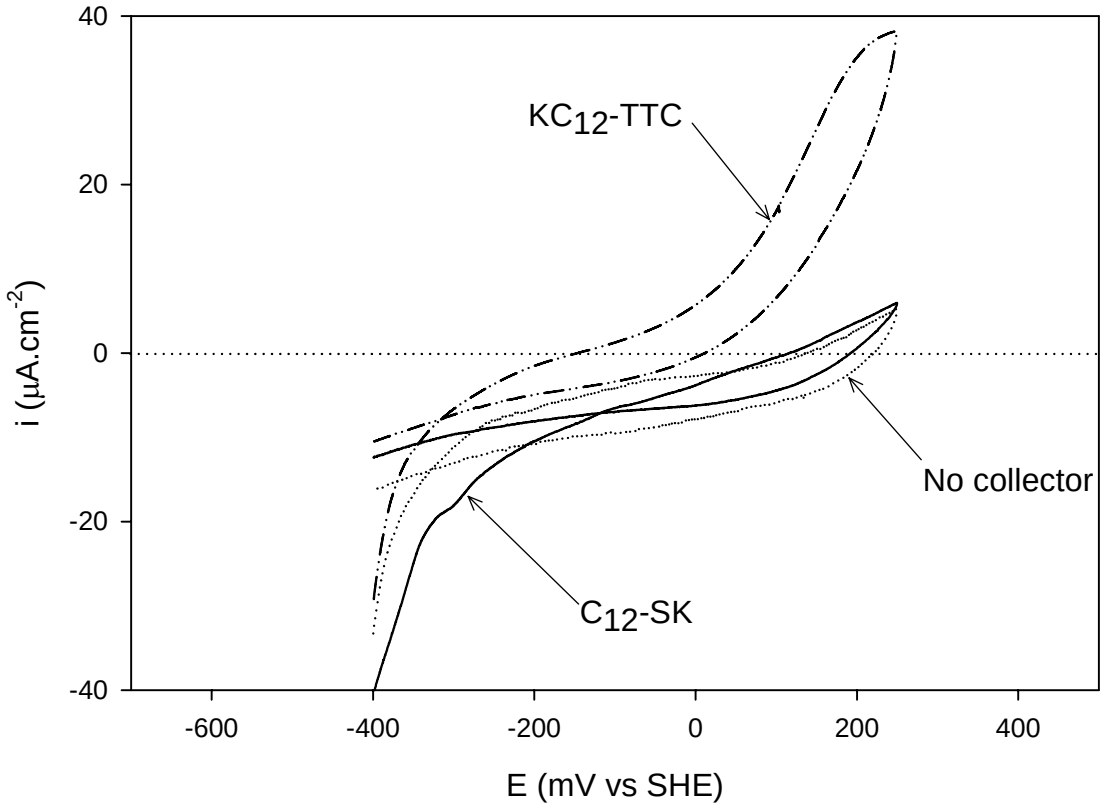

Figure 24: Cyclic voltammograms of pyrite scanned at 1 mV/s in 0.05 M borate solutions with no collector, 10^{-3} M C_{12}-TTC and 10^{-3} M C_{12}-SK.

4.1.2 Copper

It was necessary to polarise the electrode for 300 s at -800 mV (SHE) before commencing either the recording of the cyclic voltammograms or measuring the contact angles. This was to remove the copper oxides that formed during the transfer of the copper electrode from the final polishing step to the experimental solution.

Figure 25(a) shows the cyclic voltammograms recorded by changing the potential linearly with time between -800 mV (SHE) and 250 mV (SHE) at a scan rate of 1 mV/s. The cyclic voltammogram of the copper in the 0.05 M borate solution (without collectors) has two intense anodic peaks at approximately 150 mV (SHE) and 250 mV (SHE). These two peaks are caused by the formation of Cu^{2+} species (Ambrose *et al.,* 1973). The peak at approximately 150 mV (SHE) is caused by the formation of $Cu(OH)_2$ and the peak at 250 mV (SHE) is caused by the formation of CuO. The formation of CuO predominates at low sweep rates, as can be observed in this case where a sweep rate of 1 mV/s was employed (Ambrose *et al.,* 1973). The cathodic peak at -200 mV (SHE) is due to the reduction of the Cu^{2+} species.

The cyclic voltammograms of copper in the presence of 10^{-3} M KEX have an anodic peak at approximately -380 mV (SHE); this is significantly lower than the reversible potential of the xanthate/dixanthogen couple (121 mV (SHE)). It is evident from the contact angle measurements (Figure 25(b)) that the copper is hydrophobic from approximately this potential (-380 mV (SHE)). This indicates that the anodic peak is due to the interaction between the copper and the xanthate. This contrasts with the results for pyrite; pyrite only becomes hydrophobic above the reversible potential of the xanthate/dixanthogen couple. This anodic peak is ascribed to the chemisorption of the xanthate onto the copper surface (Bozkurt *et al.*, 1999). There is an anodic peak at a potential of approximately -270 mV (SHE), resulting in the formation of bulk copper xanthate or cupric xanthate. The strong increase in the anodic current from approximately 200 mV is due to the oxidation of cupric to cuprous in conjunction with the formation of dixanthogen (Bozkurt *et al.*, 1999).

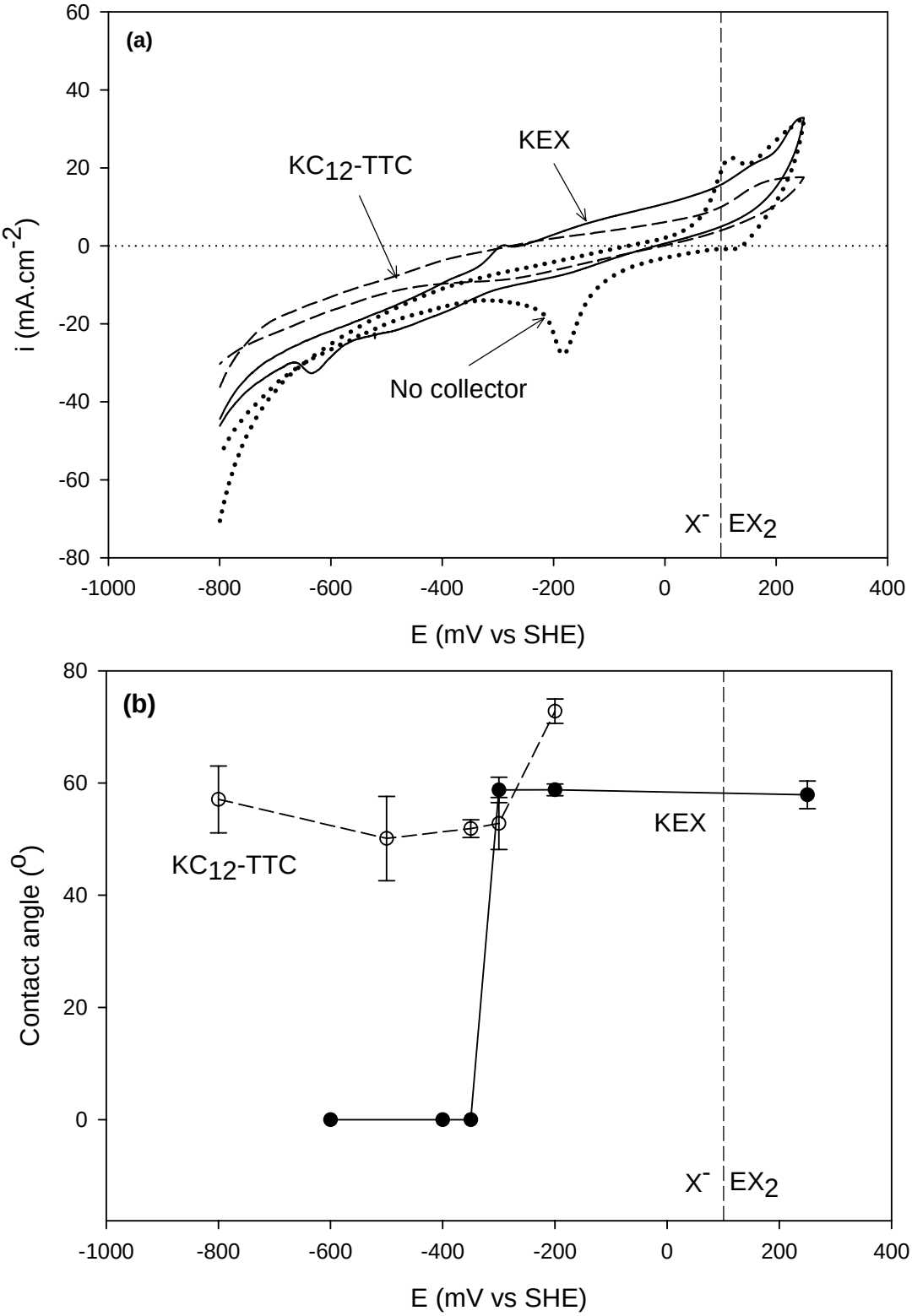

Figure 25: (a) Cyclic voltammograms scanned at 1 mV/s of copper in 0.05 M borate solutions with no collector, 10^{-3} M KEX and 10^{-3} M KC_{12}-TTC; (b) contact angles for copper electrode polarised for 300 s in 0.05 M borate solutions with 10^{-3} M KEX and 10^{-3} M KC_{12}-TTC.

An anodic current was visible from approximately -300 mV (SHE) in the presence of 10^{-3} M KC_{12}-TTC. It was possible to measure finite contact angles even when a cathodic current was observed; this was similar to the behaviour of pyrite in the presence of KC_{12}-TTC. The increase in the contact angle in the case of the copper electrode coincided with the establishment of an anodic current as was the case with the pyrite. At 250 mV (SHE) the KEX achieved a higher current density than the KC_{12}-TTC. This contrasts with the behaviour of the two collectors on pyrite; KC_{12}-TTC achieved a much higher current density. As previously indicated, the peak at 250 mV (SHE) for both KEX and KC_{12}-TTC is associated with the adsorption of the collector species as well as the oxidation of the copper. It is clear that collectors very successfully inhibit the formation of the $Cu(OH)_2$ species, but the TTC inhibits the formation of the CuO more strongly than the xanthate. Similar behaviour between different types of oxidation inhibitors on copper is reported by Subramanian and Lakshminarayanan (2002).

Figure 26 (I) indicates that the concentration of the KEX did not change significantly for successive scans in the same solution as was the case for pyrite. The successive scans in a KC_{12}-TTC solution [Figure 26 (II))] indicate a change in the solution chemistry (this result was confirmed with repeat tests). For the first two scans the observed anodic current density also decreased as was found with pyrite, but the third scan indicated an increase in the anodic current. The anodic peak at approximately 150 mV (SHE) corresponds to the formation of $Cu(OH)_2$; therefore it seems that the KC_{12}-TTC has been depleted.

The interaction between C_{12}-SK and copper was also investigated (Figure 27), since it is the most likely decomposition product. At first glance it seemed that there was some electrochemical interaction between the C_{12}-SK and the copper, with the strong anodic peak observed at approximately 150 mV (SHE). However, this peak is again probably due to the formation of $Cu(OH)_2$. Thiols adsorb via the following reduction steps (Turbeville & Yap, 2006):

$$2RSH + 2CuO \rightarrow RSSR + Cu_2O + H_2O \quad (12)$$

$$2RSH + Cu_2O \rightarrow 2RSCu + H_2O \quad (13)$$

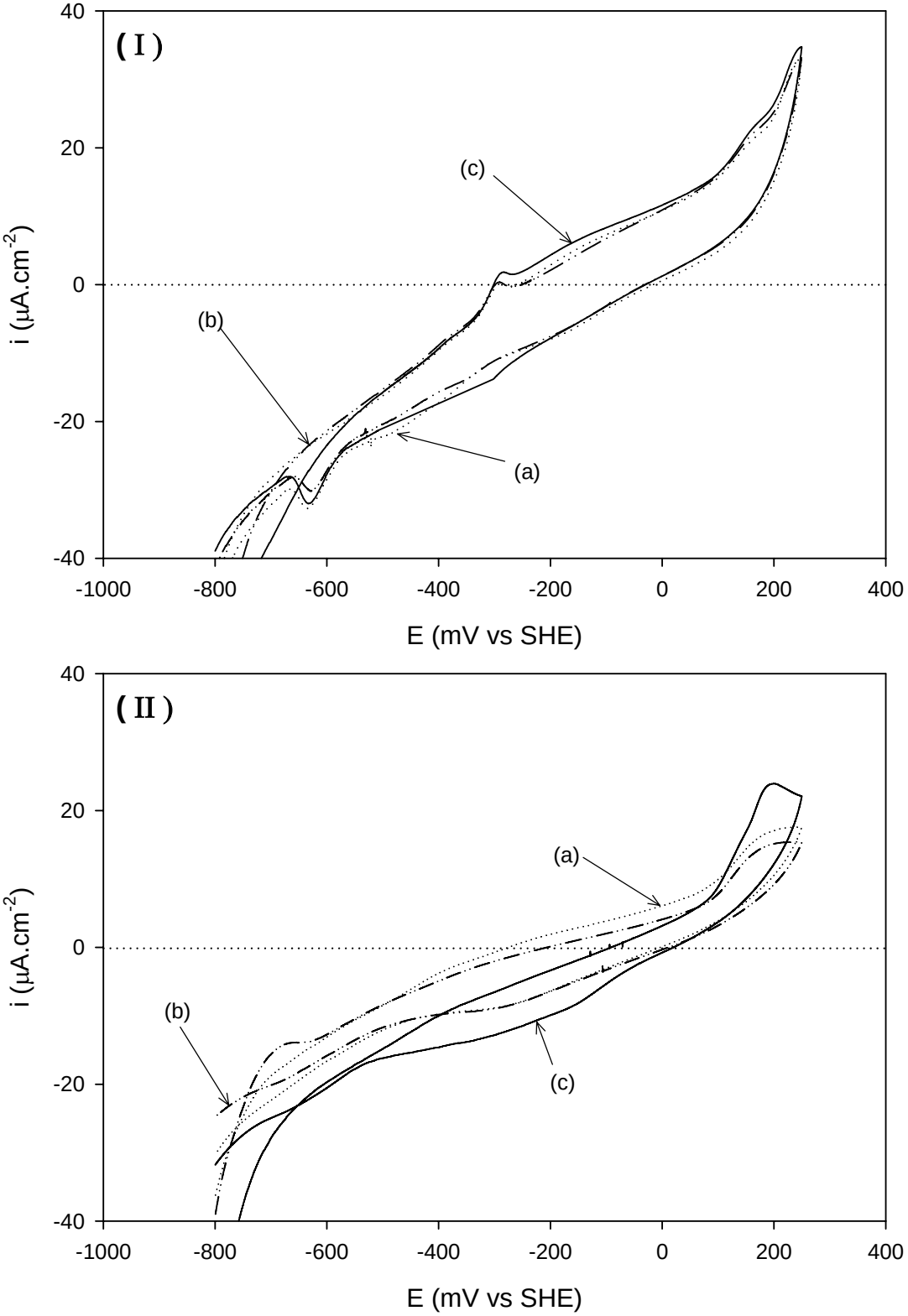

Figure 26: Cyclic voltammograms of copper scanned at 1 mV/s in 0.05 M borate solutions with (I) 10^{-3} M KEX and (II) 10^{-3} M KC_{12}-TTC; (a), (b) and (c) are successive scans in the same solution, each with a freshly prepared copper surface.

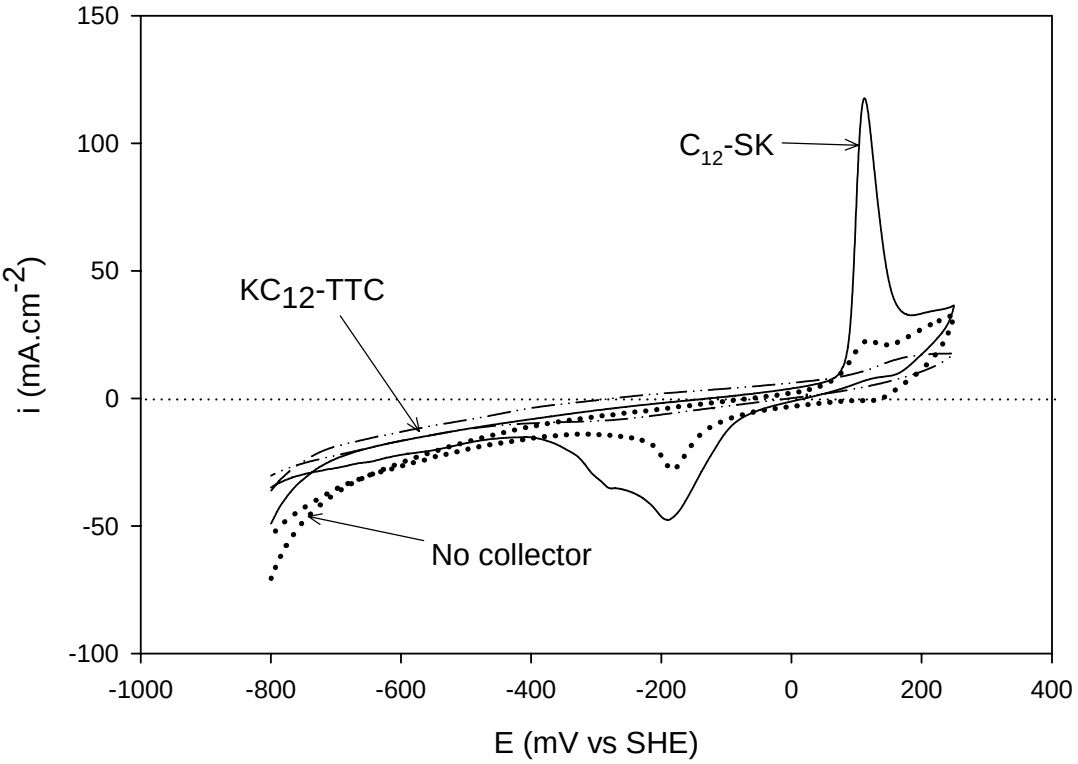

Figure 27: Cyclic voltammograms of copper scanned at 1 mV/s in 0.05 M borate solutions with no collector, 10^{-3} M C_{12}-TTC and 10^{-3} M C_{12}-SK.

Therefore the C_{12}-SK suppresses the formation of the $Cu(OH)_2$ passivation layer, resulting in an increase of the current density at approximately 150 mV (SHE). However the adsorption rate of the C_{12}-SK is low (formation for measurably thiol self-assembled monolayers (SAMs) and takes at least between 12-17 hours (Keller *et al.*, 1994 and Carbonell *et al.*, 2004)) and consequently it does not itself serve as an effective oxidation inhibitor.

4.2 Raman spectroscopy

4.2.1 Pyrite

The Raman spectrum of pyrite was recorded in the borate solution (without collectors) (Figure 28). Two very intense peaks are visible between 300 cm^{-1} and 400 cm^{-1}. These peaks are due to the Fe-S bonds that are present in pyrite (McGuire *et al*., 2001). Raman spectra for the experimental work on pyrite were recorded from above 400 cm^{-1} to preclude these intense peaks from interfering with the interpretation of the spectra of the adsorbed species. A band at approximately 870 cm^{-1} was visible in most of the Raman spectra. This band was due to borate buffer solution (Oblonsky & Devine, 1995).

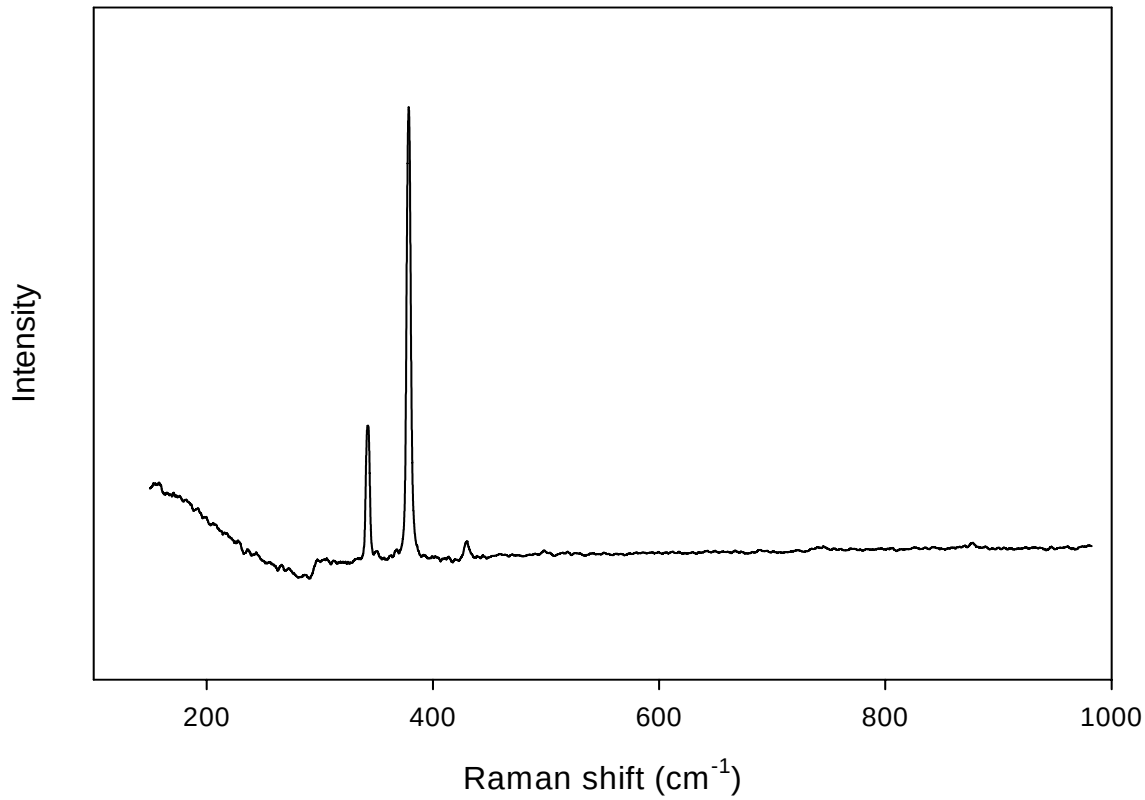

Figure 28: Pyrite in a 0.05 M borate solution (pH 9.2)

Figure 29 shows the Raman spectra recorded of purified KEX and freshly synthesised diethyl dixanthogen (EX_2) as reference. The characteristic Raman bands are listed in Table 4. Figure 29 also shows the Raman spectra recorded *in situ* of a pyrite electrode

polarised at 250 mV (SHE) for different lengths of time in a 0.05 M borate and 10^{-3} M KEX solution (note that the time indicated is from the start of the polarisation; the Raman spectra were recorded from that instant onwards, for the next 120 s). Significant Raman bands from the *in situ* Raman spectra appear only after 240 s. The only species that can be identified is the dixanthogen by the appearance of two intense peaks at 428 cm^{-1} (C-O-C trans deformation) and 498 cm^{-1} (S-S stretching vibration). The S-S stretch band is particularly significant, since this peak is not present in the case of the xanthate monomer. There are no peaks in the *in situ* Raman spectrum that would indicate the presence of the xanthate monomer.

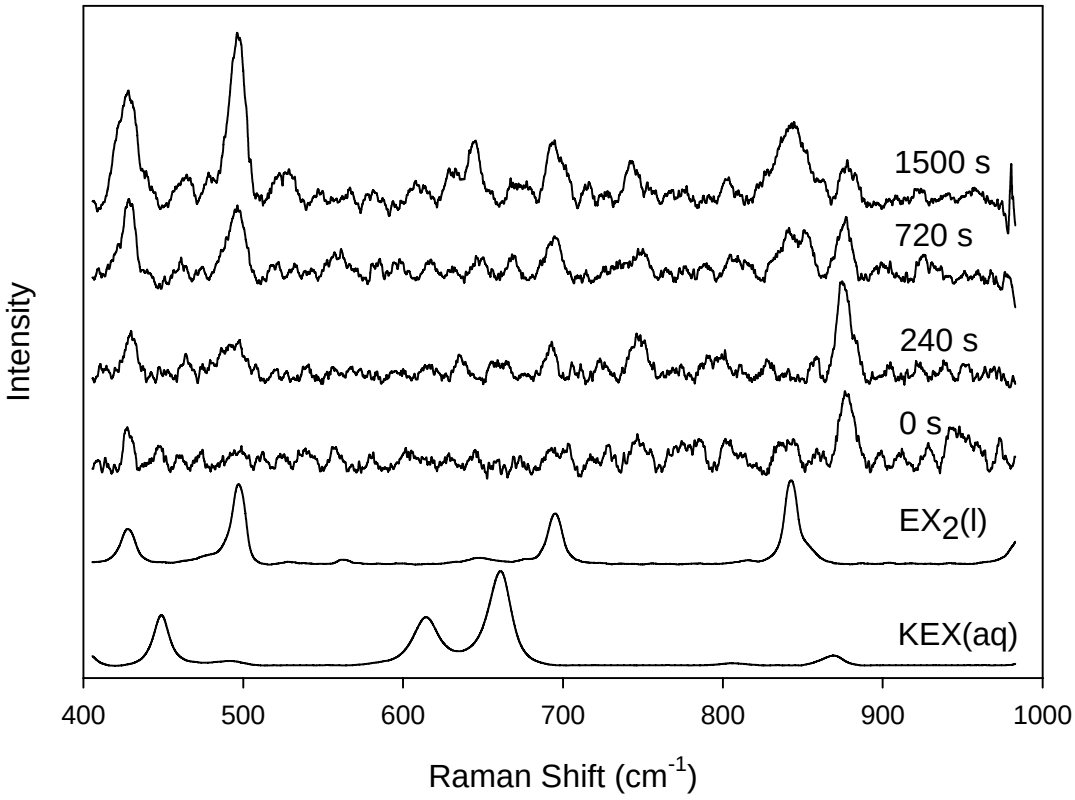

Figure 29: Comparison of the spectra of xanthate and dixanthogen with the spectra of a pyrite electrode polarised at 250 mV (SHE) for different times in a 0.05 M borate and 10^{-3} M KEX solution.

It is concluded from the Tafel slopes of the anodic peak measured during cyclic voltammetry of pyrite that the oxidation of the xanthate is preceded by the chemisorption of the xanthate monomer (Woods, 1996). It is reported that the mechanism of the interaction of xanthate with pyrite is similar to that of gold. The

chemisorption of the monomer on gold was spectrochemically verified by Woods *et al.* (1998c). The phenomenon of surface-enhanced Raman scattering (SERS) occurs on gold which makes it possible to achieve 10^3 times higher sensitivity when recording Raman spectra. Woods *et al.* (1998c) deduce from their measurements that there is a layer of chemisorbed xanthate on the surface with multilayers of dixanthogen bonded to this layer. These authors deduced this from the fact that the band intensities of the chemisorbed xanthate and dixanthogen were similar even though the concentration of the dixanthogen was much higher. In the case of pyrite, no surface enhancement is expected [occurs usually on transition metals for example gold, silver and copper (Woods *et al.*, 1998a]. Hence it was only possible to detect the dixanthogen after 240 s of polarisation when the concentration was high enough through the formation of multilayers of dixanthogen. There was no measurable evidence of any chemisorbed xanthate, presumably because the concentration of the chemisorbed xanthate was very low, possibly only a monolayer of xanthate.

Table 4: The comparative Raman bands of potassium ethyl xanthate and of diethyl dixanthogen.

	Raman shift (cm^{-1})			
	Woods *et al.* (1998a)		**Vermaak *et al.* (2005)**	
Vibration	**KEX (aq)**	**EX_2 (l)**	**KEX (aq)**	**EX_2 (l)**
CS_2 antisymmetric stretch	1046	1041	1046	1041
CCOC stretch	864	845	864	844
CS_2 symmetric stretch *trans*	660	695	659	694
CS_2 symmetric stretch *gauche*	615	646	614	646
OCS_2 out of plane *wag*	556	528	-	-
SS stretch	N/A	498	N/A.	498
COC deformation *gauche*	493	473	493	-
COC deformation *trans*	449	427	448	428
OCC deformation	399	378	401	378

N/A not applicable; l: liquid; aq: aqueous solution

Figure 30 shows the Raman spectra of potassium dodecanetrithiocarbonate (KC_{12}-TTC) and didodecane ditrithiocarbonate (C_{12}-TTC_2) compared to the Raman spectrum of the pyrite electrode (*in situ*) in a 0.05 M borate and 10^{-3} M KC_{12}-TTC solution, after polarisation at 0 mV (SHE) for 900 s. It is clear from these spectra that the species detected on the surface is neither of the two TTC species. The peak at approximately 740 cm^{-1} is characteristic of the ν(C-S) band for adsorbed alkanethiols (Kudelski, 2005).

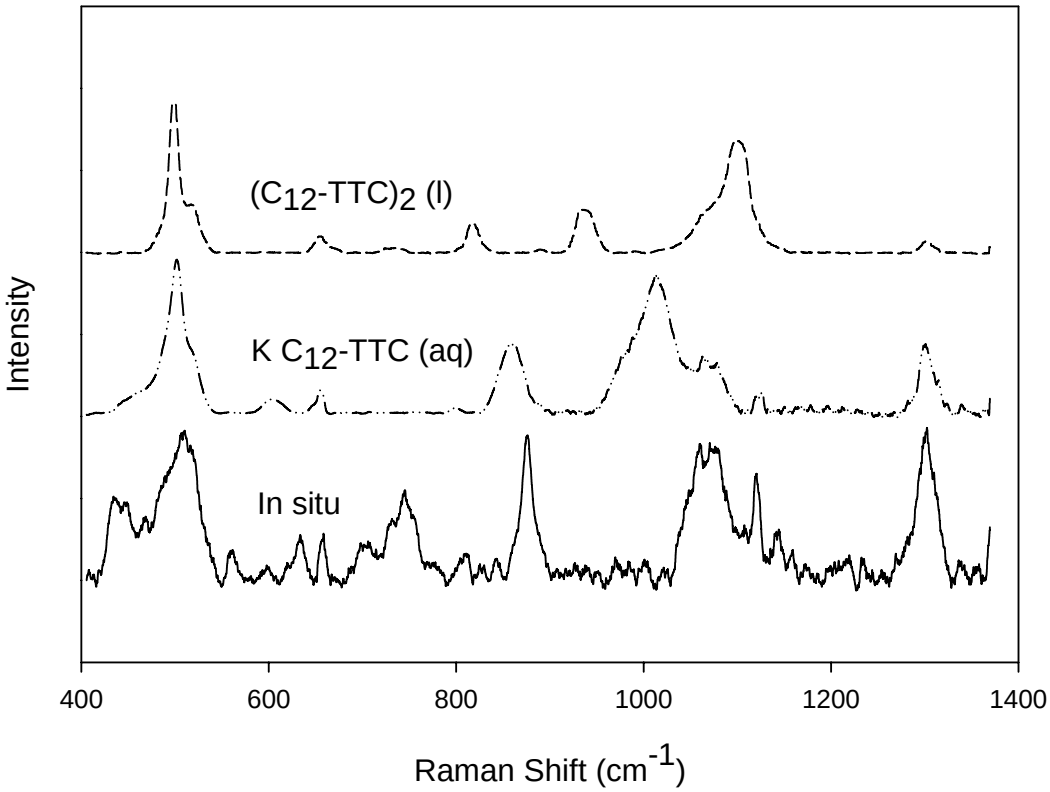

Figure 30: Raman spectra of the C_{12}-TTC monomer and dimer compared to the *in situ* spectrum of a pyrite electrode in a 0.05 M borate and 10^{-3} M potassium dodecanetrithiocarbonate solution polarised at 0 mV (SHE) for 900 s.

Figure 31 shows the Raman spectra of the dodecanethiol (C_{12}-SH) and potassium dodecanethiolate (C_{12}-SK) compared to the Raman spectrum of the pyrite electrode in a 0.05 M borate and 10^{-3} M KC12-TTC solution polarised at 0 mV (SHE) for 900 s. It is evident from these spectra that there is a strong similarity between the spectra of the two species and those of the *in situ* measurement. Table 5 contains a summary of the data in the literature on some of the most important Raman bands found in the region

of interest. These peaks (see Table 5) had been determined with SERS; the peak intensity and resolution were much higher than in the present case. It is interesting to note that the peak at approximately 740 cm^{-1} is attributed to the trans conformer of the S-C-C chain. This peak is visible in all three spectra, whereas the peak at approximately 655 cm^{-1} (the *gauche* conformer of the S-C-C chain) is only visible in the thiol and thiolate spectra. This would indicate that the *in situ* species is probably the *trans* conformer.

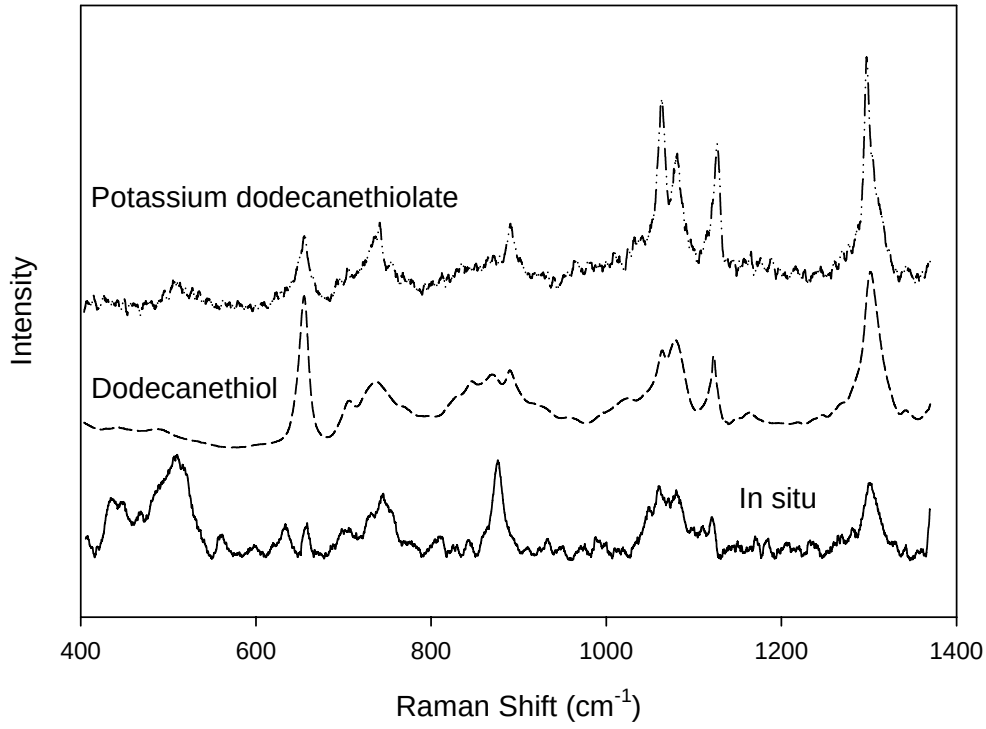

Figure 31: Raman spectra of the C_{12}-SH and C_{12}-SK compared to the *in situ* spectrum of a pyrite electrode in a 0.05 M borate and 10^{-3} M potassium dodecanetrithiocarbonate solution polarised at 0 mV (SHE) for 900 s.

There is some additional activity in the region of 400–550 cm^{-1} in the case of the *in situ* spectrum that is not present in the case of the thiol species. Figure 32 indicates that there is some thiol species present at the rest potential even though no anodic current has been applied. Compared to the spectrum of the pyrite surface polarised at 0 mV (SHE) for 900 s, the main difference is the presence of the wide band in the region of 400–550 cm^{-1}. This indicates that the TTC species, which also has bands in this region (Figure 30), may be present at more positive potentials; the TTC may serve as an adsorption intermediate for the attachment of the thiol species.

Table 5: Characteristic Raman bands of thiols adsorbed on metals (Kudelski, 2005)

Vibration	**Raman shift (cm^{-1})**
CH_2 wagging	~1300
ν(C-C)	1000-1100
CH_3 rocking	900
CH_2 rocking	700-900
$\nu(C\text{-}S)_T$	700-740
$\nu(C\text{-}S)_G$	620-650

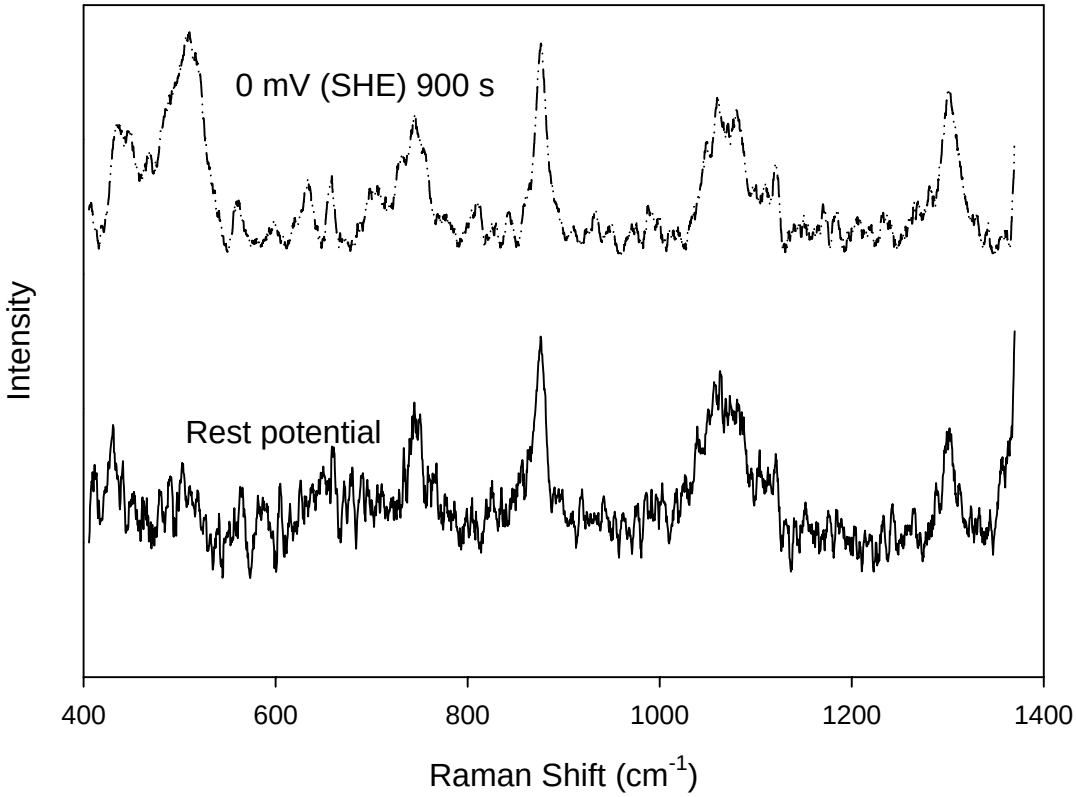

Figure 32: Raman spectra the *in situ* spectra of a pyrite electrode in a 0.05 M borate and 10^{-3} M potassium dodecanetrithiocarbonate solution polarised at 0 mV (SHE) for 900 s and at its rest potential.

4.2.2 Copper

Raman spectra for copper were recorded at -500 mV (SHE) and 500 mV (SHE) in the borate solution (without collectors) (Figure 33). The only significant peak visible between 400 cm^{-1} and 1000 cm^{-1} (at both -500 mV (SHE) and 500 mV (SHE) polarisation) is the peak at approximately 870 cm^{-1}. This peak is due to the borate buffer, as previously identified for pyrite.

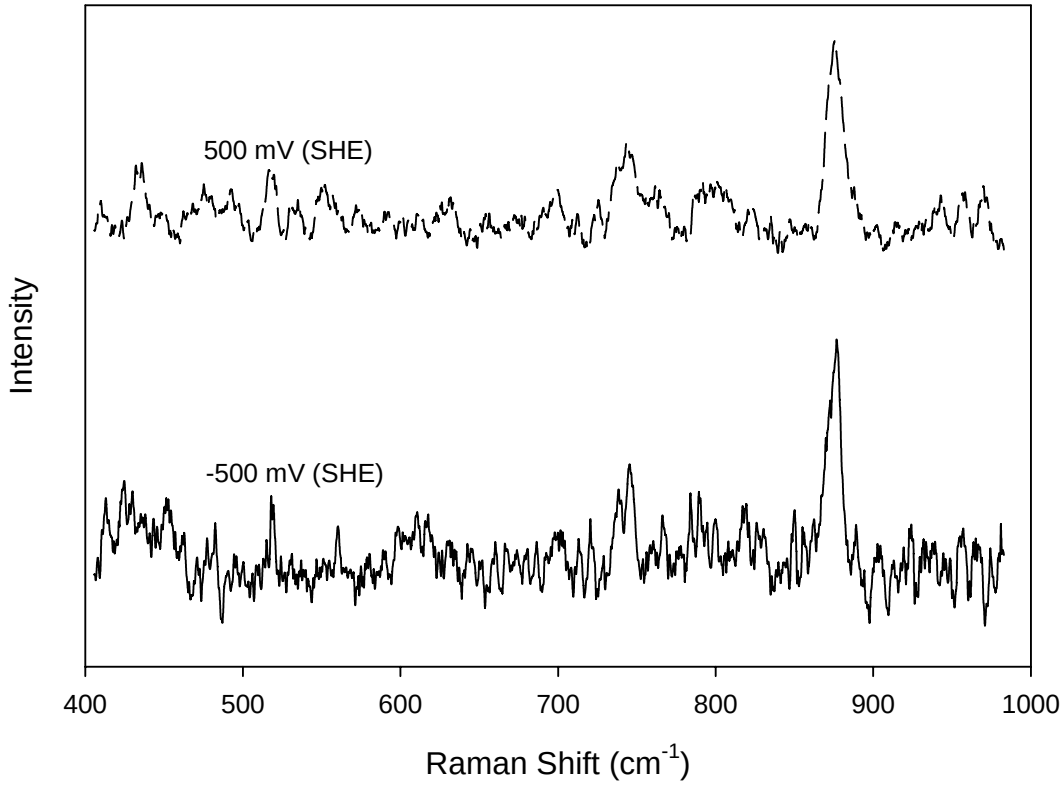

Figure 33: Comparison of the spectra of a copper electrode polarised for 480 s at -500 mV (SHE) and 500 mV (SHE) in a 0.05 M borate.

Figure 34 shows the Raman spectrum recorded *in situ* of a copper electrode polarised at 300 mV (SHE) for 3600 s in a 0.05 M borate and 10^{-3} M KEX solution. It is possible to identify xanthate on the copper electrode by the presence of the peak at 659 cm^{-1} (CS_2 symmetric stretch *gauche*). The very intense peak at 469 cm^{-1} is due to the decomposition of the xanthate on the copper; the peak can be ascribed to the formation of Cu_2S (Minceva-Sukarova *et al.*, 1997). The xanthate decomposes as a result of the reactivity of the copper combined with the energy supplied by the Ar^+-laser.

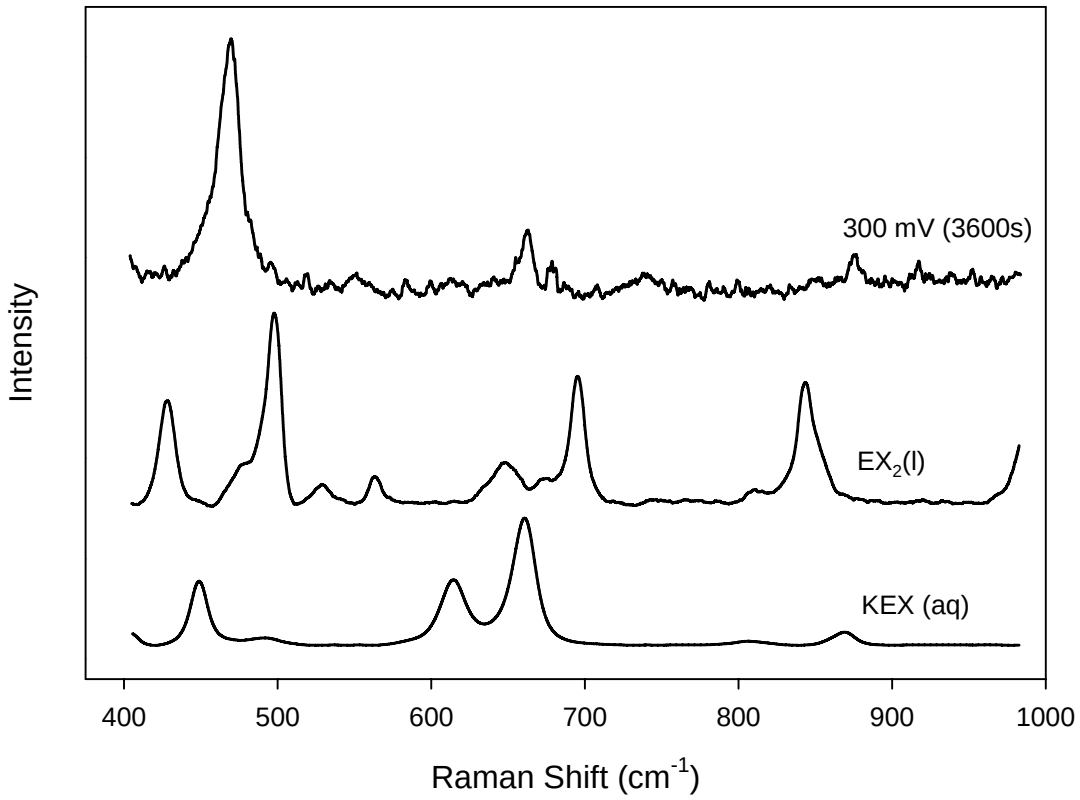

Figure 34: Comparison of the spectra of xanthate and dixanthogen with the spectrum of a copper electrode polarised at 300 mV (SHE) for 3600 s in a 0.05 M borate and 10^{-3} M KEX solution.

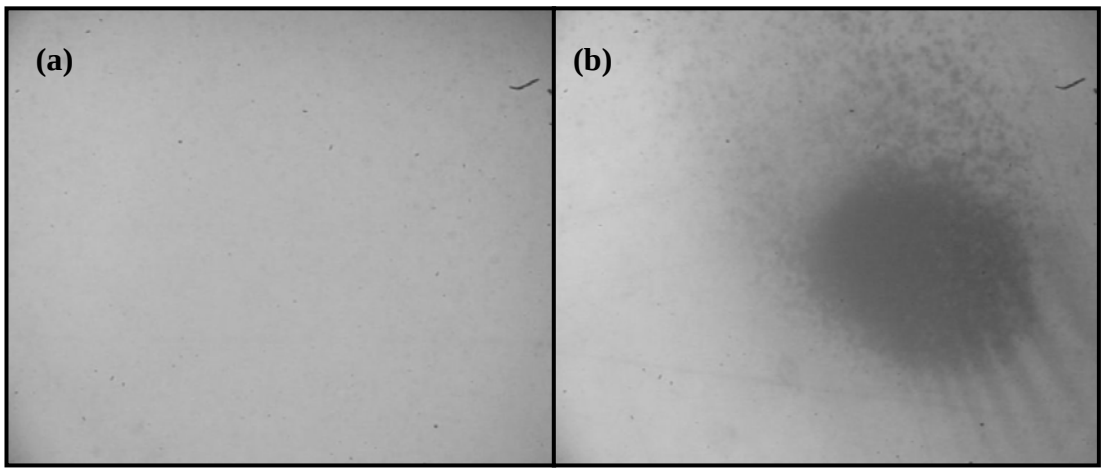

Figure 35: Microscope image of a copper electrode surface polarised for 3600 s at (a) -600 mV (SHE) and (b) 300 mV (SHE) in a 0.05 M borate and 10^{-3} M KEX solution (objective ×50) after Raman spectra were recorded.

It was possible to detect visually the decomposition effect of the laser on the copper surface when a dark spot appeared on the copper surface at the point where the laser was focused during the recording of the Raman spectrum (Figure 35(b)). At this potential (300 mV (SHE)), one would expect the presence of both the bulk copper ethyl xanthate (CuEX) and the chemisorbed ethyl xanthate (Woods *et al*, 1998b). The potential is also higher than the reversible potential of the xanthate/dixanthogen couple (121 mV (SHE)). The formation of the CuEX or EX_2 could not be visually detected as can be seen from Figure 35(b) [the surface next to the dark spot (unaffected by the laser)]. It was, however, possible to determine the presence of the ethyl xanthate and EX_2 after long polarisation times by means of Raman spectroscopy (Figure 36). The ethyl xanthate can be identified by the peaks at 448 cm^{-1} (C-O-C deformation *trans*) and 659 cm^{-1}, whereas the EX_2 can be identified by the presence of the peaks at 428 cm^{-1} and 498 cm^{-1}.

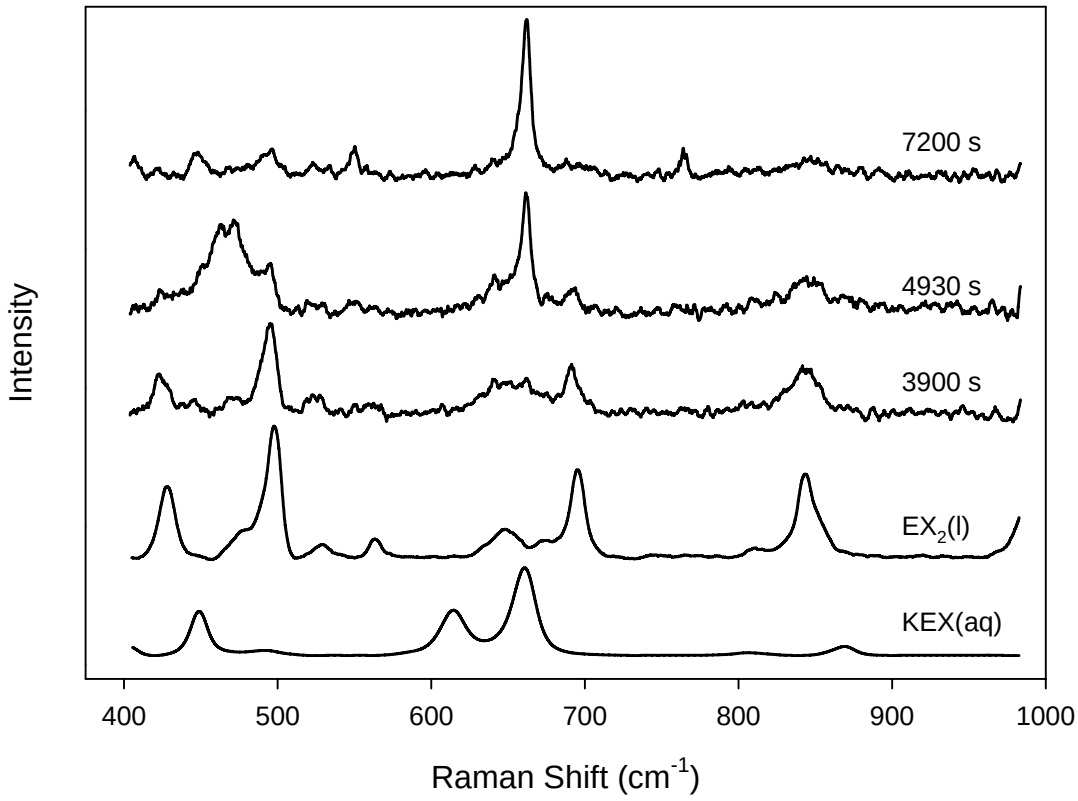

Figure 36: Comparison of the spectra of xanthate and dixanthogen with the spectra of a copper electrode polarised at 300 mV (SHE) for different times in a 0.05 M borate and 10^{-3} M KEX solution.

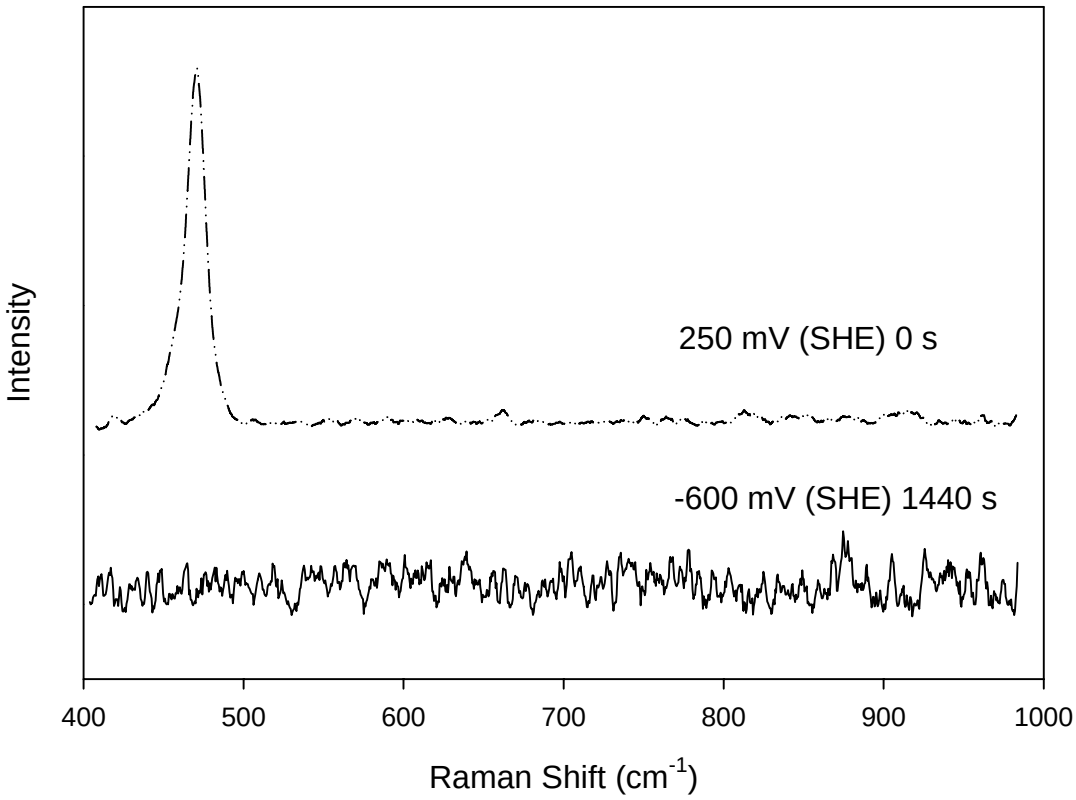

Figure 37: Raman spectra of a copper electrode polarised at -600 mV (SHE) for 1440 s and 250 mV (SHE) 0 s in a 0.05 M borate and 10^{-3} M KEX solution.

Cu_2S was formed as soon as the xanthate had adsorbed onto the surface of the copper electrode (see Figure 37). No significant peaks could be identified at potentials below the chemisorption of the xanthate (-600 mV), even for long polarisation times (Figure 37). Cu_2S could be detected on the surface of the copper electrode as soon as an anodic current was present.

It is important to note that the presence of the collector could only be detected at very long polarisation times (longer than 3600 s; see Figure 36). These extensive polarisation times allowed a sufficiently thick product layer to form, which reduced the laser-induced decomposition reaction of the xanthate on the copper electrode. This is also evident from Figure 36; as the polarisation time increases, so does the amount of CuEX (peak at 659 cm^{-1}) relative to the Cu_2S (peak at 469 cm^{-1}), eventually there is no trace of Cu_2S. The formation of the bulk CuEX also depresses the formation of EX_2 (peak 498 cm^{-1}). Woods *et al.* (1998b) were able to determine the presence of

chemisorbed ethyl xanthate and bulk CuEX at lower potentials and shorter polarisation times. This was possible due to the use of Fourier transform Raman (FT-Raman); FT-Raman uses a longer (1064 nm) laser length and shorter acquisition times, in this way reducing the energy input of the laser. This circumvents the decomposition reaction of the collector.

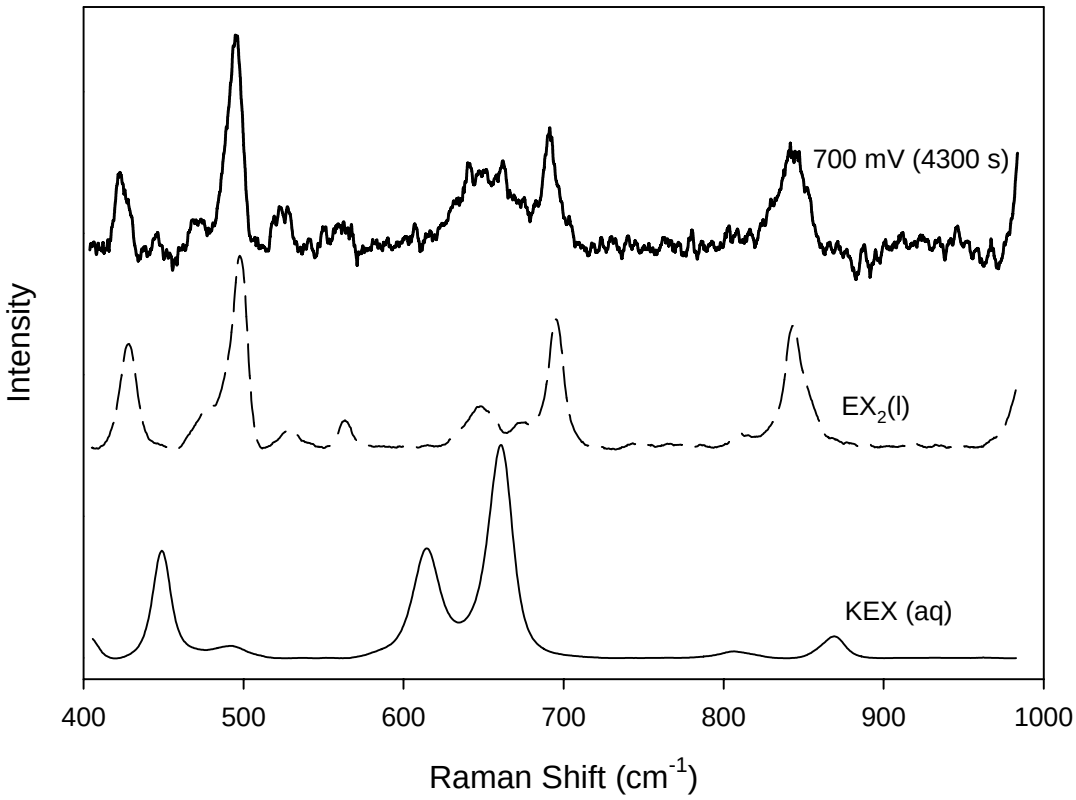

Figure 37: Comparison of the spectra of xanthate and dixanthogen with the spectrum of a copper electrode polarised at 700 mV (SHE) for 4300 s in a 0.05 M borate and 10^{-3} M KEX solution.

At a very large over-potential (700 mV (SHE)) a large amount of EX_2 can be detected with some CuEX also present (Figure 37). This was also visually confirmed with the appearance of droplets on the surface of the copper electrode (Figure 38). The pyrite electrode had a similar coverage of droplets in the presence of EX_2.

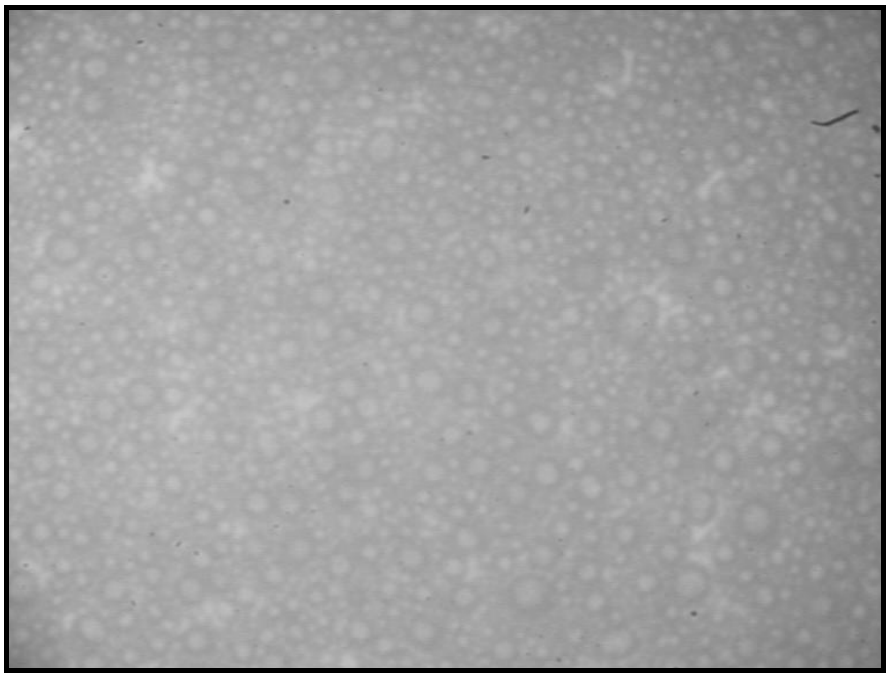

Figure 38: Microscope image of a copper electrode surface polarised for 4300 s at 700 mV (SHE) in a 0.05 M borate and 10^{-3} M KEX solution (objective ×50) after Raman spectra were recorded.

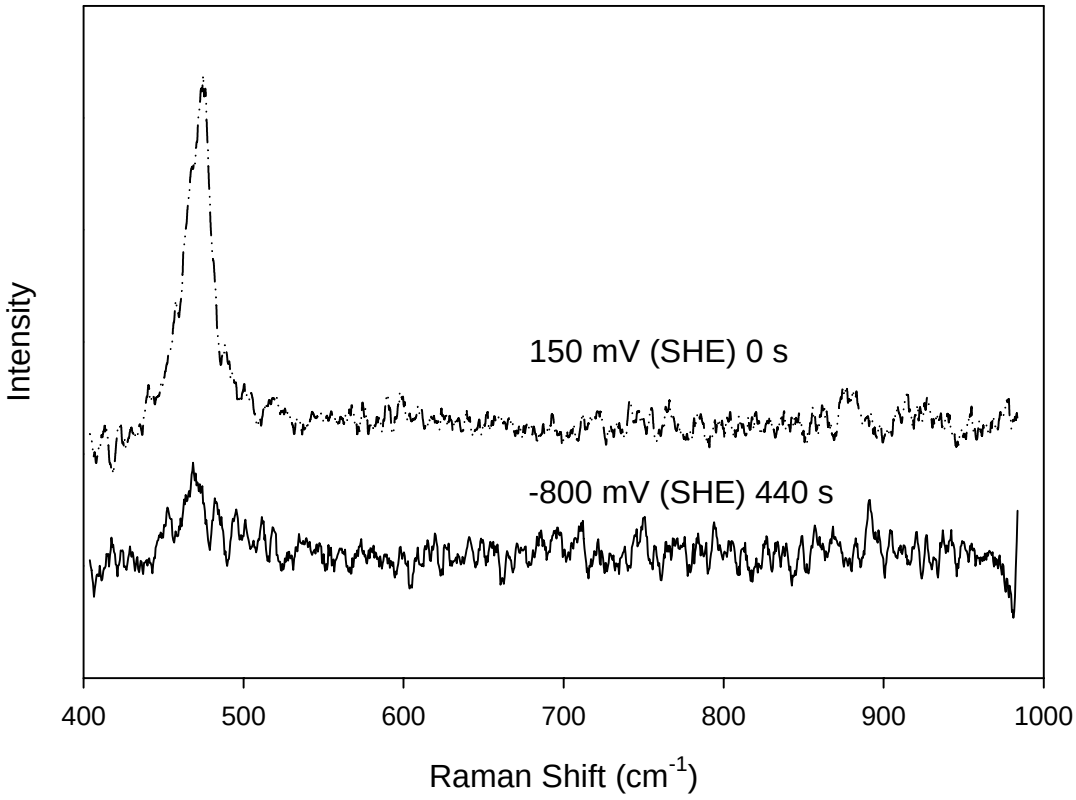

Figure 39: Raman spectra of a copper electrode polarised at -800 mV (SHE) for 440 s and at 150 mV (SHE) for 0 s in a 0.05 M borate and 10^{-3} M KC_{12}-TTC solution.

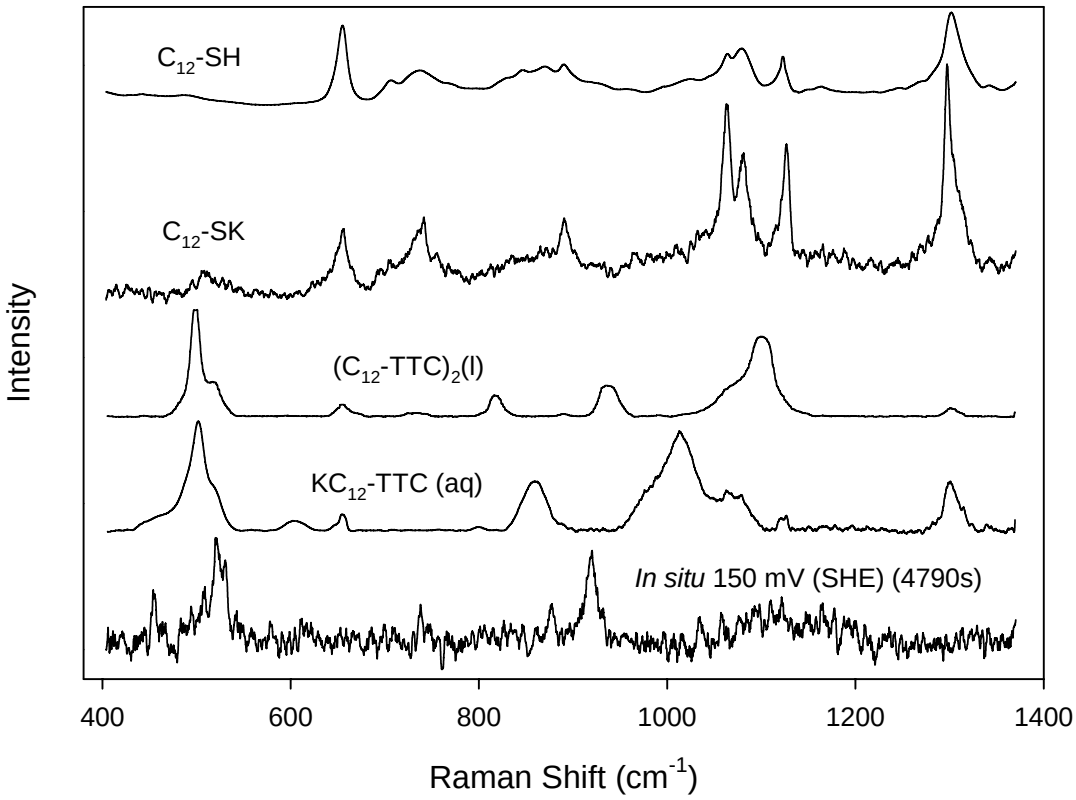

Figure 40: Raman spectra of the KC_{12}-TTC, $(C_{12}\text{-TTC})_2$, C_{12}-SK and C_{12}-SH compared to the *in situ* spectrum of a copper electrode in a 0.05 M borate and 10^{-3} M KC_{12}-TTC solution polarised at 150 mV (SHE) for 4790 s.

It was evident from the Raman experiments of the C_{12}-TTC interaction with the pyrite electrode that the C_{12}-TTC is reasonably unstable; only the thiol could be detected. It could be expected that the C_{12}- TTC would be even more reactive with the copper than with pyrite – considering the xanthate decomposition on copper forming Cu_2S. This reactivity is quite clear from the initial measurements (see Figure 39) done on the copper electrode. Cu_2S forms readily at any potential where an anodic current is present. The significant difference between the xanthate and the TTC is that Cu_2S also forms at a potential where a cathodic current is measured. This may indicate that the TTC or its decomposition products are also present at the electrode interface at these potentials.

Figure 40 shows the Raman spectra of the KC_{12}-TTC, $(C_{12}\text{-TTC})_2$, C_{12}-SK and C_{12}-SH compared to an *in situ* spectrum of the copper electrode in a 0.05 M borate solution containing 10^{-3} M KC_{12}-TTC polarised at 150 mV (SHE) for 4790 s. The *in situ* spectrum does not strongly resemble any of the collector species. Only in a few scans was it possible to detect the ν(C-C) and CH_2 wagging that should be present in the region from 1000 cm^{-1} up to 1300 cm^{-1} (indicative of adsorbed hydrocarbon chains). In addition, a strong peak appeared at approximately 920 cm^{-1} – this is due to the $\nu_{asym}(C\text{-}S_{exo})$ mode that originate from CS_3 (Cheng *et al.*, 2000). The peak at approximately 520 cm^{-1} is due to the symmetric S-C-S stretching of the CS_3 (Lin-Vien *et al.*, 1991). This indicates that the C_{12}-TTC decomposed on the surface of the copper and only the CS_3 remained on the copper surface. The peak at approximately 740 cm^{-1} (ν(C-S) band), although not as clear as in the case of the pyrite, is indicative of the presence of some kind of thiol-species. Usually the presence of this peak at approximately 740 cm^{-1} coincides with the detection of activity in the region from 1000 cm^{-1} up to 1300 cm^{-1}. Similarly to xanthate adsorption on copper, the Cu_2S formation in the presence of KC_{12}-TTC is depressed when the electrode is polarised for extended periods; a sufficient barrier forms between the collector and the copper (Figure 41). However, there is no increase in the hydrocarbon chain concentration (Raman peak intensity between 1000 cm^{-1} and 1300 cm^{-1}; not shown in this work), indicating that the C_{12}-TTC still decomposes with only the CS_3 remaining. The peak at approximately 920 cm^{-1} can also be observed after the copper electrode has been polarised for a few minutes at potentials where a cathodic current is present (not shown in this study). This confirms that the C_{12}-TTC is present on the copper surface at these low potentials. The copper probably serves as a catalyst for the decomposition of the C_{12}-TTC.

Raman spectroscopy was also conducted on a copper electrode in a 0.05 M borate solution containing 10^{-3} M C_{12}-SK (Figure 42). Raman spectroscopy indicated no difference in the behaviour of copper polarised at -800 mV (SHE) or 150 mV (SHE) in the presence of C_{12}-SK; no strong interaction was detected between the thiolate and the copper. It is well known that thiol will form a SAM on copper (Keller *et al.*, 1994), indicating that the thiolate is adsorbed directly but slowly onto the copper substrate. Therefore it seems that the TTC might be necessary as an intermediate

species for thiol adsorption on the surface (see also the results of TTC on pyrite). Importantly, it also evident from Figure 42 that the thiol does not decompose and form Cu_2S (the absence of Cu_2S was irrespective of the length of polarisation time). This furthermore indicates that the C_{12}-TTC interacts with the surface and decomposes at the surface, instead of the C_{12}-TTC decomposition products adsorbing directly onto the surface.

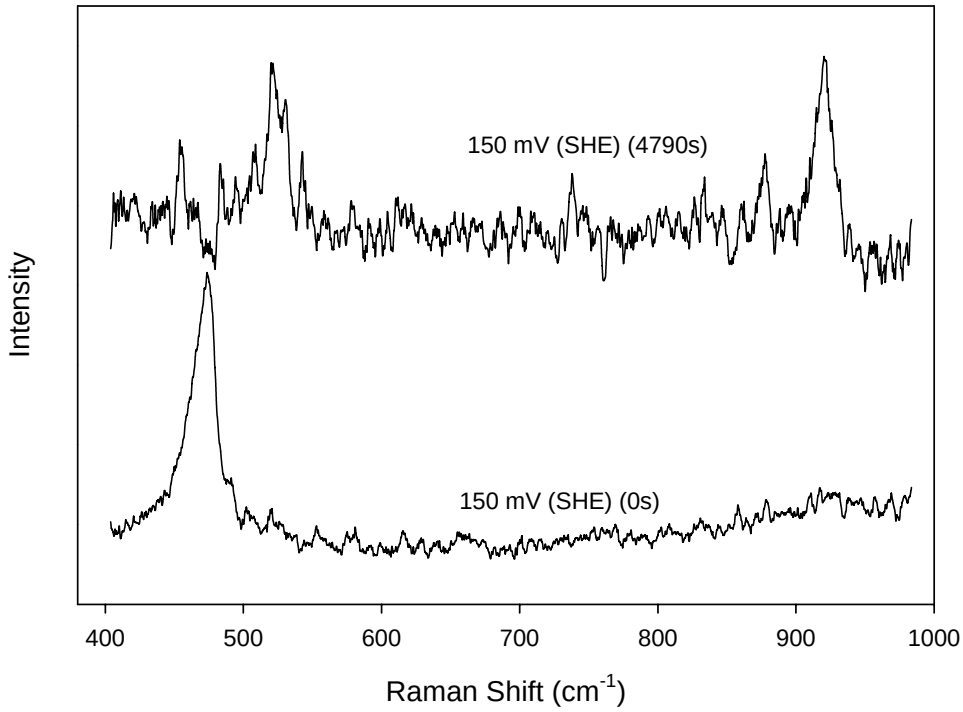

Figure 41: Raman spectra of a copper electrode polarised at 150 mV (SHE) for 0 s and 4790 s in a 0.05 M borate and 10^{-3} M KC_{12}-TTC solution.

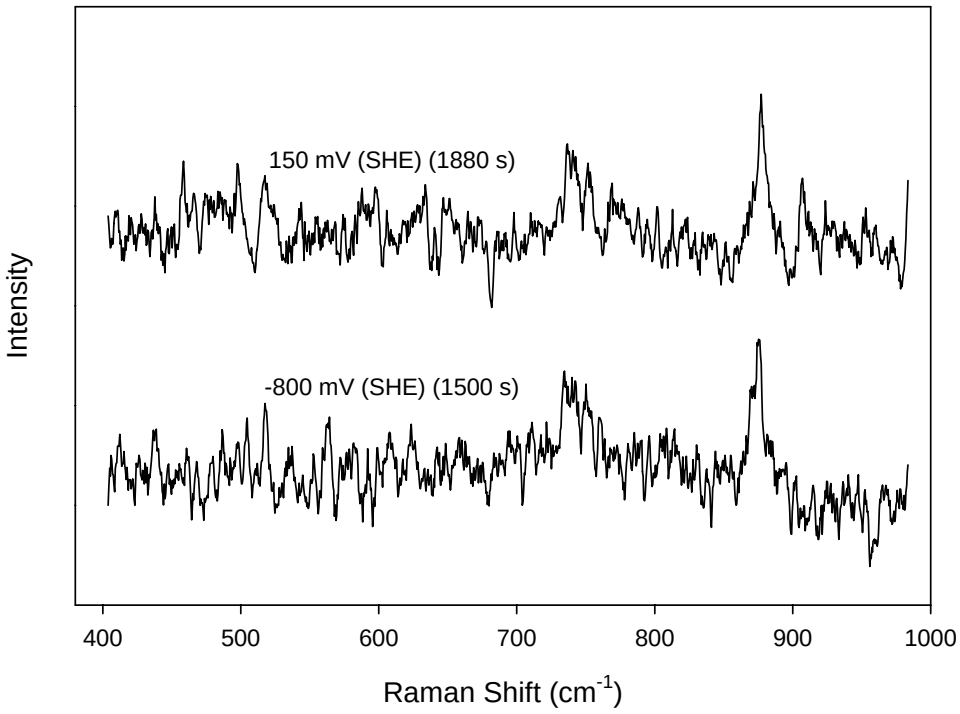

Figure 42: Raman spectra of a copper electrode polarised at -800 mV (SHE) for 1500 s and 150 mV (SHE) 1880 s in a 0.05 M borate and 10^{-3} M C_{12}-SK solution.

4.3 Electrochemical impedance spectroscopy (EIS)

In EIS a potential is applied (generally in a sine wave form) and the resulting current (also in wave form) is measured. The results of these measurements are expressed as a resistance or impedance (Z) and an associated phase angle (θ) – the phase shift between the two waves. The impedance (Z) consists of real (Z') and imaginary (Z'') components that can be calculated by means of the phase angle (θ). The real (Z') and imaginary (Z'') components are due to the behaviour of different components in the electrochemical system. The impedance measurements are generally represented in either a Nyquist plot (Z' versus –Z'') (Figure 43) or a Bode type of plot (log frequency versus log $|Z|$ and θ) (Figure 44). The electrochemical system can be modelled by electrical circuit elements such as resistors, capacitors and inductors (Silverman, 1986). A simple charge-transfer process can be modelled as a circuit that consists of a resistor (solution resistance) in series with a parallel circuit containing a capacitor (interfacial capacitance) and a resistor (polarisation resistance) (Figure 45). The Nyquist (Figure 43) and Bode (Figure 44) plots are of the typical impedance measurements obtained from a simple charge-transfer process.

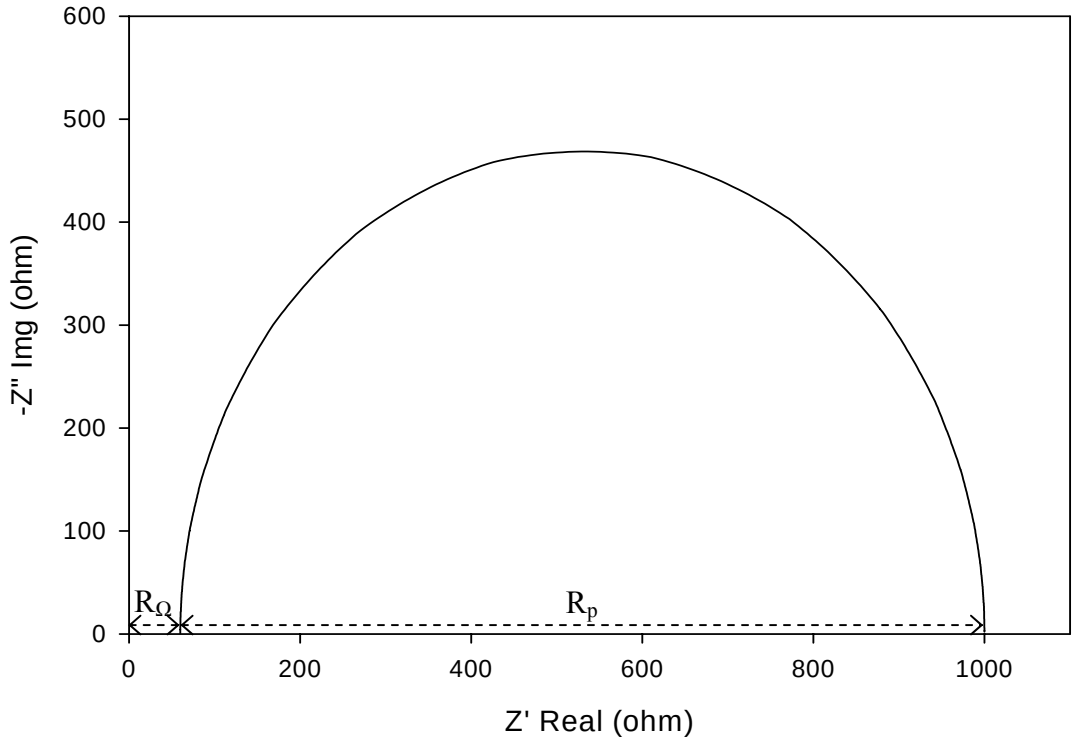

Figure 43: Nyquist plot of a simple charge-transfer process; where R_Ω = 60 Ω.cm^2, R_p = 940 Ω.cm^2 and C = 40 μF.cm^{-2}.

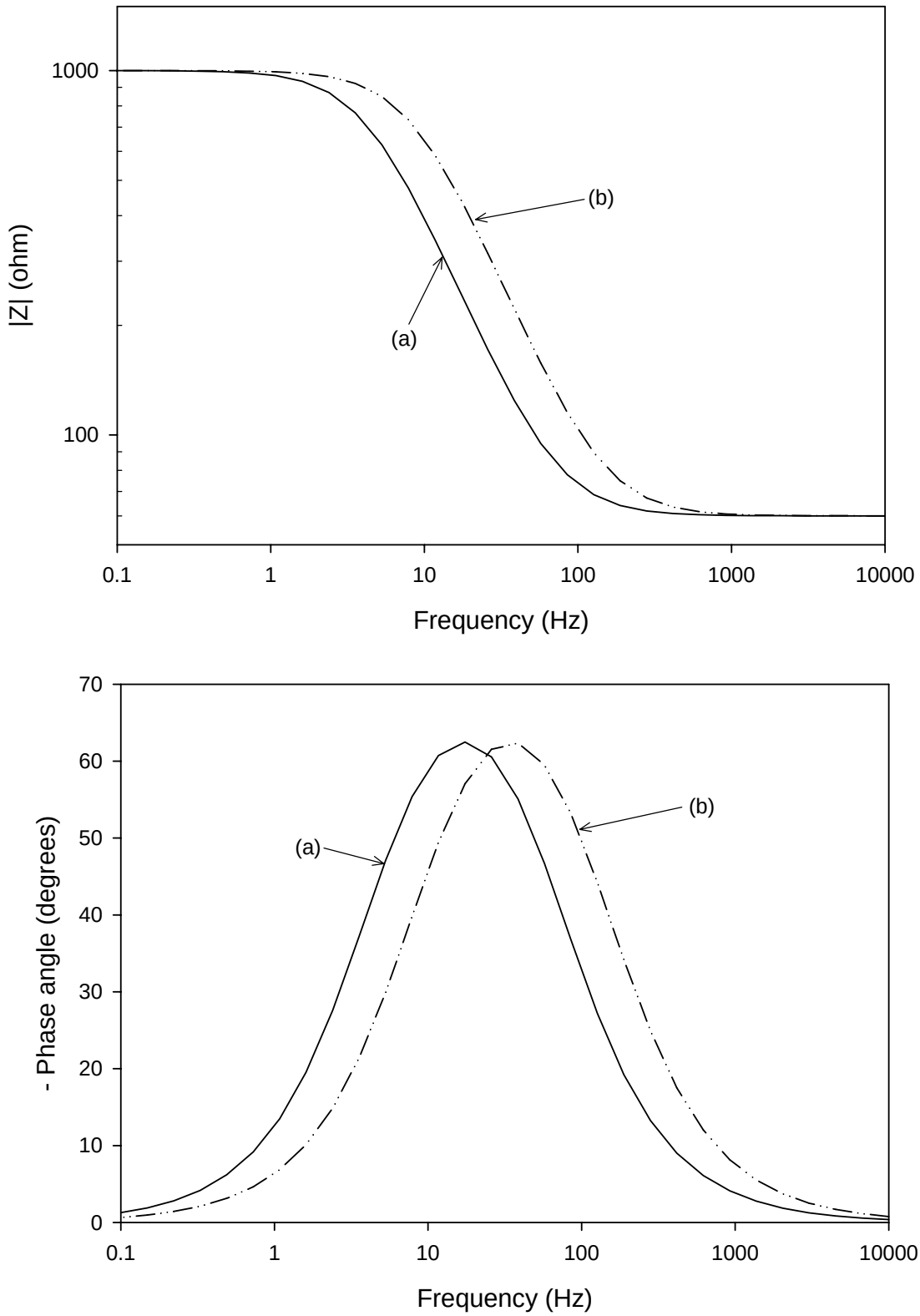

Figure 44: Bode plots of the impedance as a function of the frequency. The effect of a decrease in the capacitance is shown in the Bode plots; where R_Ω = 60 Ω.cm^2, R_p = 940 Ω.cm^2, (a) C = 40 μF.cm^{-2} and (b) C = 20 μF.cm^{-2}.

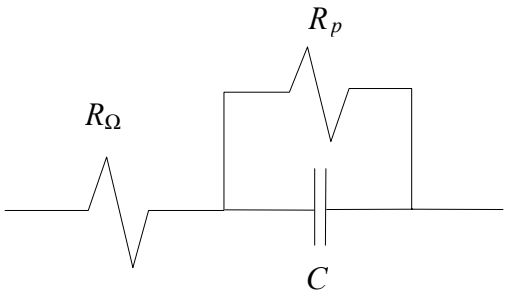

Figure 45: Circuit that models impedance in Figures 1 and 2; a simple charge-transfer process.

The circuit in Figure 45 can be described by the following equation:

$$Z = R_\Omega + \frac{R_p}{1+\omega^2 {R_p}^2 C^2} + \frac{j\omega {R_p}^2 C}{1+\omega^2 {R_p}^2 C^2} \qquad (14)$$

where R_Ω is the solution resistance, R_p is the polarisation resistance, ω is the angular frequency and C is the capacitance.

The capacitance effect is due to double-layer charging (C_D) and possible surface layers (C_S) (Vermaak *et al.*, 2004). The total electrode capacitance (C) is the series combination of C_D and C_S and can be calculated as follows:

$$\frac{1}{C} = \frac{1}{C_D} + \frac{1}{C_S} \qquad (15)$$

It is evident from Equation (15) that the formation and growth of a surface layer (with a finite and increasing value C_S) will cause a decrease in the total electrode capacitance (C) (Figure 44).

4.3.1 Pyrite

It is possible to use this simplified electric circuit model (Figure 45) in the case of a pyrite electrode (polarised at -400 mV (SHE) and 200 mV (SHE) in different solutions) at high applied frequencies (therefore low Z' and –Z'' values), as can be seen from Figure 46. It is difficult, however, to estimate the value of the polarisation resistance (R_p) because of the difficulty with extrapolatation, since the plots have not yet reached the maximum –Z'' values. However it is clear from Figure 46 that the R_p values are very large, relative to the other components. Therefore Equation (14) can be simplified to:

$$Z = R_{\Omega} + \frac{j}{\omega C} \qquad ; \text{where } R_p >>> R_{\Omega} \qquad (16)$$

The EIS measurements were performed at an open circuit potential after polarisation, so the measurements are not representative of the reactions that occur at the surface during polarisation; however, the surface layers that may have formed during polarisation would affect the capacitance, and this would be measurable at the open-circuit potential.

A few other observations are also possible from the measurements. It is evident from the Bode plots for pyrite polarised at -400 mV (SHE) for 1800s (Figure 47) that there is no major change in the behaviour of the pyrite in the solutions without a collector, 10^{-3} M KEX and 10^{-3} M C_{12}-SK. This indicates that no reaction occurred during the polarisation of the pyrite electrode; therefore no surface layer formed. This corresponds with the findings of the cyclic voltammetry and Raman spectroscopy work performed on the pyrite. However, at very low frequencies it is possible to see from the Bode plot in Figure 47 that the KEX reactions occurring are probably under diffusion control. This is shown by a larger phase angle than the borate-only solution, at the lowest frequencies (whereas the phase angles in the KEX and borate-only solutions are nearly identical at higher frequencies). However, it is clear from the Bode plot (Figure 46(a)) that R_p is very large for the KEX, therefore the resistance to a reaction between the KEX and the surface is very high under the de-aerated conditions used here.

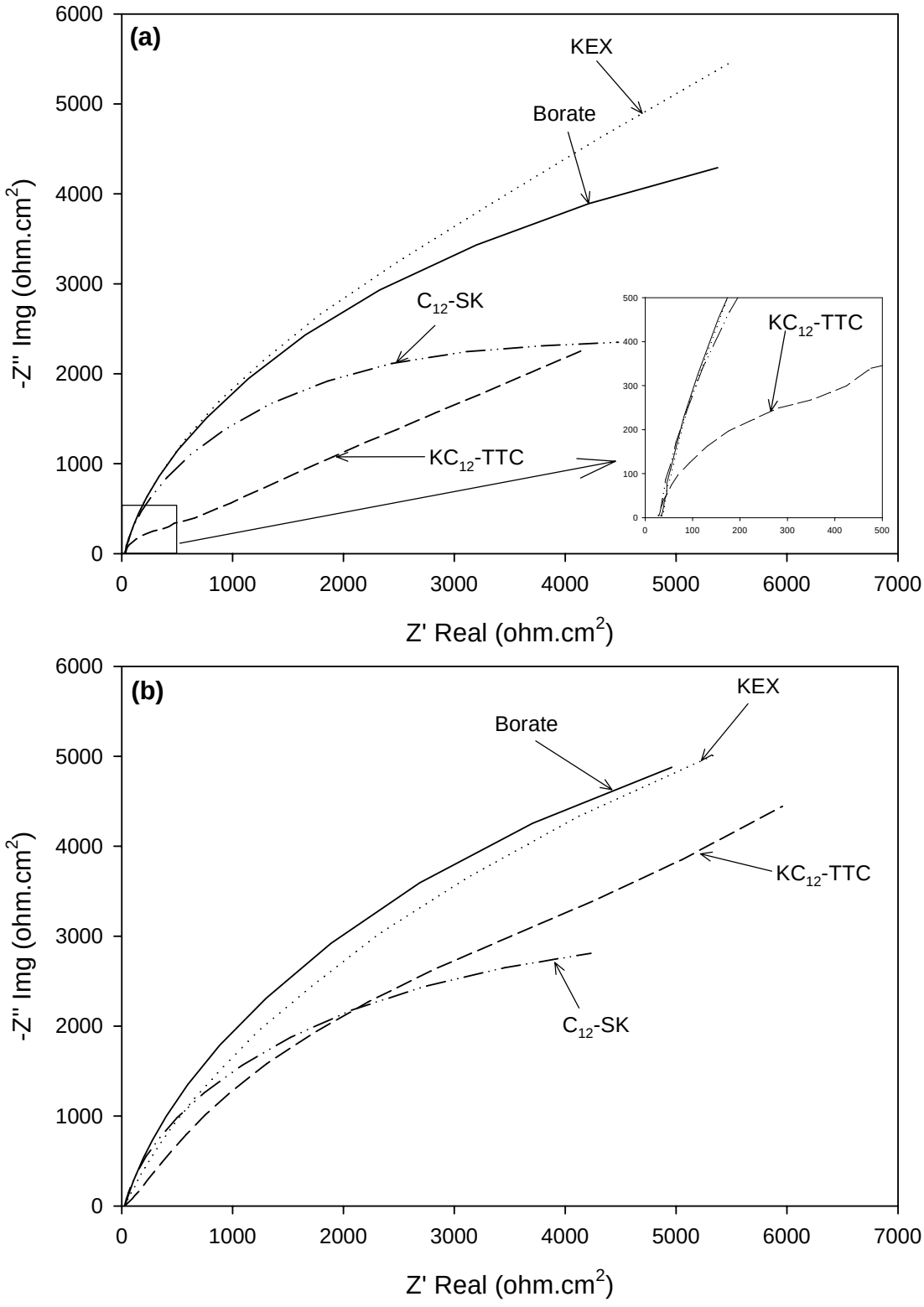

Figure 46: Nyquist plots of a pyrite electrode measured at an open circuit after polarisation for 1800 s at (a) -400 mV (SHE) and (b) 200 mV (SHE) (except in KEX solution; polarised at 300 mV (SHE)) in 0.05 M borate solutions containing: borate-only, 10^{-3} M KEX, 10^{-3} M KC_{12}-TTC and 10^{-3} M C_{12}-SK.

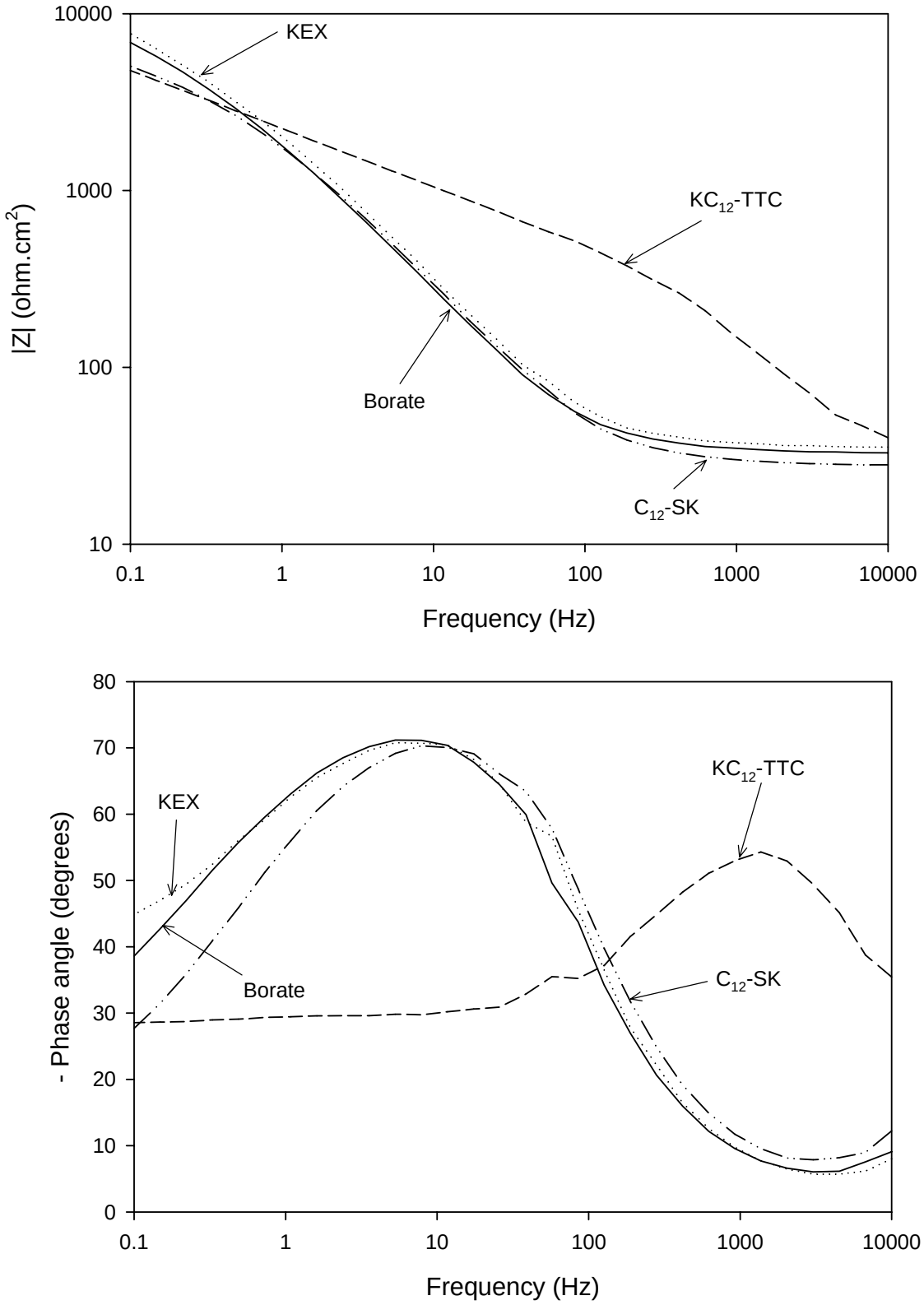

Figure 47: Bode plots for a pyrite electrode measured at an open circuit after polarisation for 1800 s at -400 mV (SHE) in a 0.05 M borate solution containing: borate-only, 10^{-3} M KEX, 10^{-3} M KC_{12}-TTC and 10^{-3} M C_{12}-SK.

The EIS performed on pyrite in a KC_{12}-TTC solution indicates a major change in the surface of the electrode compared to the electrode in the other three solutions. It is also evident from the Nyquist plot in Figure 46(a) that the pyrite electrode in the KC_{12}-TTC solution comes under diffusion control at very low Z' and –Z'' values; the semicircular part is due to kinetic control and the linear part is due to the diffusion control (Subramanian & Lakshminarayanan, 2002). The diffusion control at lower frequencies is also quite evident in the Bode plot where the phase angle is approximately constant from 0.1 Hz to approximately 20 Hz. The kinetic control is visible in the higher frequency range above 20 Hz. The appearance of the Bode plot is more characteristic of EIS performed during polarisation, indicating that some reactions still occur, even though no potential is applied. It can be seen from the Nyquist plot (Figure 46(a)) that R_p is lower for pyrite in the KC_{12}-TTC solution. This indicates that the surface is more reactive in the TTC solution than in other solutions after polarisation at -400 mV (SHE). As shown later after polarisation at -400 mV (SHE) in C_{12}-TTC solutions, the presence of a surface layer could be detected from a much lower total surface capacitance.

The pyrite electrode was polarised at 200 mV (SHE) in the different collector-containing solutions, except for the pyrite electrode in the KEX solution, which was polarised at 300 mV (SHE) to ensure that a large overpotential was applied for the interaction of the xanthate with the pyrite. The EIS measurements are shown in Figures 46 (b) (Nyquist plot) and 48 (Bode plot). There are no significant differences between the Nyquist and Bode plots for the pyrite in the borate solution after the polarisation at -400 mV (SHE) and 200 mV (SHE). Similarly there is no marked difference in the case of the C_{12}-SK. This indicates that neither of the species interacts strongly with the pyrite. By contrast, the measurements in the xanthate solution indicated a strong decrease in the capacitance of the surface. The lowering of the capacitance value is a result of the adsorption of xanthate and the formation of dixanthogen on the pyrite surface at potentials more positive than the reversible potential of the xanthate/dixanthogen couple. This is in good agreement with the work done previously in this current study.

There was clearly a large capacitance change from the investigations involving TTC as collector, polarised at -400 mV (SHE) and 200 mV (SHE). Interestingly, it can be

seen from the Nyquist plots (Figure 46) that the R_p value for the pyrite electrode in the KC_{12}-TTC solution is lower after polarisation at -400 mV (SHE) than after polarisation at 200 mV (SHE). This indicates that the pyrite surface is more reactive after the polarisation step at -400 mV (SHE); this may be related to differences in the surface coverage obtained during the different polarisation steps. From the contact angle measurements, an increase was observed in the contact angle as soon as an anodic current was applied. One would expect the increase in the contact angle to indicate an increase in the surface coverage of the electrode, suggesting that the lower polarisation resistance at -400 mV (SHE) is related to the possibility that some areas on the surface might be uncovered and could therefore still interact with the TTC. (It should be stressed that the electrochemical reaction occurring at the open-circuit potential is unknown.)

Figure 49 shows the capacitance calculated for pyrite in the different collector-containing solutions polarised for 1800 s at the indicated potentials. The capacitance was calculated from the imaginary part of Equation (16). For all the solutions, the measurements at 1000 Hz were utilised to do the calculation except for the TTC solutions that were computed from the measurements at 3000 Hz. The borate-only solution and the C_{12}-SK-containing solution showed no decrease in the calculated capacitance values; the capacitance values of approximately 15-30 $\mu F.cm^{-2}$ are in the range one would expect for a surface with no surface layer (Bard & Faulkner, 1980). This indicates that the C_{12}-SK and borate did not interact measurably with the pyrite in the potential range investigated. By contrast, the xanthate showed a decrease in the capacitance values after polarisation at 300 mV (SHE); this corresponds to the formation of a surface layer (a layer consisting mostly of dixanthogen, based on the Raman measurements).

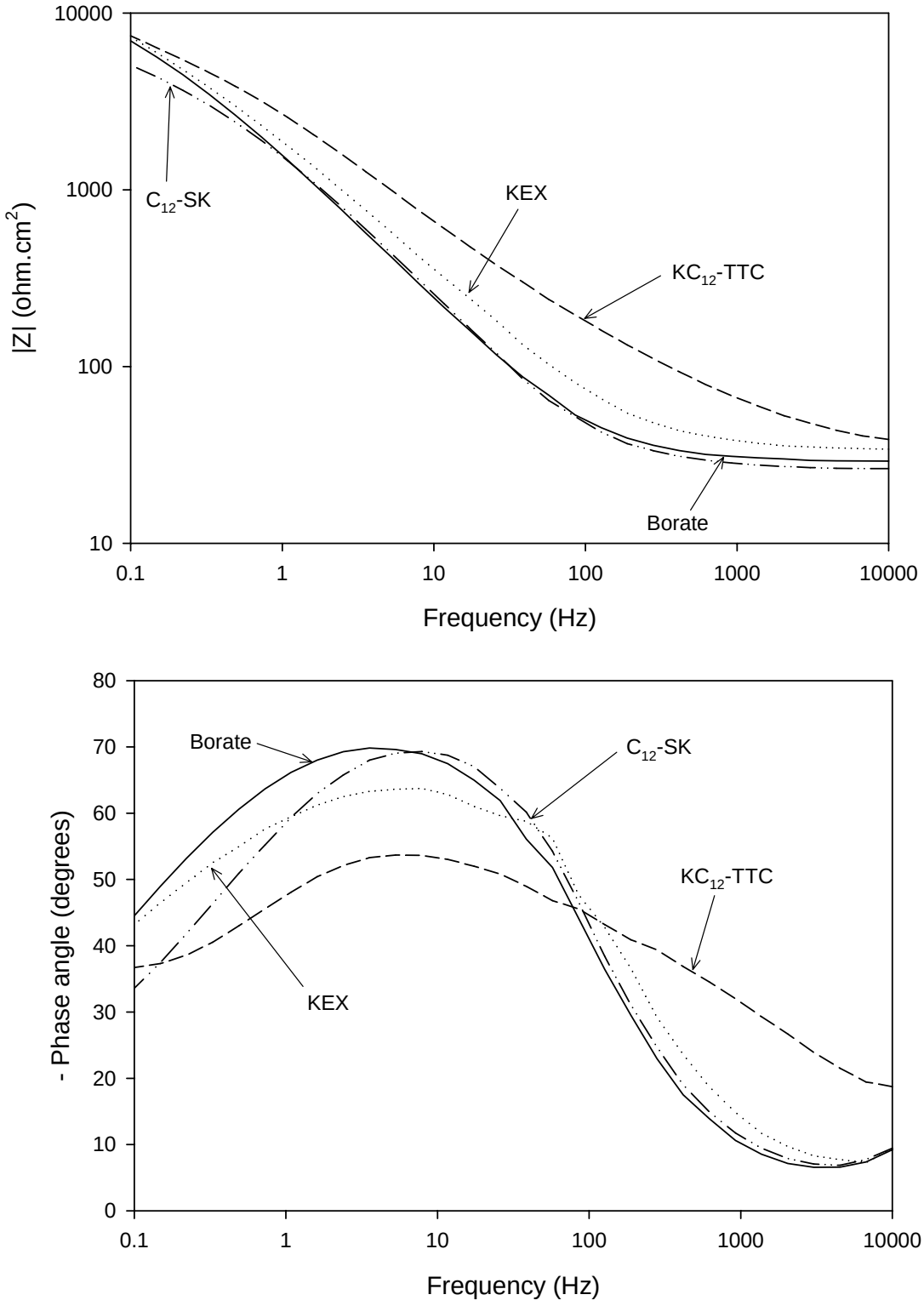

Figure 48: Bode plots for a pyrite electrode at an open circuit after polarisation for 1800 s at 200 mV (SHE) (except in KEX solution; polarised at 300 mV (SHE)) in 0.05 M borate solutions containing: borate-only, 10^{-3} M KEX, 10^{-3} M KC_{12}-TTC and 10^{-3} M C_{12}-SK.

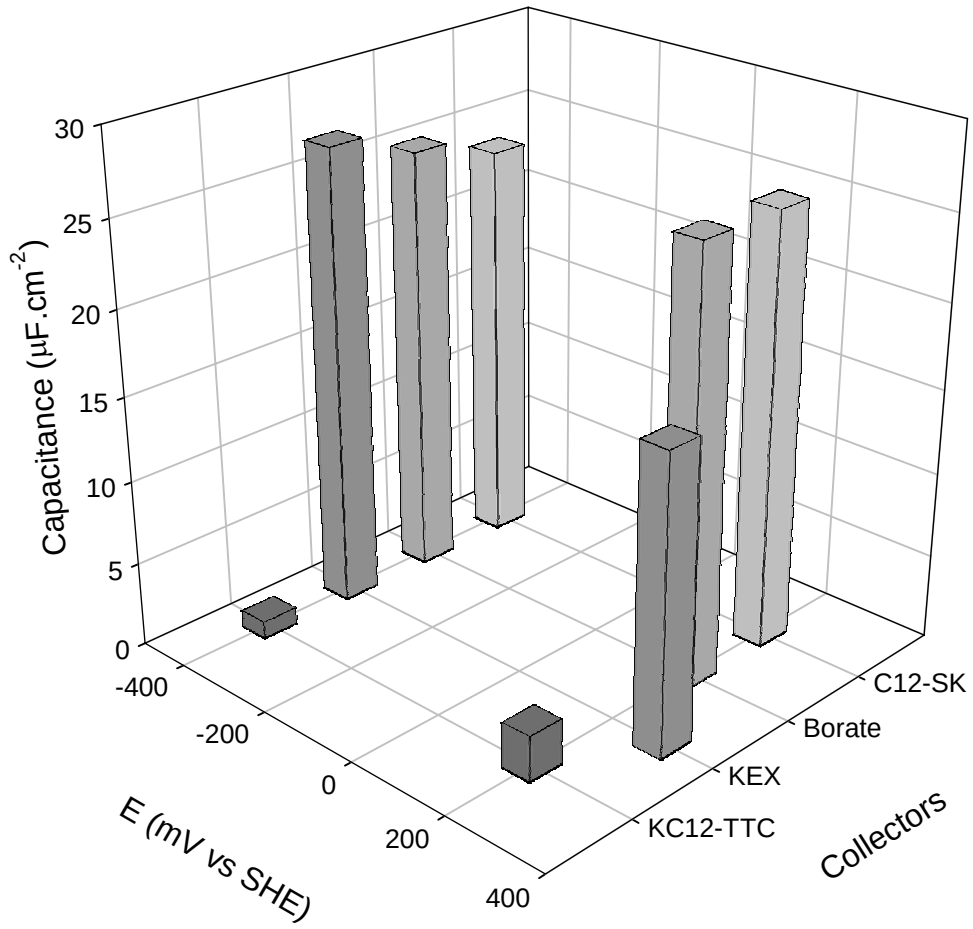

Figure 49: Capacitance of a pyrite electrode after polarisation for 1800 s at different potentials in a 0.05 M borate solution containing: borate-only, 10^{-3} M KEX, 10^{-3} M KC_{12}-TTC and 10^{-3} M C_{12}-SK.

The capacitance values of the pyrite polarised at -400 mV and 200 mV in the KC_{12}-TTC solution are much lower than in any of the other cases, indicating that a very significant surface layer has formed. This surface layer is insensitive to the applied potential. Interestingly, the capacitance measured after holding at a negative applied potential (-400 mV (SHE)) is lower than after polarisation at a higher potential. This would seem to contradict the conclusions drawn from the previous investigations in this study, namely that the TTC serves as an intermediate for the attachment of the thiol species; as the TTC interacts electrochemically with the surface, so the extent of the surface layer should increase. To test this, Figure 50 shows the change in capacitance over time for a pyrite electrode during polarisation at

-400 mV and 200 mV in 0.05 M borate solution containing no collectors and 10^{-3} M KC_{12}-TTC. In the KC_{12}-TTC solutions it is obvious that the surface layer forms more quickly at the more positive potential (as shown by the decrease in capacitance). This concurs with the findings of the TTC serving as an adsorption intermediate; at anodic currents an increased adsorption of TTC is expected. Again it can be observed that the final capacitance of the pyrite in the TTC solution polarised at -400 mV (SHE) is slightly lower than in the case of the more positive polarisation potential. This is probably due to the effect of a change in the semi-conductor properties of pyrite during polarisation, indicated by the change in the capacitance values of the pyrite electrode polarised in the 0.05 M borate solutions containing no collectors: during polarisation at -400 mV (SHE) in borate there is a decrease in the capacitance, but at 200 mV (SHE) there is an increase in the capacitance. These capacitance values during polarisation differ from the capacitance measurements at an open circuit potential after polarisation (Figure 49); at an open circuit there is no difference in the capacitance of pyrite polarised at -400mV (SHE) or 200 mV (SHE). Pyrite is a semi-conductor, but exhibits pseudometallic behaviour in solution, as a result of surface states. These surface states may be affected by polarisation, giving stronger semi-conductor behaviour (for example, a decrease in capacitance).

The decomposition behaviour of the TTC was again investigated (Figure 51) by performing successive scans on the same solution; a new pyrite surface was created (by polishing) in between the experimental runs. As the C_{12}-TTC decomposes the capacitance increases, indicating a decrease in the thickness of the surface layer. This is more marked in a case where successive scans were performed in the 0.05 M borate solutions containing 10^{-3} M KC_{12}-TTC polarised at 200 mV (SHE). This is probably because more TTC is adsorbed or oxidised at anodic currents and therefore the TTC decomposes faster on the surface, depleting the solution of TTC for the successive experimental runs. Consequently the concentration of the TTC decreases more rapidly in the solutions where the electrode is anodically polarised. The measurement (c) in Figure 52(I) is for a solution which was allowed to decompose for lengthy periods of time (several hours); there was no real formation of a surface layer, although the capacitance was lower from the onset of the polarisation than in solutions containing no collectors.

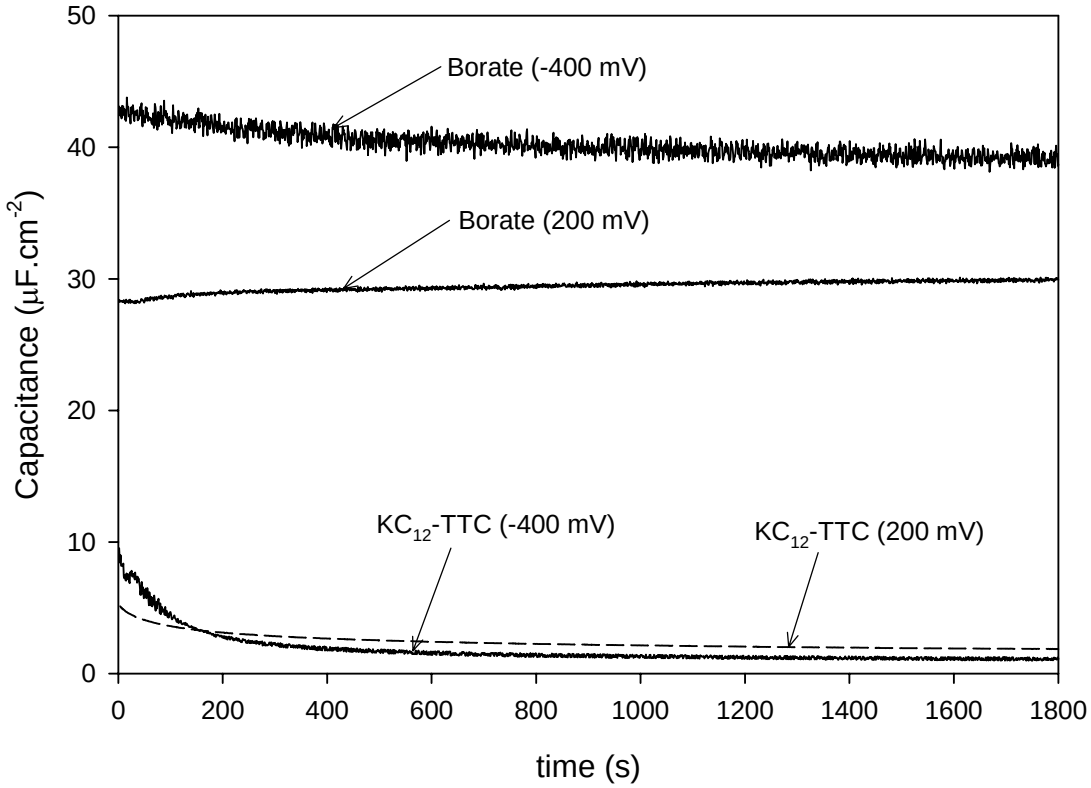

Figure 50: Capacitance measurements as a function of time for a pyrite electrode polarised at -400 mV (SHE) and 200 mV (SHE) in 0.05 M borate solutions containing no collectors (measured at 1000 Hz) and 10^{-3} M KC_{12}-TTC (measured at 3000 Hz).

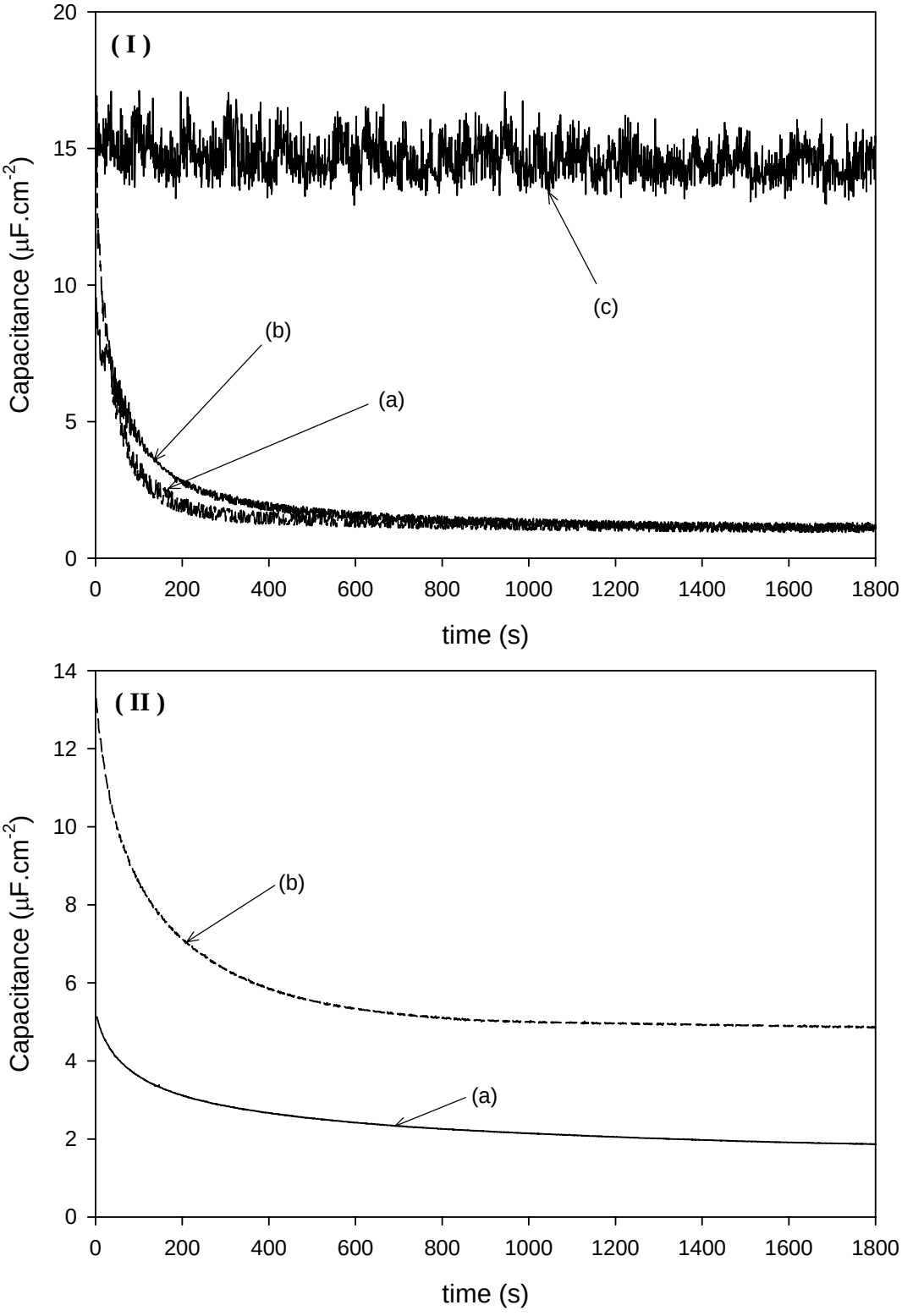

Figure 51: Capacitance measurements as a function of time at 3000 Hz for a pyrite electrode in 0.05 M borate solutions with 10^{-3} M KC_{12}-TTC polarised at (I) -400 mV (SHE) and (II) 200 mV (SHE); (a) and (b) are consecutive measurements; (c) was measured several hours later.

4.3.2 Copper

An EIS investigation was also done for copper polarised at -400 mV (SHE) and 200 mV (SHE) for 1800s in 0.05 M borate solutions containing: no collectors, 10^{-3} M KEX, 10^{-3} M KC_{12}-TTC and 10^{-3} M C_{12}-SK respectively. The same electrochemical circuit shown in Figure 45 was employed to model the copper electrochemical system. Similarly to pyrite, the R_p values at an open circuit are very large; see the Nyquist plots in Figure 52. This means that the system can again be described by Equation 16 at high frequencies. It is evident from the Bode plots in Figures 53 and 54 that after polarisation at both potentials in the borate-only solution, the open-circuit reactions become diffusion controlled. This indicates that the borate interacts with the copper surface. Yin and Lin (1996) found that borate can adsorb weakly onto copper surfaces. This has also been confirmed by the calculated capacitance values (calculated similarly to the pyrite electrode) for the copper electrode at the two polarisation potentials (-400 mV (SHE) and 200 mV (SHE)) (Figure 55). The capacitance values are lower (less than 10 $\mu F.cm^{-2}$) than expected for a surface without any surface layer (15-30 $\mu F.cm^{-2}$) indicating some adsorbed borate on the copper surface. The measured borate capacitance values are similar for both the polarisation potentials, indicating that the borate adsorption is not of an electrochemical nature. For the more positive potential, formation of copper oxide may contribute to the decreased capacitance.

When xanthate is added to the solution, the capacitance decreases, as expected, with an increase in the polarisation potential (Figure 55). The Bode plot of the copper electrode in the xanthate solution after polarisation at 200 mV (SHE) (Figure 54) clearly indicates the decrease in the capacitance characteristics (due to the formation of a product layer). It could be expected that the xanthate would adsorb at potentials higher than approximately -380 mV (SHE); the increase in the R_p values after polarisation at 200 mV (SHE) (Figure 52) does indicate lower open-circuit activity. Therefore the adsorbed xanthate appears to inhibit surface interactions. The slight decrease in the capacitance of the copper electrode in the xanthate solution compared with the solution without any collector after polarisation at -400 mV (SHE), is probably because the EIS measurements were performed at open-circuit potentials, where some xanthate adsorption would be possible.

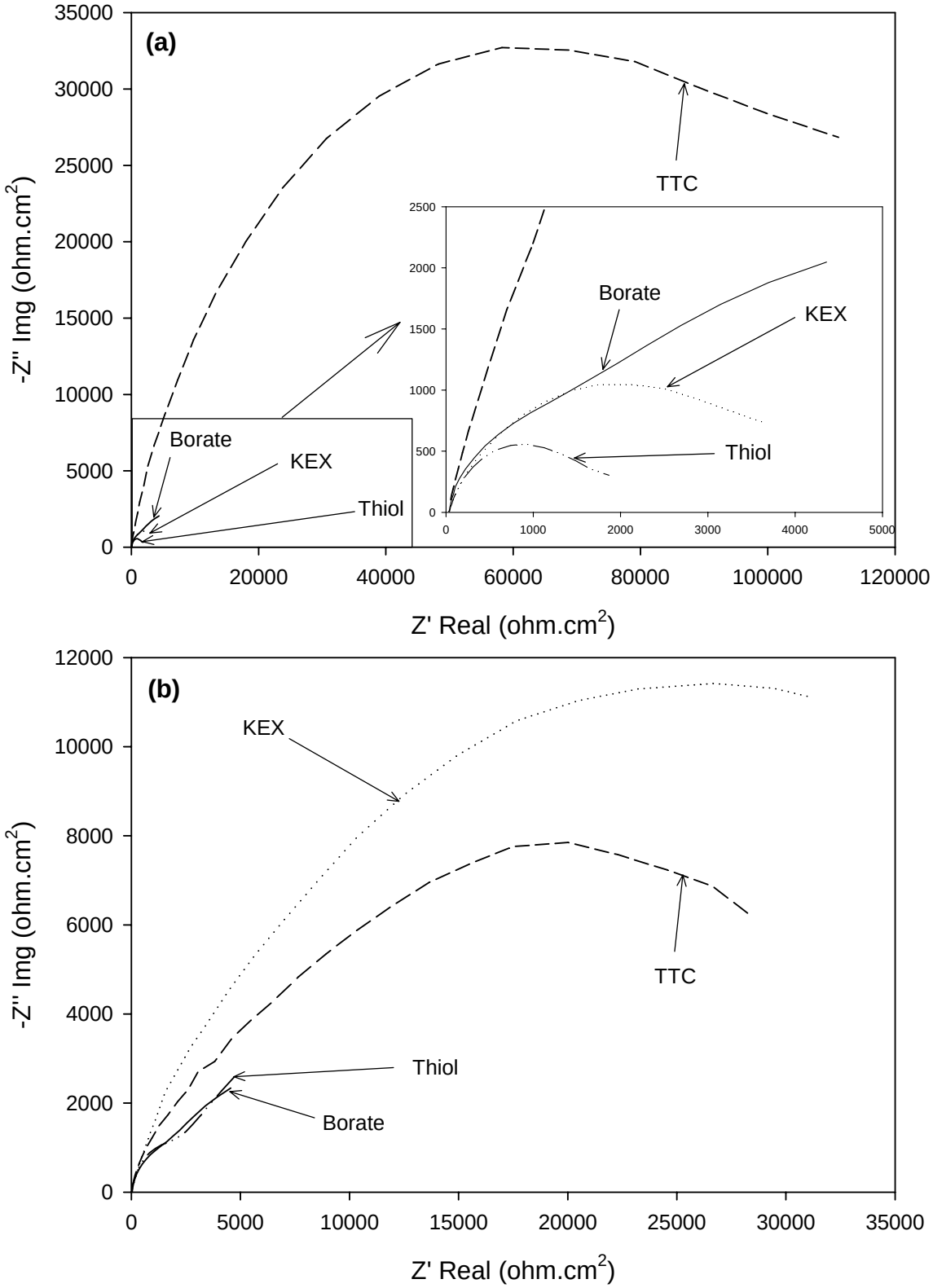

Figure 52: Nyquist plots of a copper electrode polarised for 1800 s at (a) -400 mV (SHE) and (b) 200 mV (SHE) in 0.05 M borate solutions with: no collectors, 10^{-3} M KEX, 10^{-3} M KC_{12}-TTC, and 10^{-3} M C_{12}-SK respectively.

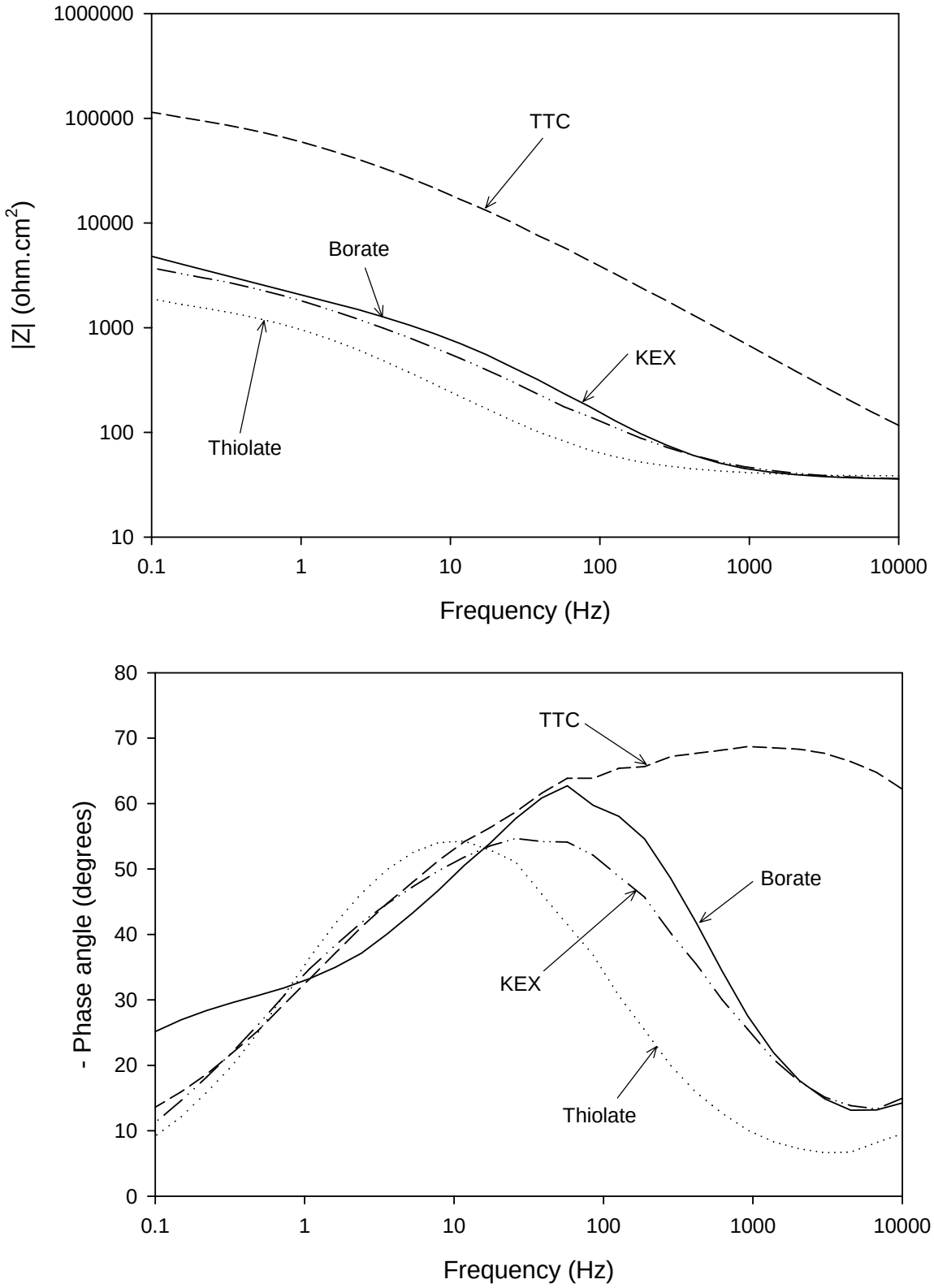

Figure 53: Bode plots for a copper electrode after polarisation for 1800 s at -400 mV (SHE) in a 0.05 M borate solution containing: no collectors, 10^{-3} M KEX, 10^{-3} M KC_{12}-TTC and 10^{-3} M C_{12}-SK respectively.

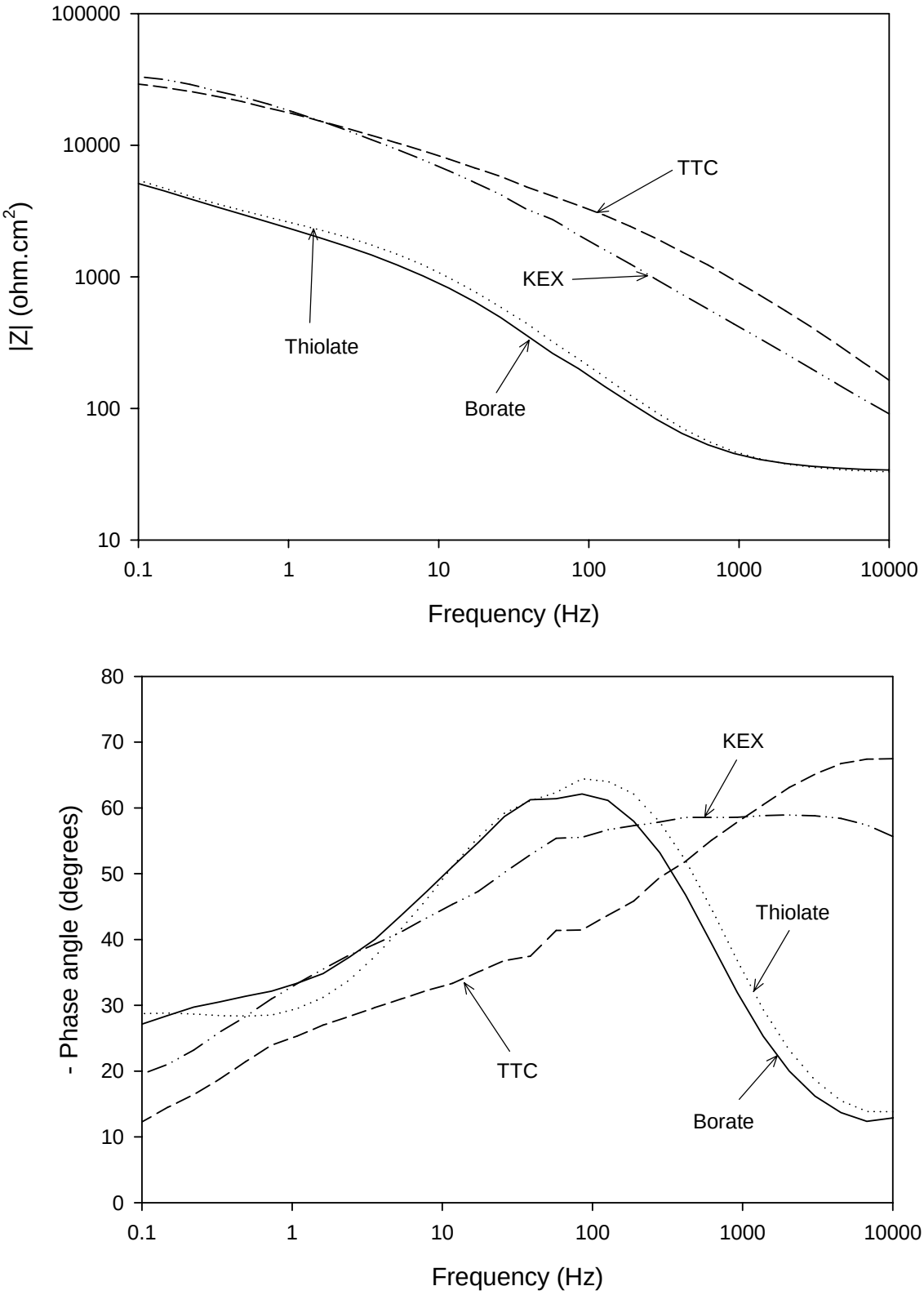

Figure 54: Bode plots for a copper electrode after polarisation for 1800 s at 200 mV (SHE) in a 0.05 M borate solution containing: no collectors, 10^{-3} M KEX, 10^{-3} M KC_{12}-TTC and 10^{-3} M C_{12}-SK respectively.

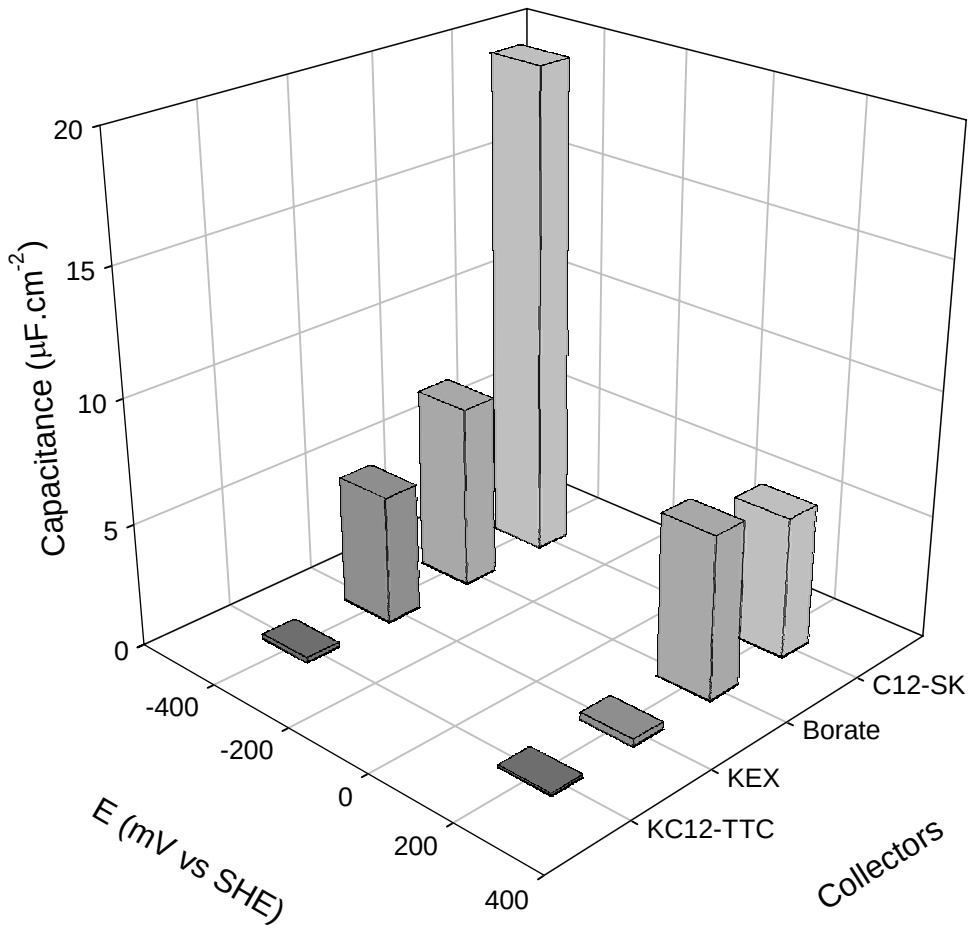

Figure 55: Capacitance of a copper electrode after polarisation for 1800 s at -400 mV (SHE) and at 200 mV (SHE) in a 0.05 M borate solution containing: no collectors, 10^{-3} M KEX, 10^{-3} M KC_{12}-TTC and 10^{-3} M C_{12}-SK respectively.

The capacitance measured of the copper electrode polarised at -400 mV (SHE) in the C_{12}-SK solution (Figure 55) is in the region one would expect for a clean electrode surface. The capacitance is higher, however, than that for the electrode in the borate solution without any collector. The results suggest that the thiolate inhibits the interaction between the surface and the borate, but does not adsorb onto the surface itself. Thiols interact with copper to form self-assembled monolayers (SAMs); this may occur (as previously discussed) through the reduction of the copper oxides or it may occur by the reduction of the thiol itself (Turbeville & Yap, 2006):

$$2RSH + 2Cu \rightarrow 2RSCu + H_2 \qquad (17)$$

As this reaction is quite slow, no real detectable layer is produced in 1800 s. However, such a presumed layer may inhibit the adsorption of borate on the copper surface.

By contrast, the interaction between the thiolate and the copper electrode during polarisation at 200 mV (SHE) is significant with a clear decrease in capacitance. This can probably be ascribed to two effects:

1) The adsorption of the thiol onto the surface via the reduction of the copper oxides formed at a potential of 200 mV (SHE).
2) The adsorption of the thiol is through a two-step process, firstly reduction of the Cu^{2+} and secondly the reduction of the Cu^{+}. The second step seems to be the step determining the rate of the adsorption of the C_{12}-SH; since the adsorption is slow, the thiol does not form a sufficient inhibitor layer on the surface to eliminate the oxidation of the Cu. This was evident in the increased current densities observed during the voltammetric measurements, resulting in an increase in the thickness of the oxide layer formed. This was visually observed when a coloured oxide layer formed on the copper surface (Figure 56).

Figure 56: Copper electrode polarised at 200 mV (SHE) for 1800 s in a 0.05 M borate and 10^{-3} M C_{12}-SK solution.

The adsorption of the thiol through the reduction of the copper oxides is much more effective than the adsorption through the direct reduction of the thiol by the copper. This was shown by Carbonell *et al.* (2004); the XPS investigations indicated a significant increase in the observed sulphur (thiol) species on the oxidised surface compared to an unoxidised copper surface.

The capacitances for the copper electrode polarised at -400 mV (SHE) and 200 mV (SHE) in the KC_{12}-TTC solution (Figure 55) were as expected; with an increase in the potential there is a decrease in the capacitance (the capacitance halved), indicating an increase in the thickness of the surface layer. After polarisation at 200 mV (SHE), the product layer would probably consist of not only the TTC adsorption products, but also some Cu^{2+} species. This is evident from the Nyquist plots (Figure 52), indicating that the open-circuit R_p value for the copper electrode decreases after polarisation at the more positive potential. This is contrary to the finding obtained in the case of the pyrite electrode. This increased reactivity of the electrode is probably due to the adsorption of the thiol onto the copper surface via the reduction of the Cu^{2+} species.

Figure 57 shows the change in the capacitances during the polarisation of a copper electrode in a solution containing only 0.05 M borate solution, together with the results for a TTC solution. At -400 mV (SHE) there is no change in the capacitance in the borate solution, but at 200 mV (SHE) the initial capacitance is lower and it continues decreasing over time, probably due to the formation of copper oxides. In the presence of TTC the capacitance decreases faster at the more positive potential. This correlates with the increased rate of adsorption of the TTC, or the formation of oxidation products.

The effect of the decomposition of TTC in the bulk solution was again investigated (Figure 58). The product layer formed during polarisation decreased significantly (for both of the polarised potentials) during the successive scans. The decrease was more evident in the case of the more positive potential, indicating that an anodic current enhanced the TTC adsorption on the electrode and also increased the decomposition of the TTC in solution.

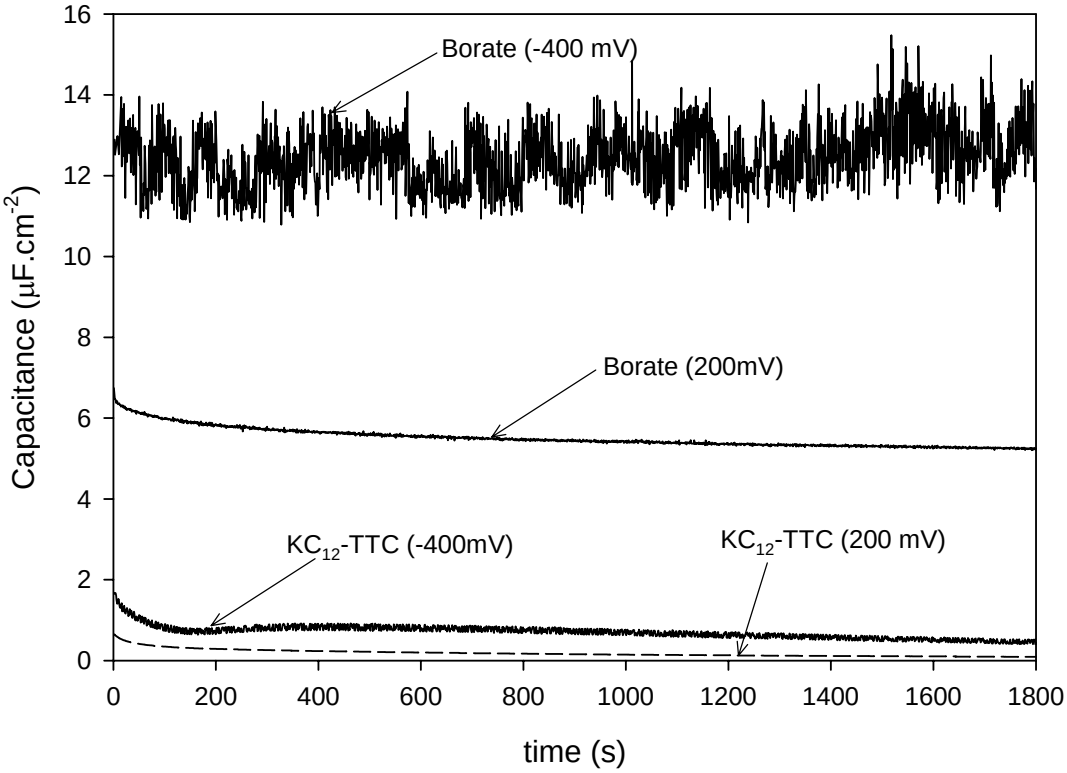

Figure 57: Capacitance measurements as a function of time for a copper electrode polarised at -400 mV (SHE) and 200 mV (SHE) in 0.05 M borate solutions containing no collectors (measured at 1000 Hz) and 10^{-3} M KC_{12}-TTC (measured at 3000 Hz).

In order to compare the rate of adsorption of TTC onto copper and pyrite it is necessary to normalise the capacitance measurement so that the differences in the dielectric constants between the systems are negated. Subramanian and Lakshminarayanan (2002) state that one can determine the relative rate of adsorption by expressing it as a function of surface coverage (θ) versus time. This surface coverage is calculated as follows:

$$\theta = \frac{C_0 - C_t}{C_0 - C_f} \tag{18}$$

where θ is the surface coverage, C_0 is the capacitance of the bare electrode, C_t is the capacitance at any time t and C_f is the capacitance after long adsorption times.

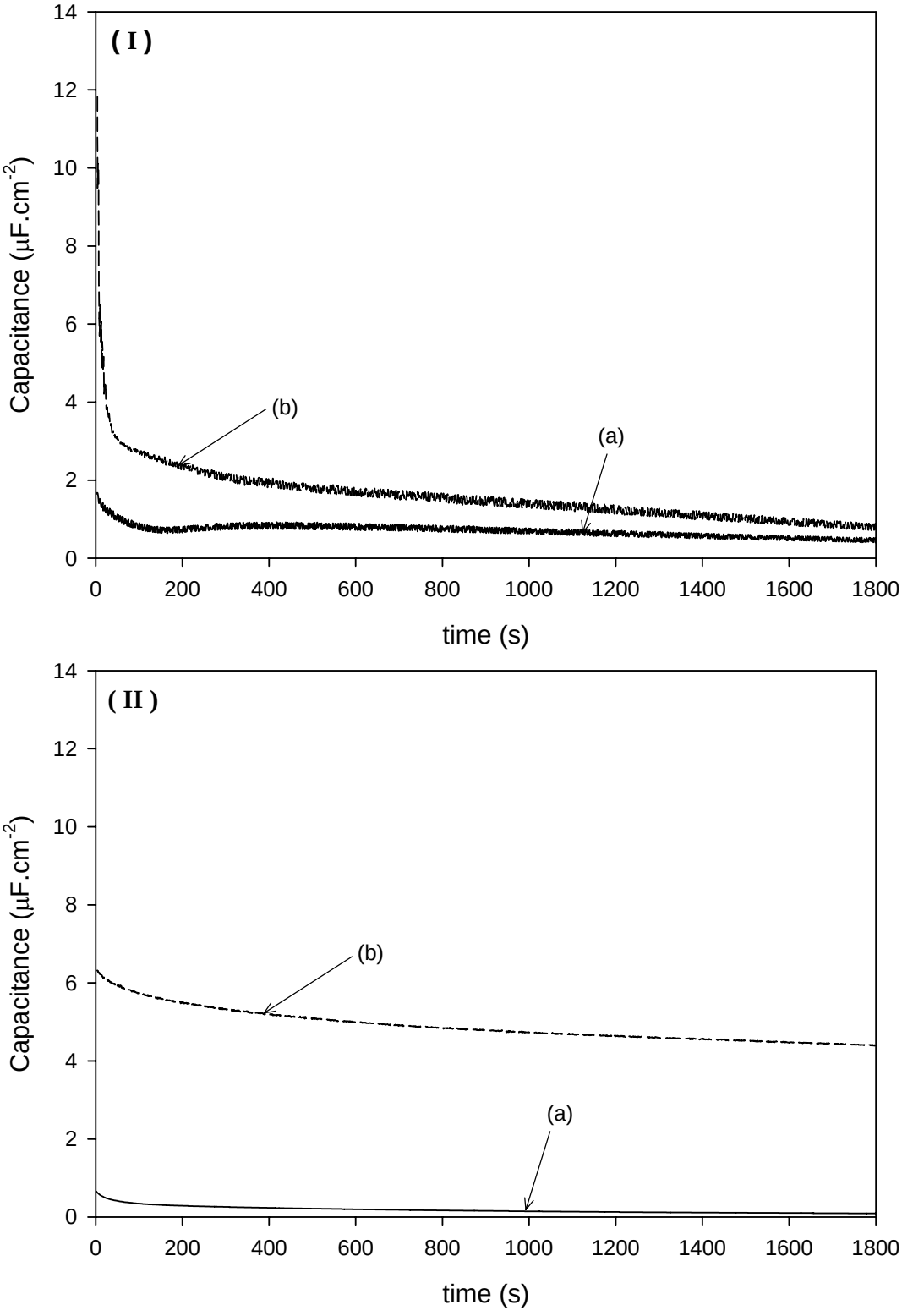

Figure 58: Capacitance measurements at 3000 Hz as a function of time for a copper electrode in 0.05 M borate solutions with 10^{-3} M KC_{12}-TTC polarised at (I) -400 mV (SHE) and (II) 200 mV (SHE); (a) and (b) are successive measurements in the same solution, using a fresh electrode in each case.

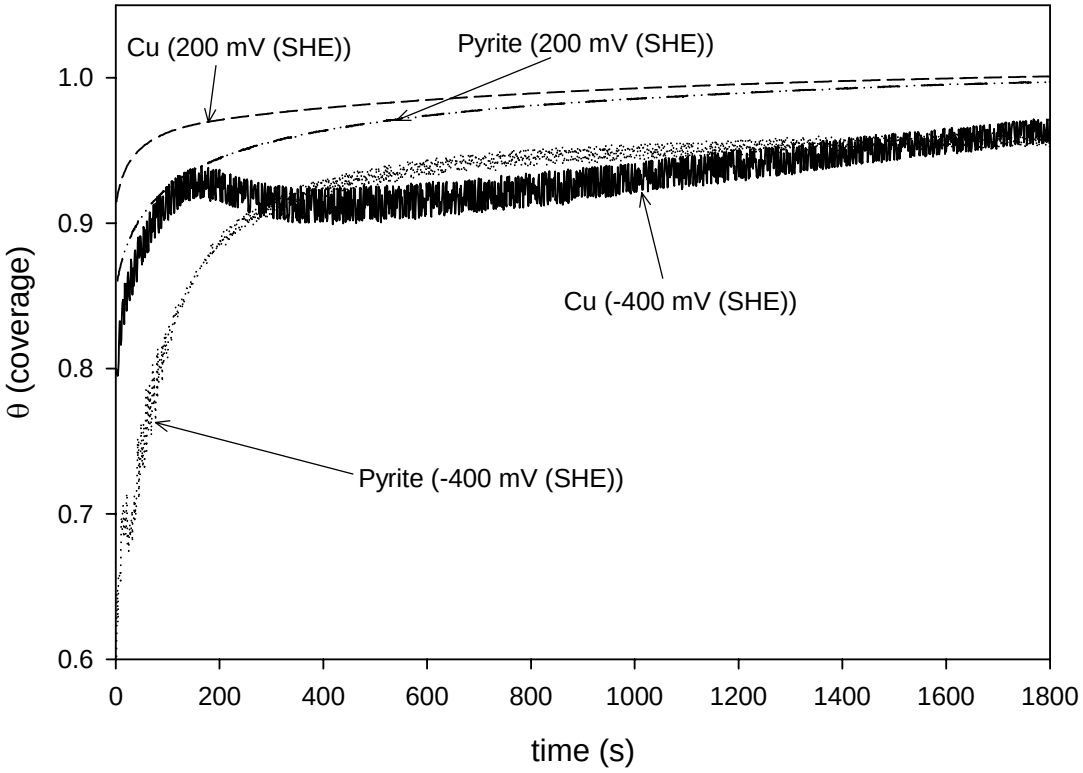

Figure 58: Change in coverage (θ) over time for a pyrite and copper electrodes respectively, measured at 3000 Hz, polarised at -400 mV (SHE) and 200 mV (SHE) in 0.05 M borate solutions containing 10^{-3} M KC_{12}-TTC.

Figure 58 displays the results of this analysis. It is clear that, for both electrodes, the rate of adsorption is higher for the more positive polarisation potentials. The TTC also adsorbs faster onto the copper than the pyrite, at the more positive polarisation potential. It is not clear what causes the inflection visible in the case of the copper electrode polarised at -400 mV (SHE), but this may reflect some restructuring of the surface layer hence changing the dielectric constant.

4.4 Decomposition of TTC in solution

Initially a UV-visible scan was performed between 200 nm and 400 nm (Figure 59). It is evident from these spectra that the peaks at 303 nm and 333 nm [these peaks can be assigned to the TTC (Du Plessis, 2003)] decrease with time.. The peak at 206 nm increases with time because of the decomposition of the TTC. The most likely decomposition products of the TTC are CS_2 and C_{12}-S^- (depending on pH C_{12}-SH might form). The CS_2 has an absorption peak at around 206 nm (Sun & Forsling, 1997). One would expect that the thiol species would also have an absorption peak in the region of 195 nm (Williams & Fleming, 1966). In Figure 60 the UV absorption spectrum of C_{12}-SK is compared to that of the aged TTC (measured after 15 minutes). In the case of the C_{12}-SK there is no CS_2 present; the peak at 206 nm is due solely to the C_{12}-S^- species. This peak corresponds to the peak found during the decomposition of the TTC.

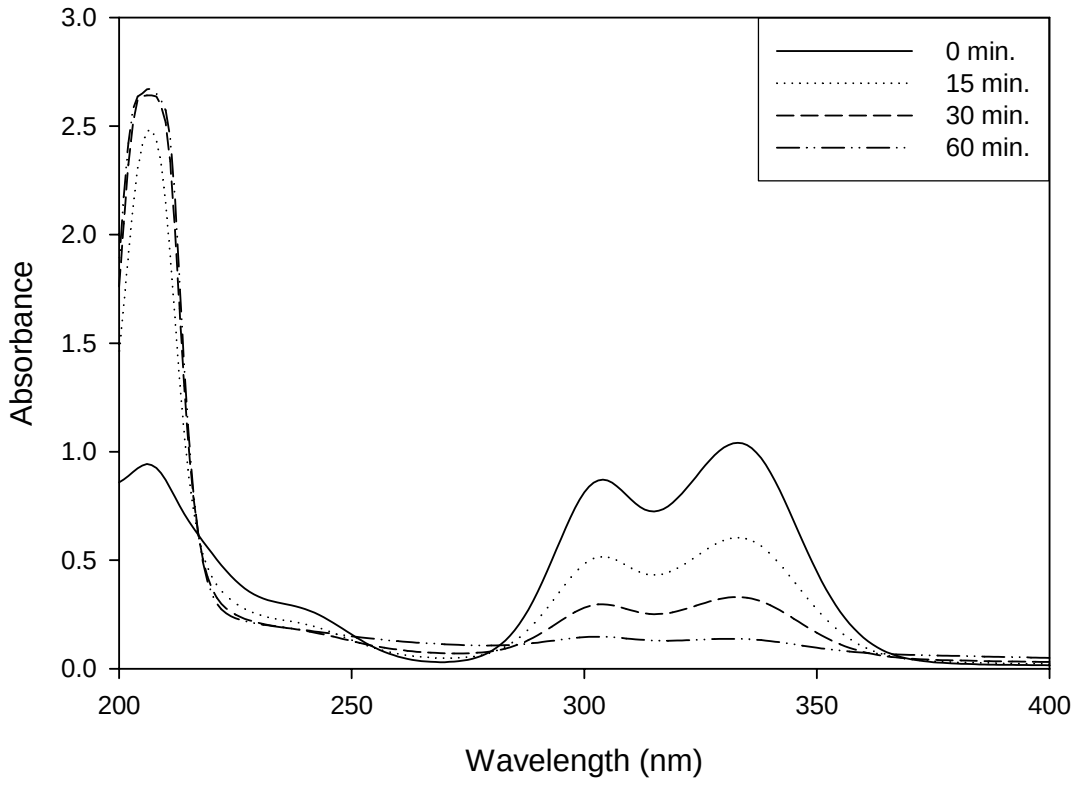

Figure 59: UV-visible spectra of a 0.05 M borate solution (pH 9.2) initially containing 10^{-4} M KC_{12}-TTC recorded at 0 min., 15 min., 30 min. and 60 min.

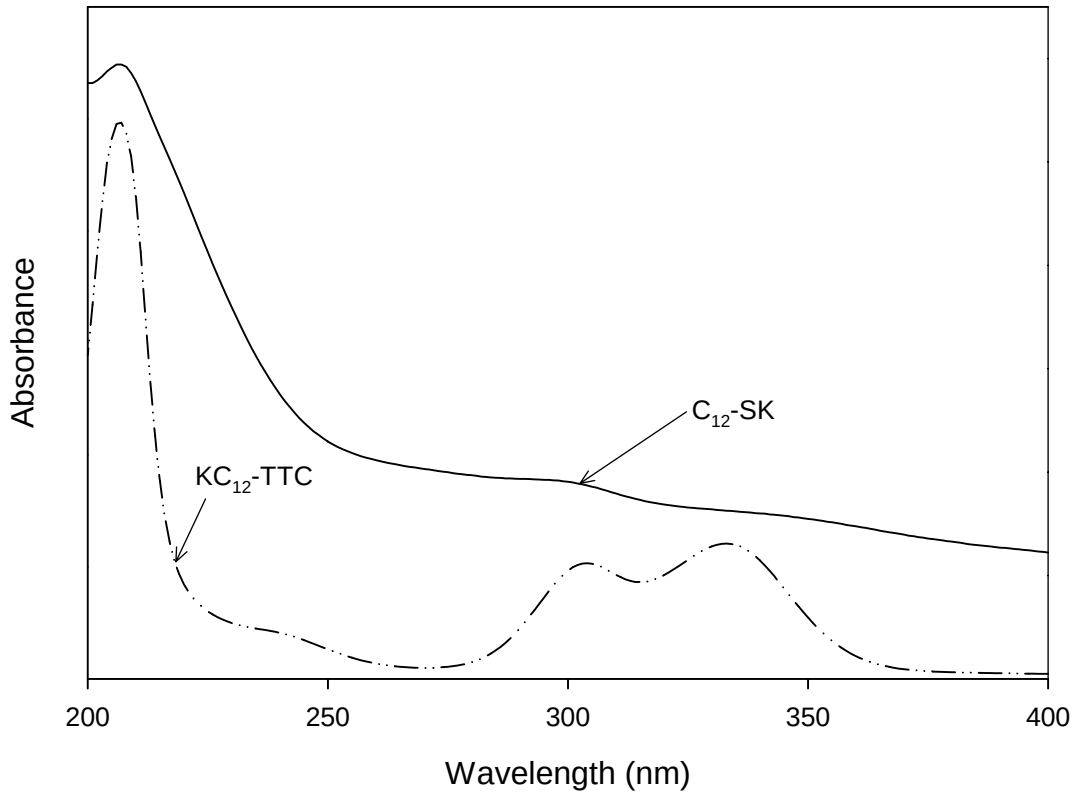

Figure 60: UV-visible spectra of 0.05 M borate solutions containing KC_{12}-TTC and C_{12}-SK respectively.

Sun and Forsling (1997) mention that in the case of ethyl xanthate, the decomposition follows a first-order reaction rate. Assuming that the decomposition of the TTC also follows a first-order reaction rate, the decomposition is as follows:

$$C_{12}\text{-}TTC^{-}(aq) = CS_2\,(aq) + C_{12}\text{-}S^{-}(aq) \qquad (19)$$

Therefore the decomposition rate can be expressed as follows:

$$\frac{d[C_{12}\text{ - }TTC^{-}]}{dt} = -k[C_{12}\text{ - }TTC^{-}] \qquad (20)$$

where k is the rate constant.

Therefore

$$[C_{12} - TTC^-] = [C_{12} - TTC^-]_0 e^{-kt} \quad (21)$$

where $[C_{12} - TTC^-]_0$ is the initial concentration.

This implies that if the decomposition of the TTC is a first-order reaction, the plot of $\ln[C_{12} - TTC^-]$ versus t should produce a straight line with a slope of –k.

Normally, in order to determine the concentration of species with UV spectroscopy, it is necessary to prepare a set of solutions with known concentrations so that a calibration curve can be established by employing Beer's law:

$$A = \varepsilon bc \quad (22)$$

where A is the absorbance at a fixed wavelength, ε is the molar absorptivity ($M^{-1}.cm^{-1}$) of the compound, b is the path length (cm) through the measurement cell and c is the concentration (M).

In this study it was not possible to prepare quantitative solutions, since the TTC decomposes quite rapidly. But ε and b are constant for the different solutions, so:

$$A \propto c \quad (23)$$

therefore plotting ln ΔA versus t should also produce a straight line with a slope of –k for a first-order reaction. The degradation plots in Figure 61 for TTC in unbuffered pH 4-11 solutions all seem to be fairly straight lines, indicating that the TTC follows a first-order reaction rate. It is clear from these plots that the TTC decomposes faster at low pH values and slower at high pH values.

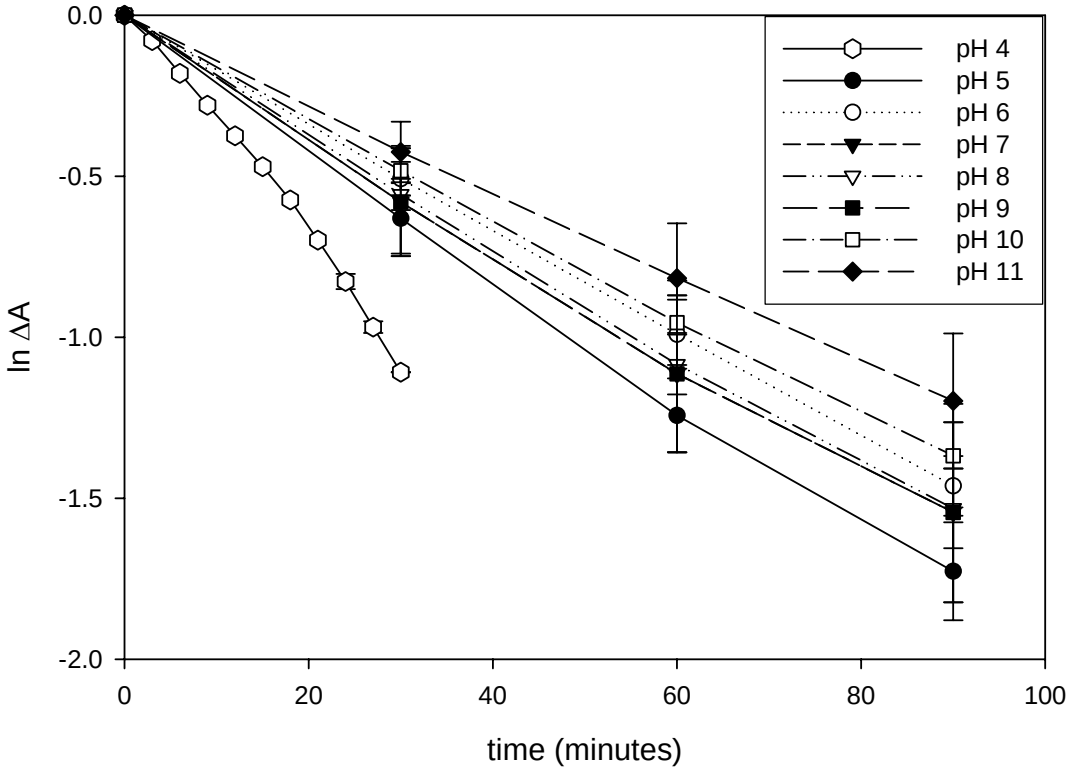

Figure 61: TTC degradation plots as a function of time for pH 4-11 solutions at 18 ˚C.

The pH of each solution was measured directly after the UV measurements (90 minutes from the first measurement). All the solutions had pH values of about 10.2 (Figure 62). The pK_a of C_{12}-SK is approximated 10.2 (indicated in Figure 62), calculated by utilising the ChemAxon Marvin software at the United States National Library of Medicine website at <http://chem.sis.nlm.nih.gov/chemidplus/>. Therefore the solutions are buffered at this pH. After three days, the pH values for the different solutions dropped (Figure 62). This was due to the C_{12}-SH that separates from the water due to its low solubility and volatilisation. The hydroxide concentration is dependent on the following equilibria:

$$RS^-(aq) + H_2O\ (l) = RSH\ (aq) + {}^-OH\ (aq) \quad (24)$$

$$2H_2O\ (l) = H_3O^+\ (aq) + {}^-OH\ (aq) \quad (25)$$

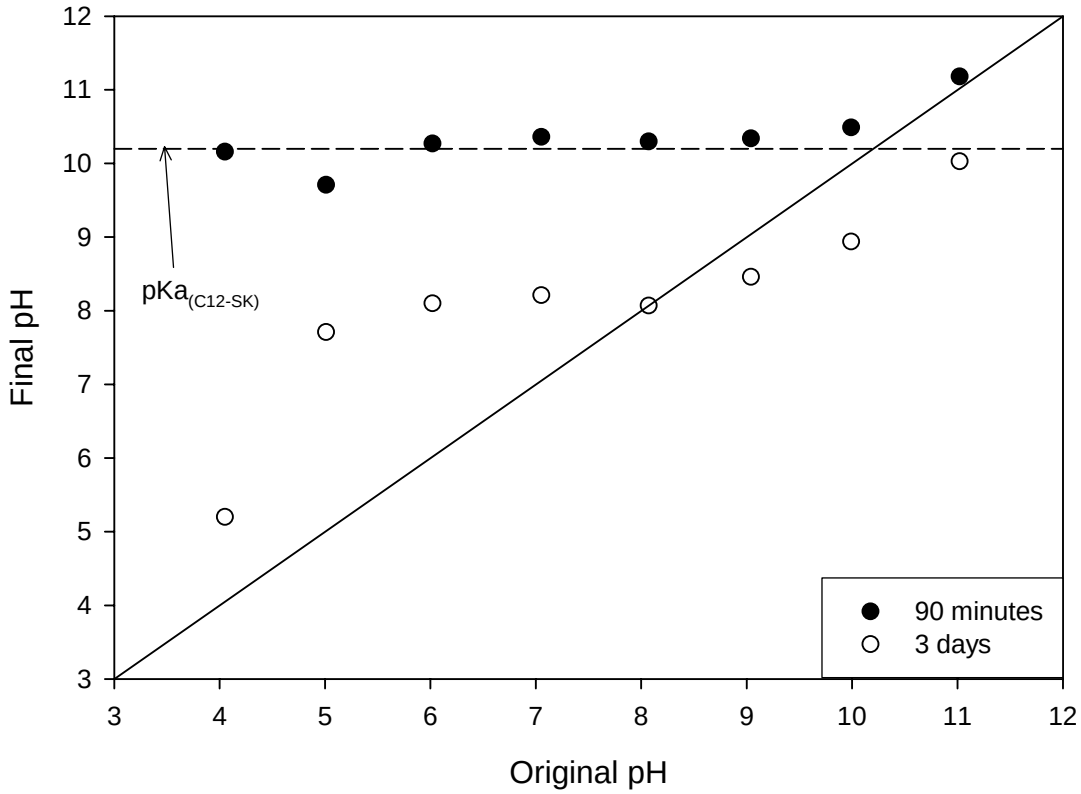

Figure 62: Change in the pH of the solutions during the decomposition of TTC; after 90 min. and three days at 18˚ C.

The [$^{-}$OH] due the dissociation of the water is equal to [H_3O^+], and the [$^{-}$OH] due to the reaction (25) is equal to the [RSH]. Hence the total [$^{-}$OH] in the system can be described as follows:

$$[^{-}OH] = [H_3O^+] + [RSH] \quad (26)$$

This indicates that as the concentration of the RSH decreases, the pH declines too.

It is clear from Figure 62 that after three days all the solutions, except the ones at a pH of 4 and 11, had a pH close to 8. This is due to the fact that at lower pH values, only the thiol would be present in the solution, so the solution is buffered at a pH of 8 until almost all of the thiol has separated from the water. It seems that after removing the thiol/thiolate buffer action, the solution would return to approximately its original pH (indicated in Figure 62). This behaviour of the pH during decomposition indirectly confirms that the decomposition products are thiolate and CS_2. The decomposition

tests were repeated for a 0.05 M borate solution buffered at pH 9.2 to remove the effects of the unstable pH. Figure 63 indicates that the TTC decomposition still follows a first-order reaction rate. The rate constants were calculated from the degradation plots and used to calculate the half-life ($t^{1/2}$) of the TTC as follows:

$$t^{1/2} = \frac{\ln 2}{k} \tag{27}$$

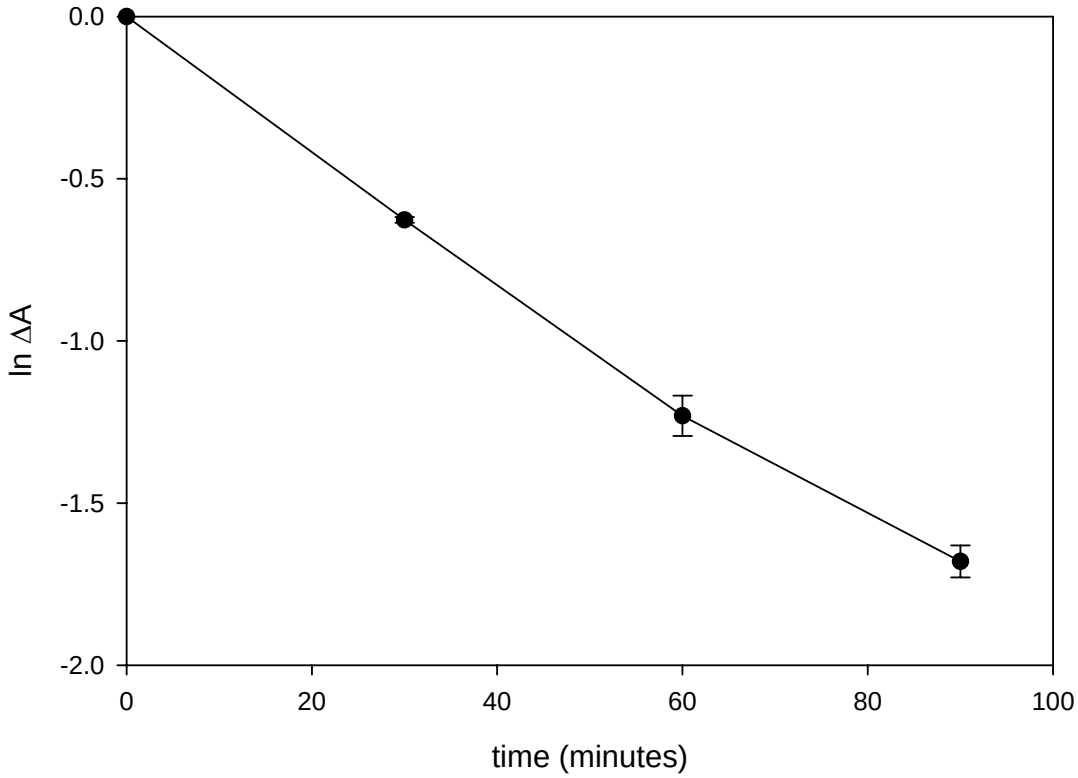

Figure 63: TTC degradation plots as a function of time for a 0.05 M borate solution buffered at a pH of 9.2 at 18° C.

It is clear from the half life plot (Figure 64) that the TTC is very unstable and independent of the solution pH. The degradation is slower at higher pH values ($t^{1/2} \approx 57$ minutes at pH of 11), but is still very high compared to that of xanthate (Sun & Forsling, 1997). The half-life times of xanthates vary from 42 minutes to 340 hours for pH 4-11. The half-life of the TTC in the buffered solution does not differ much from that of the unbuffered solution; the unbuffered solution was originally buffered at a pH of 10.2 compared to the buffered solution at a pH of 9.2. During the course of the measurements, the difference in the pH values of the two solutions was not

expected to be significant. However, if the solution were buffered in the lower pH range, the half-life of the TTC would probably increase due to the increase in the removal rate of the thiolate species. At higher pH values the rate of decomposition is lower due to the protonation of the thiolate and the subsequent reformation of the TTC.

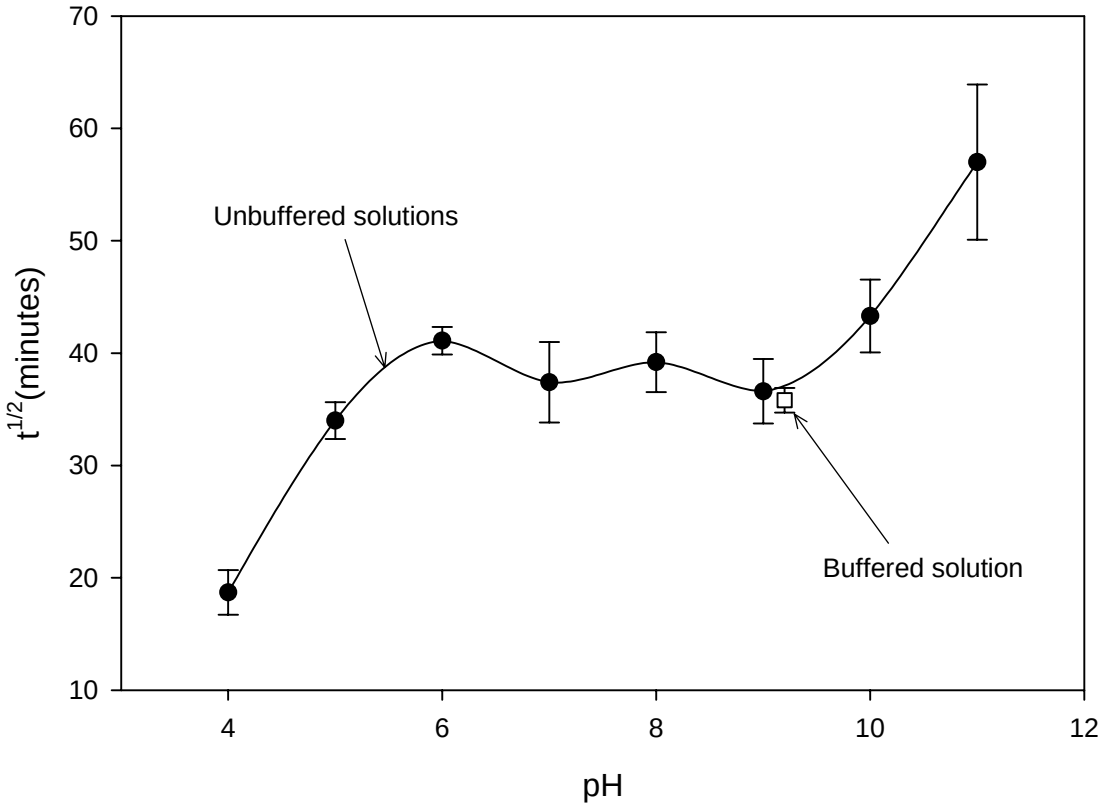

Figure 64: Half-life of TTC in unbuffered solutions (pH 4-11) and a 0.05 M borate solution buffered at pH 9.2 at 18˚ C.

4.5 Microflotation of pyrite

Figure 65 displays the results of the microflotation tests. It is clear from the test work that, in the presence of the freshly prepared TTC, the initial rate of flotation is significantly higher than that of xanthate. After 10 minutes nearly all the pyrite was floated with the freshly prepared TTC, compared to only approximately 45% recovered after 20 minutes with xanthate. This concurs with the findings in the EIS work that a more significant layer is formed by the TTC than by the xanthate. During the float, the presence of the dixanthogen, as expected under these conditions, could be detected by its distinctive odour.. The TTC that decomposed for four hours (approximate concentration of 5×10^{-7} M) still outperformed the xanthate. This indicates that the TTC has a much higher affinity to the pyrite than the xanthate has. One would expect that if full release curves (as much pyrite is floated as possible) were performed, the xanthate would ultimately float more pyrite than the decomposed TTC (the TTC would be completely depleted after extended periods).

The rate of recovery of the decomposed TTC was significantly lower than that of the fresh TTC. This was also as expected from the previous test work, that indicated that as the TTC decomposed it became less effective in interacting with the substrate. The thiol was very inefficient as a collector. The inability of the thiolate to attach to the pyrite surface was illustrated with the EIS measurements; there was no really noticeable formation of a surface layer. The inability of the thiol to act as a collector is in agreement with Keller *et al.* (1994) who found that no significant flotation was possible at low thiol concentrations (on copper).

Du Plessis *et al.* (2002) (Figure 66) and Breytenbach *et al.* (2003) state that there is a synergistic effect when using a combination of xanthate and TTC. These authors also found that the synergism effect had an optimum when using only a small amount of xanthate. The efficiency of the TTC probably decreases as its concentration increases, due to its ability to act as a frother and its stabilising effect on the bubbles, resulting in an increase in water recovery decreasing the grade and ultimately also the recovery. The microflotation tests suggest that the use of a small amount of TTC would increase the initial rate of recovery of the ore, compensating for the slow recovery rate

achieved with xanthate. The small amount of TTC does not have a noticeable affect on the froth stability. As was seen from the decomposed TTC test, only a very small amount is required for improved recovery rates. The slower-adsorbing xanthate would probably target particles that are not well liberated and therefore require longer conditioning times.

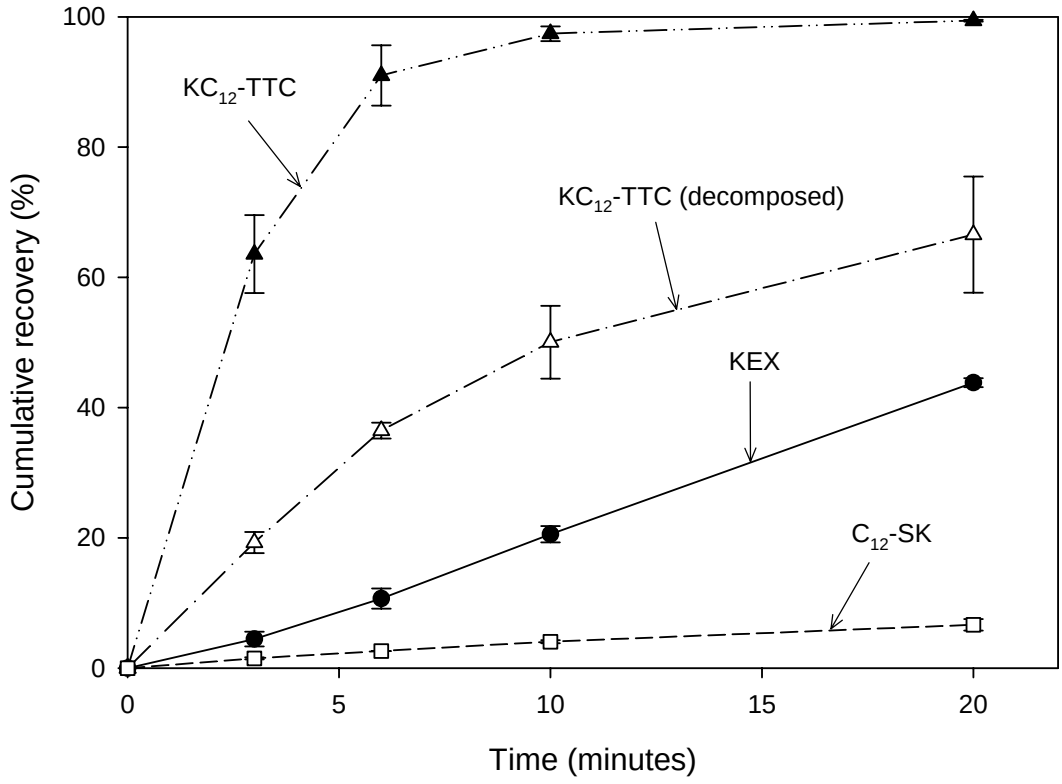

Figure 65: Microflotation of pyrite in 0.05 M borate solutions containing 5 $\times 10^{-5}$ M KC_{12}-TTC, 5 $\times 10^{-5}$ M C_{12}-SK, 5 $\times 10^{-5}$ M KEX and decomposed (for 4 hours) KC_{12}-TTC respectively.

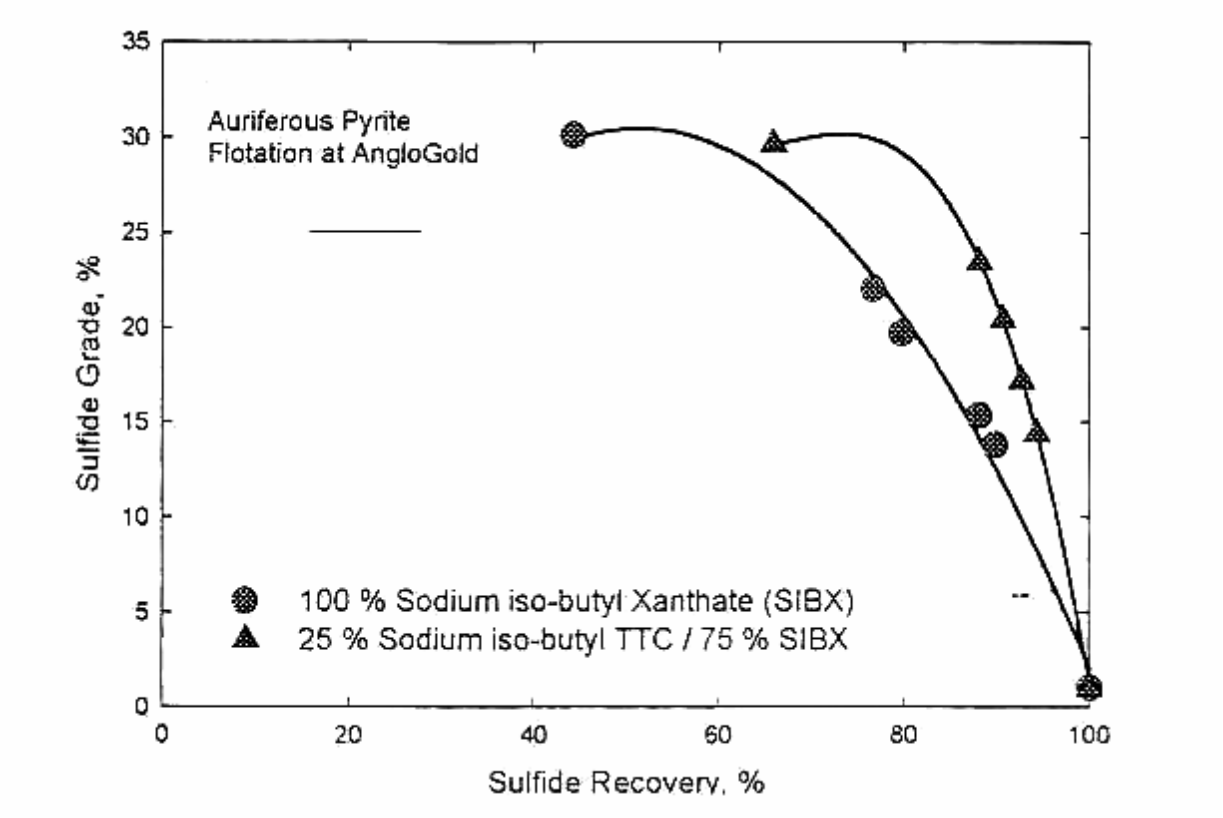

Figure 66: Grade-recovery curve illustrating improved recoveries when sodium isobutyl xanthate is used in conjunction with sodium isobutyl trithiocarbonate (Du Plessis *et al*., 2002)

5. Proposed mechanism

The current study has shown that there are significant differences in the adsorption mechanisms of the TTC and the xanthate. It appears that the TTC decomposes and that the thiol/thiolate is ultimately the final surface species that renders the particles hydrophobic. The specific surfaces act as catalysts for the decomposition of the TTC. The decomposition products do not directly interact strongly with the substrates; this was clearly illustrated by the high inefficiency of the thiol in floating the pyrite.

It is proposed that the TTC could interact in two different ways with the surface:

Firstly, the surface acts solely as a catalyst, thus just lowering the activation energy of the following reaction:

$$TTC^- \xrightarrow{M_{surf}} thiolate_{ads} + CS_2 \qquad (27)$$

This was evident from the Raman spectroscopy performed under potential control indicating that only the decomposition products could be detected in the presence of a cathodic current. The EIS measurements also confirmed the presence of an adsorbed layer on the substrates.

Secondly, the TTC chemisorbs onto the surface, similarly to xanthates, thus:

$$M_{surf} + TTC^- \rightarrow M_{surf}TTC_{ads} + e^- \qquad (28)$$

This was evident from the electrochemical experiments that indicated an anodic peak at more positive potentials and which was supported by Raman spectroscopy that indicated the presence of the CS_3-functional group at the surface. The EIS measurements indicated an increase in the amount of adsorbed species on the anodically polarised substrates as compared to the measured layer when the substrates where under cathodic control.

This is the followed by the decomposition reaction:

$$M_{surf}TTC_{ads} \rightarrow M_{surf}thiolate_{ads} + CS_2 \quad (29)$$

This was the only detectable species in this study with Raman spectroscopy.

Or the oxidation of the TTC:

$$M_{surf}TTC_{ads} \rightarrow TTC_2 + M_{surf} \quad (30)$$

One would expect in cases where the potential is more positive than the reduction potential of the TTC monomer/dimer couple, that some oxidation of the TTC should occur [see Reaction (30)]. This was indeed found by Du Plessis (2003). Reaction (28) is the reason for the increase in the rate of adsorption, as measured with EIS. This increased rate in adsorption would also cause an increase in the surface coverage compared to reducing conditions; this was observed during the contact angle measurements with the increase in the contact angle. It is clear from the results that the TTC could be utilised in more reducing or less oxidative conditions than the xanthate; TTC should be very useful in cases where ores are easily oxidised, but it would not be restricted solely to those conditions. The ability of the thiols to adsorb onto oxides combined with the ability of the TTC to carry the species to the surface may also be useful in the flotation of oxide ores. However, the stabilisation of the bubbles and ultimately the froth may restrict the concentration range in which TTC can be added.

6. Conclusions

The main conclusions from this study are as follows:

I) The C_{12}-TTC can interact with the substrate independent of the surface potential, making it possible to use the C_{12}-TTC in reducing conditions compared to xanthate that requires an oxidant for adsorption.

II) The C_{12}-TTC has two different mechanisms of adsorption; in the presence of a cathodic current the substrate only serves as a catlyst for the decomposition of the C_{12}-TTC, while in the presence of an anodic current the C_{12}-TTC chemisorbs via a charge transfer process.

III) The C_{12}-TTC is very unstable in solution (pH 4-11); half-life varies from as short as 18 minutes (pH 4) up to 57 minutes (pH 11).

IV) The C_{12}-TTC decomposes to its corresponding thiol or thiolate; these decomposition products on their own are very weak flotation collectors.

V) Only a small amount of C_{12}-TTC is required to increase the rate of recovery during flotation; decomposed C_{12}-TTC (only approximate 10% of the original concentration) still had a higher rate of recovery than a fresh xanthate solution.

7. Recommendations

For a complete elucidation of the mechanism of adsorption it would be useful to perform SERS on gold, copper and silver by employing longer wavelengths (1064 nm) and therefore lower energies; the sensitivity of the analysis would be increased by up to three orders of magnitude. Due to the instability of the TTC it is important that the tests should be performed *in situ* and should be less destructive so as not to change the surface species. The interaction of the laser with the TTC on the copper was a very prevalent problem during the current study. Other less intrusive tests, for example IR spectroscopy, could also be useful in this regard. Specifically attenuated total reflectance (ATR) FTIR can be useful since it is an *in situ* technique. However, water absorption of the IR can possibly limit the use of ATR FTIR.

Further work needs to be done on the synergism between the TTC and the xanthate. Microflotation tests with the individual collectors and combinations of them are needed to investigate whether the synergism is only a sum of the two collectors' recovery rates. In addition, the froth characteristics of the TTC would need to be quantified and taken into consideration during the flotation work.

8. References

ACKERMAN, P.K., HARRIS, G.H., KLIMPEL, R.R. & APLAN, F.F. 1987. Evaluation of flotation collectors for copper sulfides and pyrite, I. Common sulfhydryl collectors. *International Journal of Mineral Processing***,** Vol. 21, pp. 105-127.

AMBROSE, J., BARRADAS, G. & SHOESMITH, D.W. 1973. Investigations of copper in aqueous alkaline solutions by cyclic voltammetry. *Electroanalytical Chemistry and Interfacial Electrochemistry,* Vol. 47, pp. 47-64.

BARD, A.J. & FAULKNER, L.R. 1980. *Electrochemical methods: fundamentals and applications*, New York: John Wiley & Sons, pp. 502.

BRADSHAW, D.J., CRUYWAGEN, J.J. & O'CONNOR, C.T. 1995. Thermochemical measurements of the surface reactions of sodium cyclohexyl-dithiocarbamate, potassium *n*-butyl xanthate. *Minerals Engineering*, Vol. 8, pp. 1175-1184.

BRADSHAW, D.J. & O'CONNOR, C.T. 1996. Measurements of the sub-process of bubble loading in flotation, *Minerals Engineering*, Vol. 9, pp. 443-448.

BREYTENBACH W., M.K.G. VERMAAK & DAVIDTZ, J.C. (2003). Synergistic effects among dithiocarbonates (DTC), dithiophosphate (DTP) and trithiocarbonates (TTC) in the flotation of Merensky ores. *Journal of the South African Institute of Mining and Metallurgy,* Vol. 103(10), pp. 667–670.

BOZKURT, V., XU, Z., BRIENNE, S.H.R., BUTLER, I.S. & FINCH, J.A. 1999. *In situ* orientation study of xanthate on copper under potential control. *Journal of Electroanalytical Chemistry*, Vol. 475, pp. 124-129.

CARBONELL, L. WHELAN, C.M., KINSELLA, M. & MAEX, K. 2004. A thermal stability study of alkane and aromatic thiolate self-assembled monolayers on copper surfaces. *Superlattices and Microstructures*, Vol. 36, pp.149-160.

CHENG, E.C-C., LEUNG, K-H., MISKOWSKI, V.M., YAM, V.W-W. & PHILLIPS, D.L. 2000. Electronic and resonance Raman spectra of $[Au_2(CS_3)_2]^{2-}$.

spectroscopic properties of a "short" Au(I)-Au(I) Bond. *Inorganic Chemistry*, Vol. 39, pp. 3690-3695.

DRAKE J.E. & YANG J. 1994. Synthesis and spectroscopic characterization of *S*-ethyl, *S*-isopropyl, *S*-*n*-propyl and *S*-*n*-butyl trithiocarbonate (Trixanthate) derivatives of Trimethyl- and Triphenylgermane and Diphenyldigermane. Crystal structure of $Ph_2Ge[S_2CS(i\text{-}Pr)]_2$. *Inorganic Chemistry,* Vol. 33, pp. 854–860.

DU PLESSIS, R., DAVIDTZ, J.C. & MILLER, J.D. 1999. Preliminary examination of the electrochemical and spectroscopic features of trithiocarbonate collectors for sulfide mineral flotation. *Prepared for the Proceedings of the 1999 International Workshop on the Electrochemistry of the Sulfide Mineral Flotation, honouring Professor Wang Dianzuo for his 50 years of contributions to mineral processing,* 5-7 November 1999, Changsa, China.

DU PLESSIS, R., DAVIDTZ, J.C. & MILLER, J.D. 2002. The development of trithiocarbonate collectors for precious metals recovery by sulfide mineral flotation. *Internal report.*

DU PLESSIS, R. 2003. The thiocarbonate flotation chemistry of auriferous pyrite. *PhD thesis,* University of Utah, United States of America.

FINKELSTEIN N.P. & POLING G.W. 1977. The role of dithiolates in the flotation of sulphide minerals. *Mineral Science Engineering*, Vol. 9 No. 4, pp. 177–197.

FUERSTENAU, D.W. & RAGHAVAN, S. 1976. Some aspects of the thermodynamics of flotation. *Flotation: A.M. Gaudin Memorial Volume*. Edited by M.C. Feurstenau. Vol.1. Baltimore: Port City Press Inc., pp.21-65.

GARDNER J.R. & WOODS R. 1977. An electrochemical investigation of contact angle and of flotation in the presence of alkylxanthates. II galena and pyrite surfaces. *Australian Journal of Chemistry,* Vol. 27**,** pp**.** 981–991.

GROOT D.R., HARKEMA S.H.M. & VERMAAK M.K.G. 2005. The application of cyclic voltammetry coupled with surface plasmon resonance measurements to thiol-

collector interactions with gold surfaces. *Journal of the South African Institute of Mining and Metallurgy,* Vol. 105, pp. 645–652.

KARTIO, I., LAAJALEHTO, K., SUONINEN, E., KARTHE, S. & SZARGAN, R. 1992. Technique for XPS measurements of volatile adsorbed layers: application to studies of sulphide flotation. *Surface and Interface Analysis*, Vol. 18, pp. 807-810.

KELLER, H., SIMAK, P., SCHREPP, W. & DEMBOWSKI, J. 1994. Surface chemistry of thiols on copper: an efficient way of producing multilayers. *Thin Solid Films*, Vol. 244, pp. 799-805.

KUDELSKI, A. 2005. Characterization of thiolate-based mono- and bilayers by vibrational spectroscopy: a review. *Vibrational Spectroscopy*, Vol. 39, pp. 200-213.

LAAJALEHTO, K., LEPPINEN, J., KARTIO, I. & LAIHO, T. 1999. XPS and FTIR study of the influence of electrode potential on activation of pyrite by copper or lead. *Colloids and Surfaces A: Physicochemical and Engineering Aspects*, Vol. 154, pp. 193-199.

LEJA, J. 1982. *Surface chemistry of froth flotation.* Plenum Press: New York, pp. 230-243.

LEPPINEN, J.O., YOON, R.-H. & MIELCZARSKI, J.A. 1991. FT-IR studies of ethyl xanthate adsorption on gold, silver and gold-silver alloys. *Colloids and Surfaces*, Vol. 61, pp. 189-203.

LIN-VIEN, D., COLTHUP, N.B., FATELY,W.G. & GRASSELLI, J.G. 1991. *The handbook of infrared and Raman characteristic frequencies of organic molecules.* San Diego: Academic Press Inc., p. 239.

McGUIRE, M.M., JALLAD, K.N., BEN-AMOTZ, D. & HAMERS, R.J. 2001. Chemical mapping of elemental sulfur on pyrite and arsenopyrite surfaces using near-infrared Raman imaging microscopy. *Applied Surface Science,* Vol. 178, pp. 105-115.

MIELCZARSKI, J.A., MIELCZARSKI, E. & CASES, J.M. 1998. Influence of chain length on adsorption of xanthates on chalcopyrite. *International Journal of Mineral Processing*, Vol. 52, pp. 215-231.

MIELCZARSKI, J. & YOON, R.H. 1989. Orientation of thiol collectors on chalcocite. *Processing of Complex Ores: Proceedings of the International Symposium on Processing of Complex Ores*, August 20-24, Halifax.

MINCEVA-SUKAROVA, B., NAJDOSKI, M., GROZDANOV, I. & CHUNNILALL, C.J. 1997. Raman spectra of thin solid films of some metal sulfides. *Journal of Molecular Structure*, Vol. 410-411, pp. 267-270.

OBLONSKY L.J. & DEVINE T.M. 1995. A surface enhanced Raman spectroscopic study of the passive films formed in borate buffer on iron, nickel, chromium and stainless steel. *Corrosion Science,* Vol. 37, pp. 17–41.

POLING, G.W. 1976. Reactions between the thiol reagents and sulphide minerals. *Flotation: A.M. Gaudin Memorial Volume*. Edited by M.C. Feurstenau. Vol.1. Baltimore: Port City Press Inc., pp.334-363.

RAO, S.R. 1971. *Xanthates and related compounds*. New York: Marcel Dekker, pp. 15-18, 154-183 & 255.

SILVERMAN, D.C. 1986. Primer on the AC Impedance Technique. *Electrochemical techniques for corrosion engineering.* Edited by R. Baboian. Houston: NACE, pp 73-79.

SLABBERT, W. 1985. The role of trithiocarbonates and thiols on the flotation of some selected South African sulfide ores. *M.Sc. dissertation,* Potchefstroom University, South Africa.

STEYN, J.J. 1996. The role of collector functional groups in the flotation activity of Merensky reef samples. *M.Eng. (Chem.) dissertation,* Potchefstroom University, South Africa.

SUBRAMANIAN, R. & LAKSHMINARAYANAN, V. 2002. Effect of adsorption of some azoles on the copper passivation in alkaline medium. *Corrosion Science*, Vol. 44, pp. 535-554.

SUN, X. & FORSLING, W. 1997. The degradation kinetics of ethyl-xanthate as a function of pH in aqueous solution. *Minerals Engineering*, Vol. 10 No. 4, pp. 389-400.

TURBEVILLE, W. & YAP, N. 2006. The chemistry of copper-containing sulfur adsorbents in the presence of mercaptans. *Catalysis Today*, Vol. 116, pp. 519-525.

UNITED STATES NATIONAL LIBRARY OF MEDICINE. 2007. National Institute of Health, Specialized Information Services, Bethesda, viewed 25 January 2007, <http://chem.sis.nlm.nih.gov/chemidplus/>.

VERMAAK M.K.G., PISTORIUS P.C. & VENTER J.A. 2005. Electrochemical and Raman spectroscopic studies of the interaction of ethyl xanthate with Pd-Bi-Te. *Minerals Engineering,* Vol. 18**,** pp. 575–584.

VERMAAK M.K.G., VENTER J.A. & PISTORIUS P.C. 2004. Electrochemical studies of the interaction of ethyl xanthate with Pd-Bi-Te. *Journal of the South African Institute of Mining and Metallurgy,* Vol. 104(11), pp. 667–670.

VOS, C.F., DAVIDTZ, J.C. AND MILLER, J.D. 2006 Trithiocarbonates for PGM flotation. *International Platinum Conference 'Platinum Surges Ahead'*, SAIMM. Sun City, South Africa, pp. 169-174.

WANG, X., FORSSBERG, K.S.E. & BOLIN, N.J. 1989. Thermodynamic calculations on iron-containing sulphide mineral flotation systems, I. The stability of iron-xanthates. *International Journal of Mineral Processing*, Vol. 27, pp. 1-19.

WILLIAMS, D.W. & FLEMING, I. 1996. *Spectroscopic methods in organic chemistry*. London: McGraw-Hill, pp.10.

WILLS, B.A. 1997. *Mineral processing technology.* 6th Edition. Oxford: Butterworth-Heinemann, pp. 258-276.

WINTER, G. & WOODS, R. 1973. The relation of collector redox potential to flotation efficiency: monothiocarbonates. *Separation Science*, Vol. 8, No.2, pp. 261-267.

WOODS, R. 1976. Electrochemistry of sulfide flotation. *Flotation: A.M. Gaudin Memorial Volume*. Edited by M.C. Fuerstenau. Vol.1. Baltimore: Port City Press Inc., pp.298-333.

WOODS, R., BASILIO, C.I., KIM, D.S. & YOON, R.-H. 1994. Chemisorption of ethyl xanthate on silver-gold alloys. *Colloids and Surfaces A: Physicochemical and Engineering Aspects*, Vol. 83, pp.1-7.

WOODS, R. 1996. Chemisorption of thiols on metals and metal sulfides. *Modern Aspects of Electrochemistry*, Vol. 29, pp. 401-453.

WOODS, R. & HOPE, G.A. 1998a. Spectroelectrochemical investigations of the interaction of ethyl xanthate with copper, silver and gold: I. FT-Raman and NMR spectra of the xanthate compounds. *Colloids and Surfaces A: Physicochemical and Engineering Aspects*, Vol. 137, pp.319-328.

WOODS, R., HOPE, G.A. & BROWN, G.M. 1998b. Spectroelectrochemical investigations of the interaction of ethyl xanthate with copper, silver and gold: II. SERS of xanthate adsorbed on silver and copper surfaces. *Colloids and Surfaces A: Physicochemical and Engineering Aspects*, Vol. 137, pp.329-3337.

WOODS, R., HOPE, G.A. & BROWN, G.M. 1998c. Spectroelectrochemical investigations of the interaction of ethyl xanthate with copper, silver and gold: III. SERS of xanthate adsorbed on gold surfaces. *Colloids and Surfaces A: Physicochemical and Engineering Aspects*, Vol. 137, pp.339-344.

YIN, K.-M. & LIN B.-T. 1996. Effects of boric acid on the electrodeposition of iron, nickel and iron-nickel. S*urface and Coatings Technology*, Vol. 78, pp. 205-210.